SYSTEMS TECHNOLOGY, INC

13766 S. HAWTHORNE BOULEVARD • HAWTHORNE, CALIFORNIA 90250-7083 • PHONE (310) 679-2281
email: sti@systemstech.com FAX (310) 644-3887

Working Paper 1439-10

System identification studies with the stiff wing miniMUTT Fenrir – Flight 20

Started: June 3, 2015
Latest Revision: June 11, 2015

Brian P. Danowsky
Principal Research Engineer
310.679.2281x128

Prepared for

NASA NRA Grant:
Performance Adaptive Aeroelastic Wing
Contract No. NNX14AL36A

This page intentionally left blank

1.0 INTRODUCTION

A successful flight test with the stiff wing miniMUTT, formerly named Fenrir, was conducted on 27 May 2015. The purpose of this flight was to gather preliminary data for system identification focused on low frequency rigid body dynamics. No augmentation was used during the 1st flight on this day, which is formally flight 20. This working paper analyzes flight 20 only. 3-2-1-1 pitch excitations were sent to individual symmetric surface pairs coincident with normal pilot inputs.

For reference, a preliminary model of the stiff wing Fenrir (developed by D. K. Schmidt) at a flight condition of 65 ft/s (19.8 m/s) indicates a short period mode at 9.02 rad/s with a damping ratio of 0.658 and a phugoid mode at 0.569 rad/s with a damping ratio of -0.0251. It is expected that the actual aircraft dynamics will differ but these dynamic parameters provide a good baseline for ballpark values for comparison to the flight test data.

Analysis of these data were performed in both the frequency and time domains. Short period system parameters were identified using two approaches: 1) frequency domain equation error, and 2) subspace system identification in the time domain.

1.1 Test Inputs

This test consisted of a straight and level flight with five separate 3-2-1-1 inputs commanded to different sets of symmetric surface pairs. Figure 1 displays the aircraft with the control surface layout.

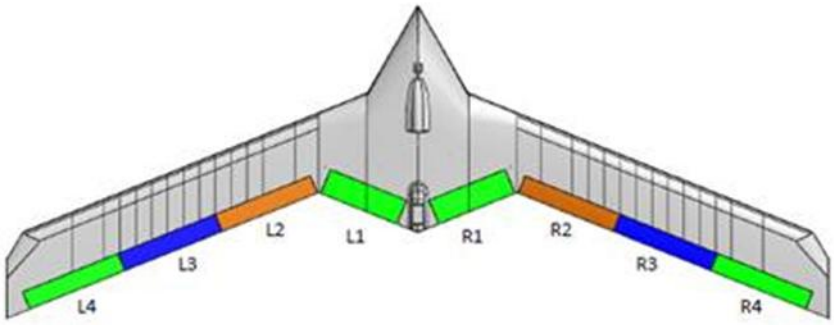

Figure 1: Fenrir control surface layout.

Collective inputs were applied in the following order: 1) L3/R3, 2) L4/R4, 3) L1/R1, 4) L3/R3, and 5) L4/R4.

The approximate frequency range of excitation based on half energy is $\mu_{min} \cong 0.3/\Delta t$ rad/s, $\mu_{max} \cong 2.7/\Delta t$ rad/s.[1] The normalized power spectral density of a 3-2-1-1 input is shown in Figure 2, which displays the frequency content above half power. All inputs for this test used a 0.16 sec pulse width which corresponds to an excitation range of 1.875 rad/s < μ < 16.875 rad/s.

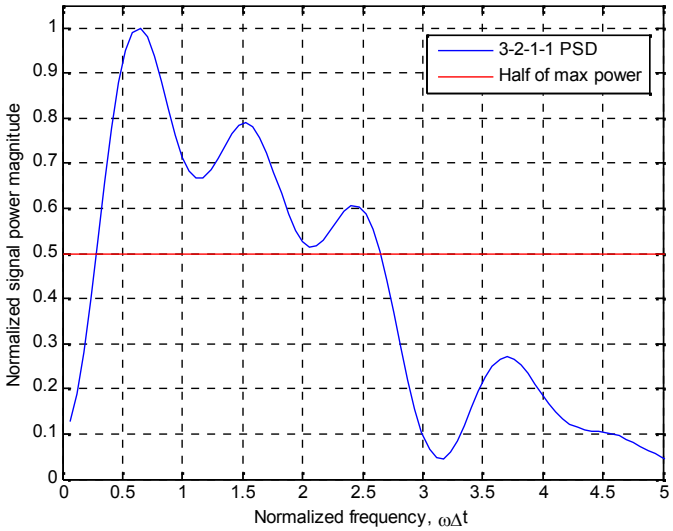

Figure 2: Power Spectral Density of a 3-2-1-1 input.

1.2 System architecture and time domain data

The control surface inputs are due to 1) the pilot, and 2) the excitation system. Referring to Figure 1, a pilot elevator input commands L4, L3, R3, R4 collectively. A pilot aileron input commands L2 and R2 differentially while also commanding L4 and R4 differentially. Excitation was applied independent of this pilot input and was applied at single symmetric surface pairs only. The elevator and all surface commands are defined as positive deflection down. A positive aileron is left deflection down, right deflection up.

The data segment from 1255 to 1280 seconds was considered since this included the excitation commands at the airspeed remained relatively consistent near 20 m/s (~65.6 ft/s) [$\overline{IAS} = 20.8$ m/s, $\pm_{IAS} = 2.57$ m/s]. Figure 3 through Figure 5 display the airspeed, excitation signals, pilot elevator command and pitch rate response.

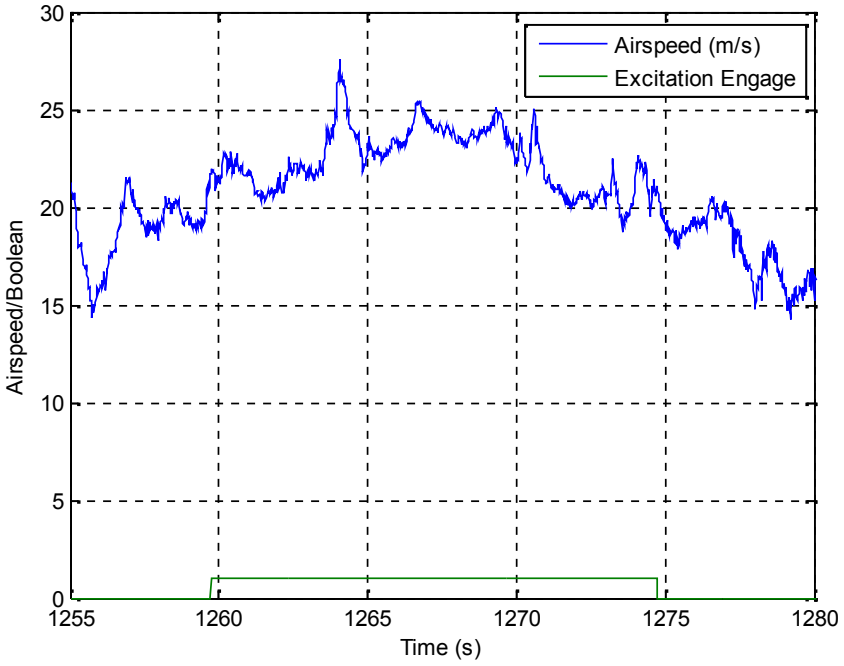

Figure 3: Airspeed and excitation engagement.

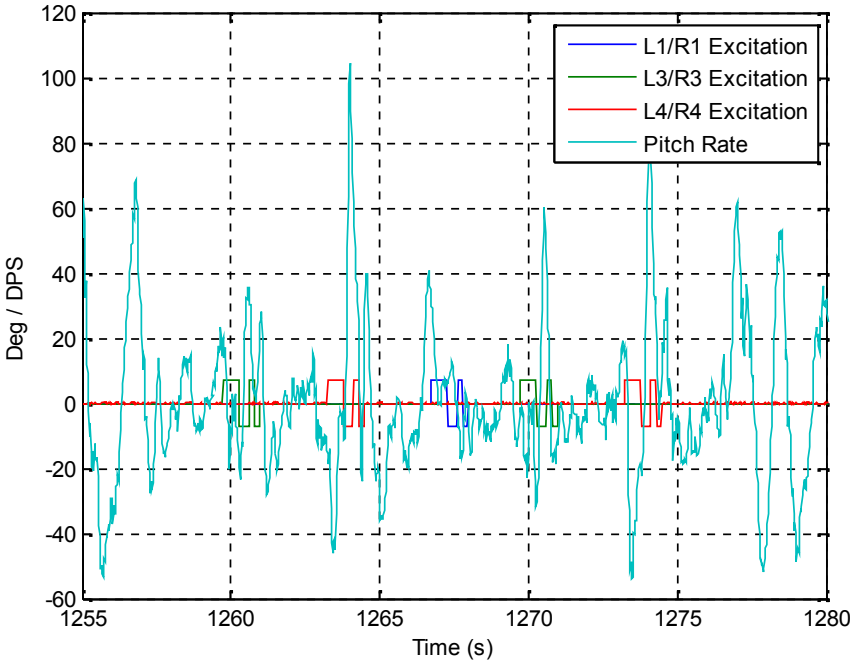

Figure 4: Excitation signals and pitch rate.

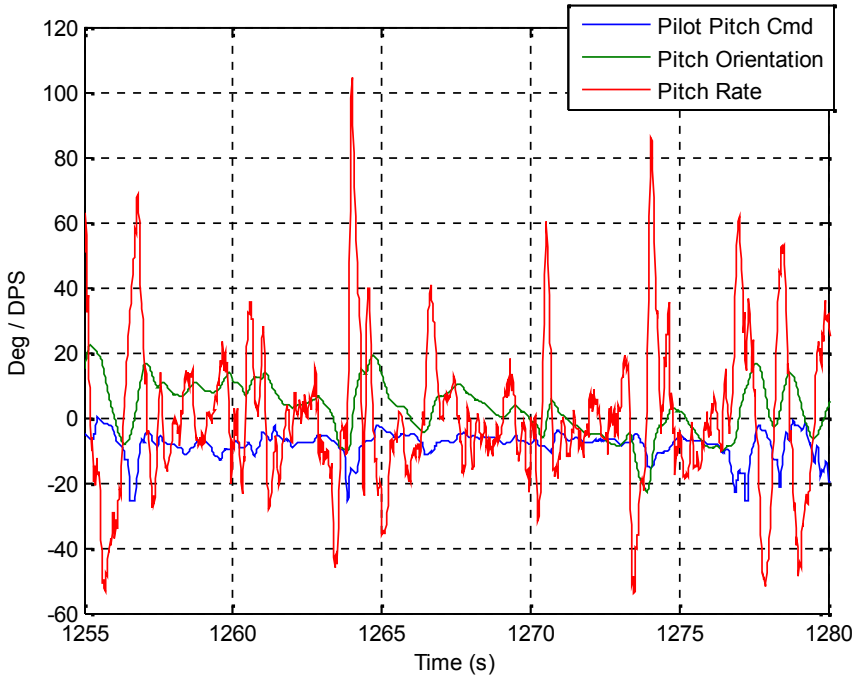

Figure 5: Pilot elevator command (pitch command), pitch orientation, and pitch rate response.

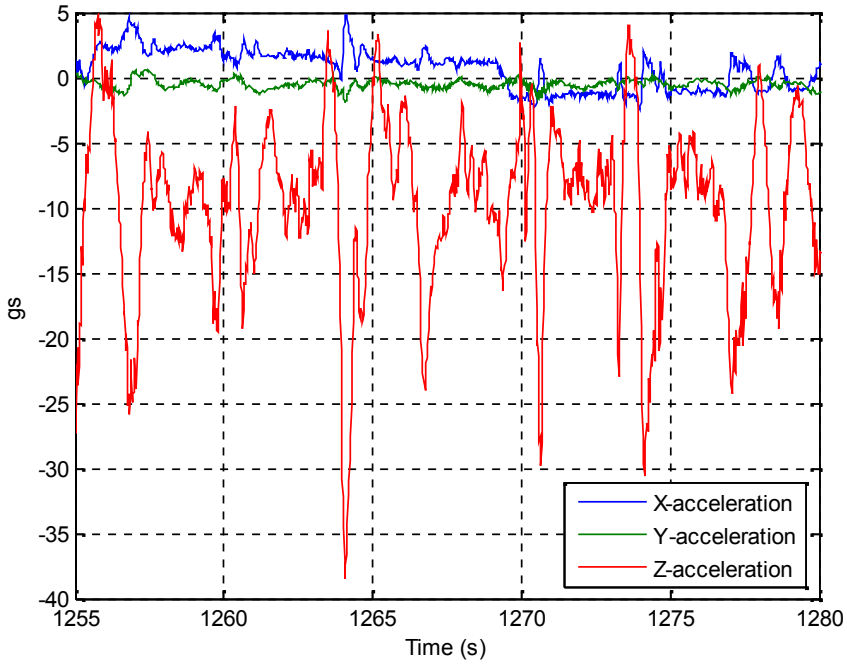

Figure 6: IMU acceleration response.

The commands to the individual surfaces are shown in Figure 7 through Figure 10.

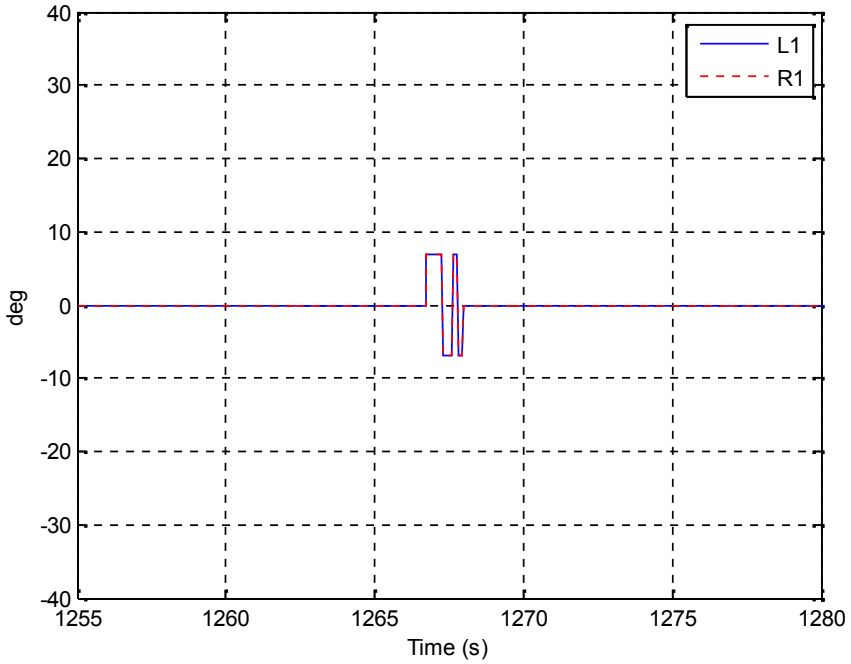

Figure 7: Surface commands to L1 and R1.

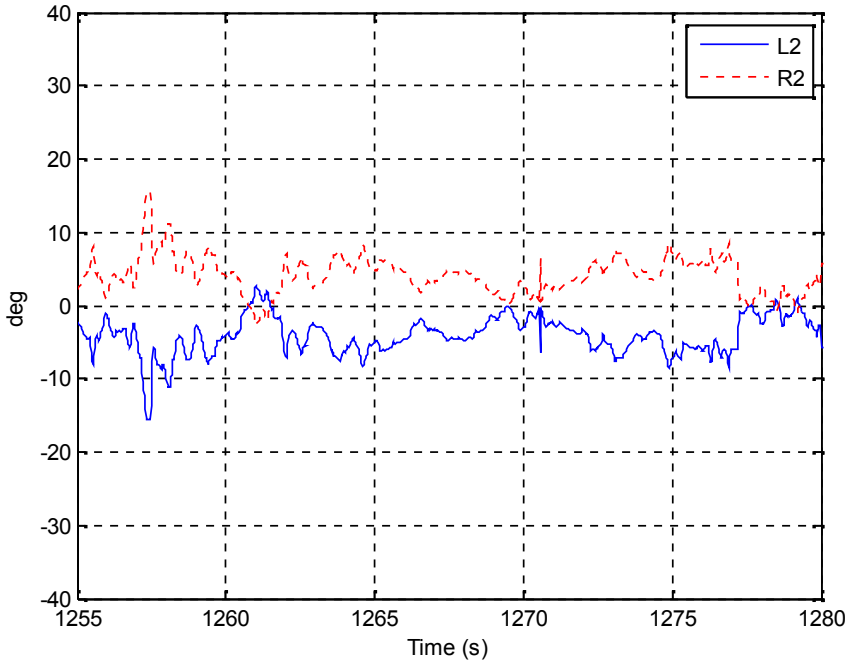

Figure 8: Surface commands to L2 and R2.

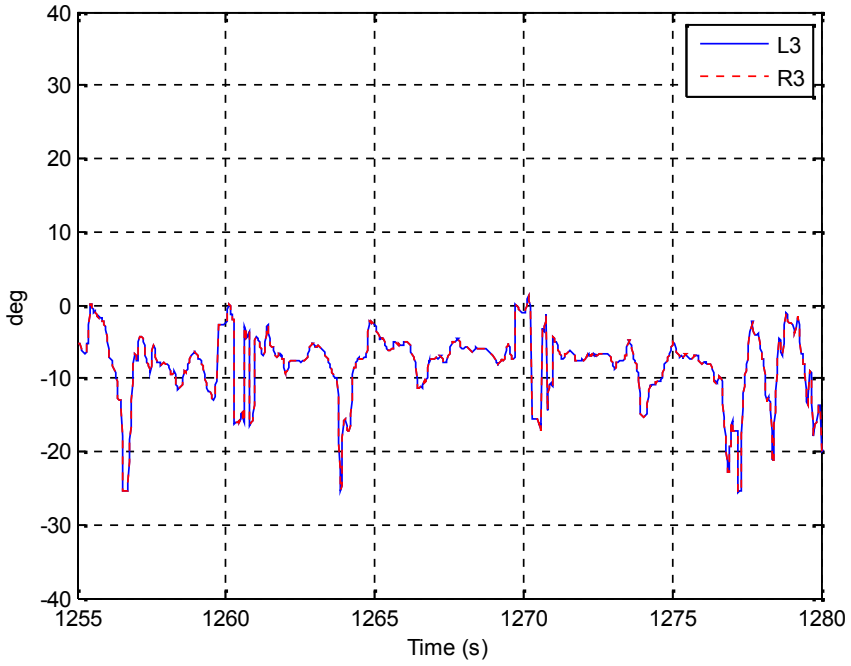

Figure 9: Surface commands to L3 and R3.

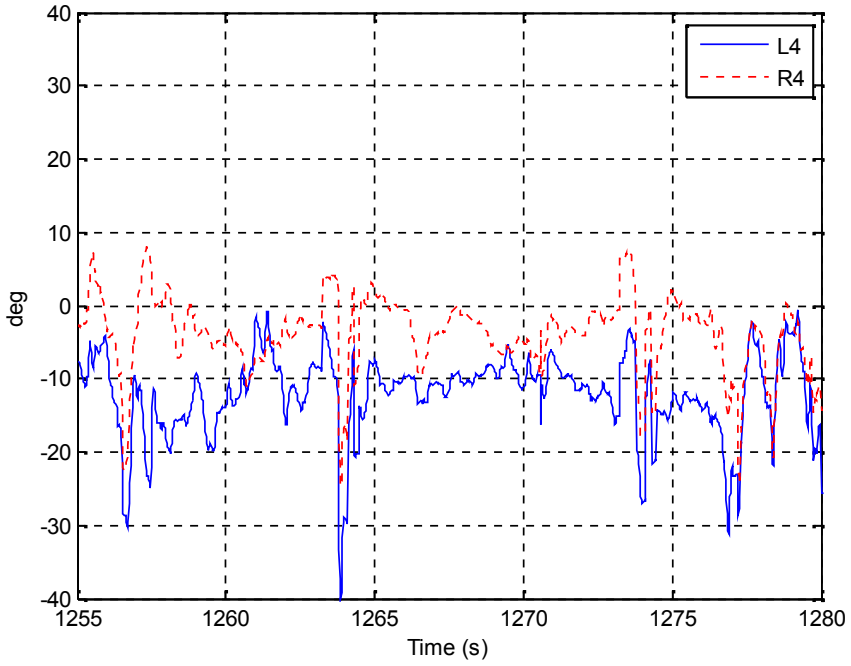

Figure 10: Surface commands to L4 and R4.

2.0 SYSTEM IDENTIFICATION USING FFT-BASED METHODS

2.1 Signal power spectral densities

The PSDs using the entire data segment for longitudinal responses of pitch orientation and pitch rate are shown in Figure 11 and Figure 12 below. For these data, FREDA settings used a bin ratio of 1.07 and a bin size of 3.

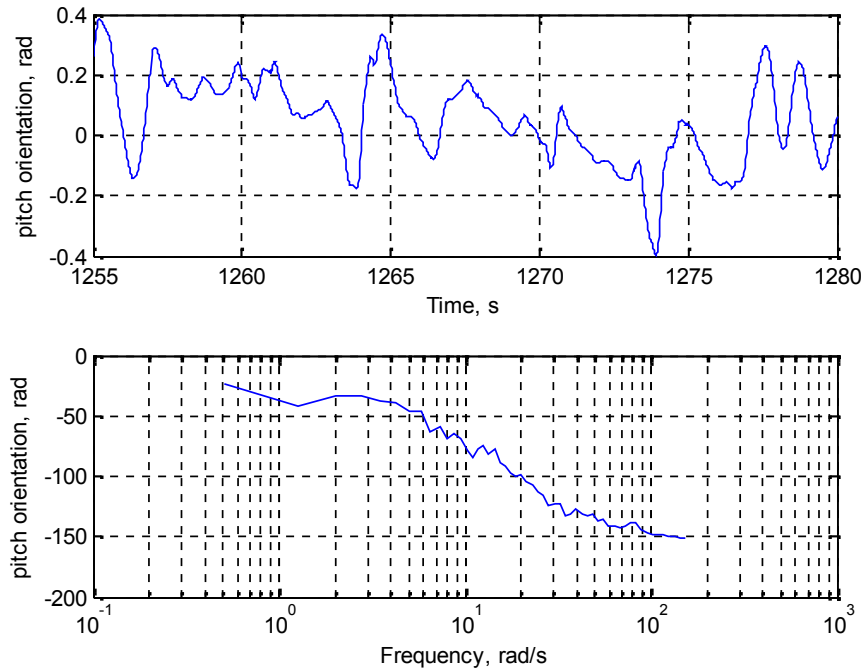

Figure 11: Pitch orientation response.

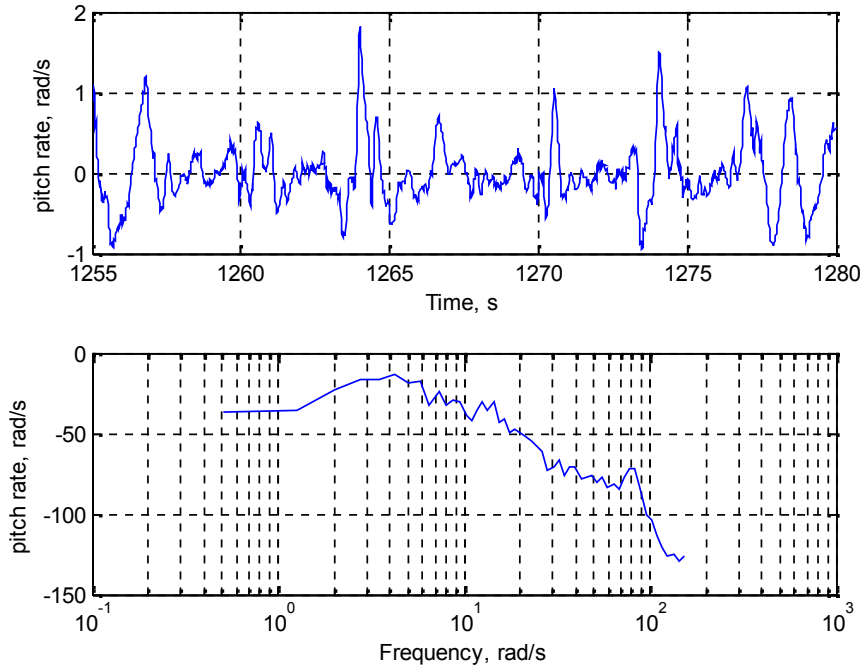

Figure 12: Pitch rate response.

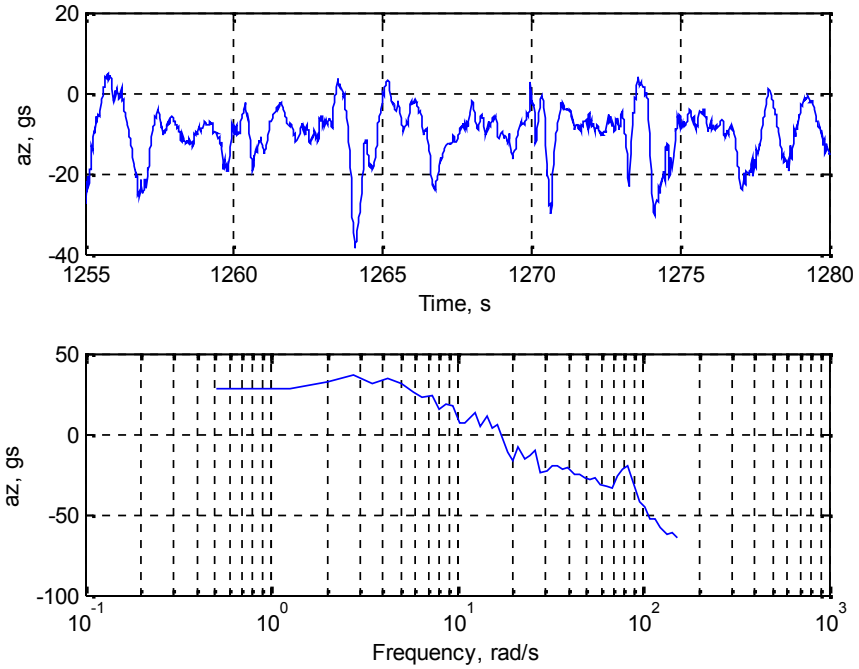

Figure 13: Vertical acceleration response.

The PSDs for the left surface commands are shown in Figure 14 through Figure 17 below. This test consisted of mainly pitch excitation with minimal roll inputs. It is the goal to use only the left surface inputs for identification (excluding surfaces L2 and R2 since these are used exclusively for roll).

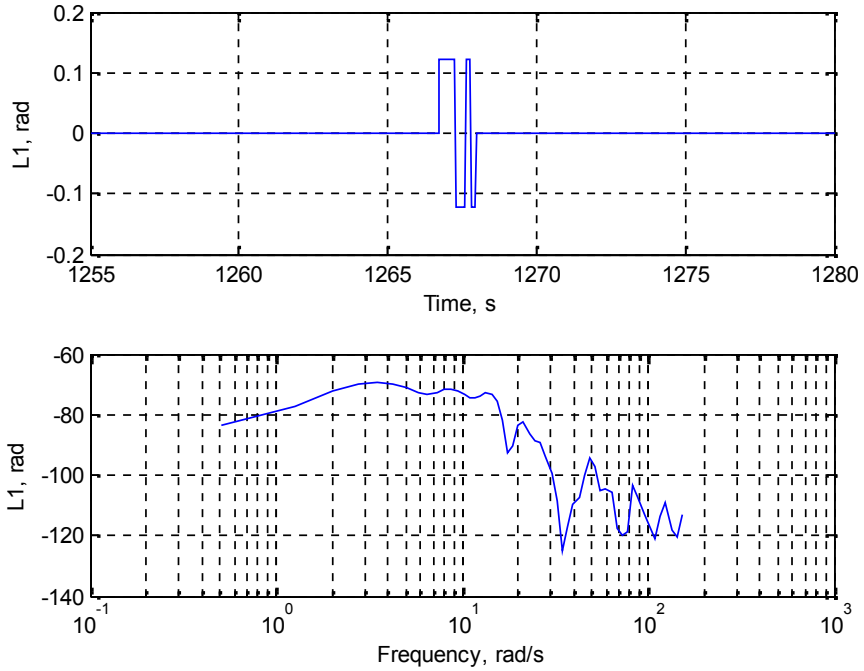

Figure 14: L1 command.

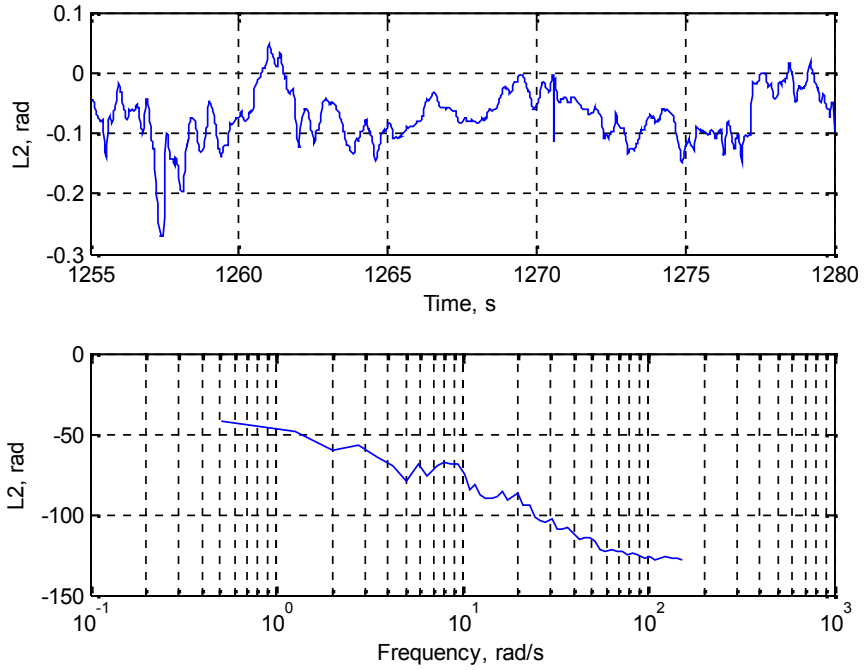

Figure 15: L2 command.

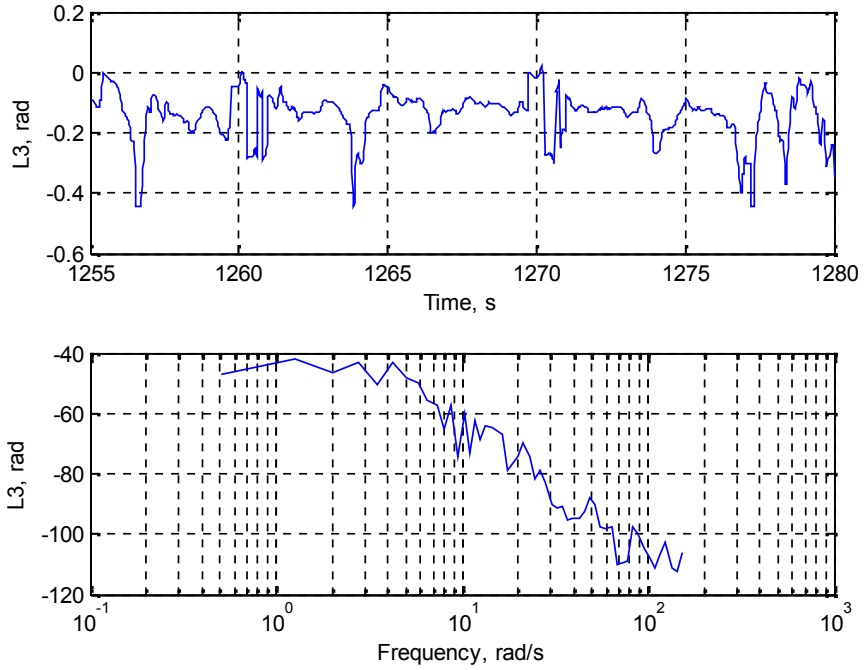

Figure 16: L3 command.

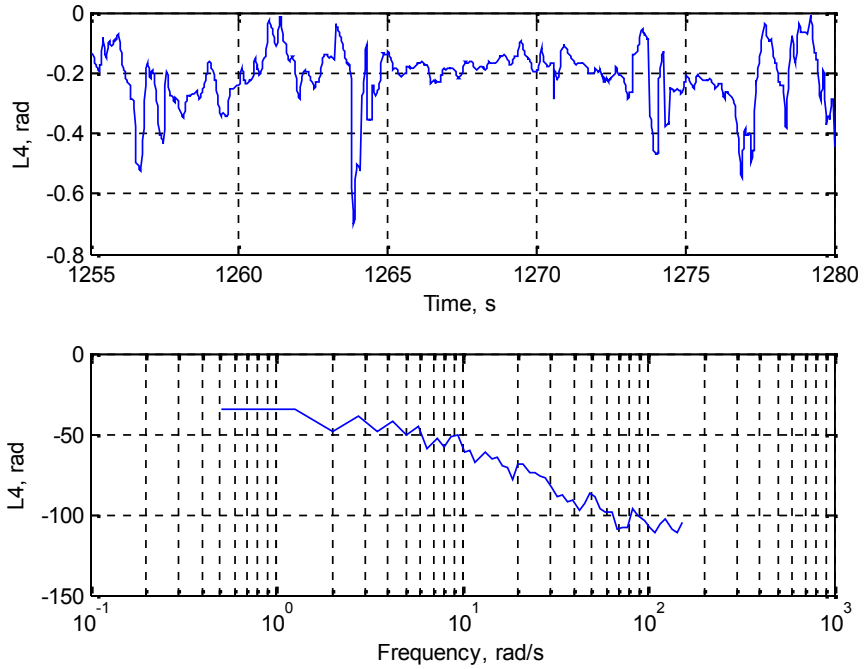

Figure 17: L4 command.

Note the expected similarity of Figure 14 to Figure 2 since the L1 command involves only the 3-2-1-1 excitation.

2.2 SISO FREDA Identification

2.2.1 L1/R1 excitation

A single-input-single-output (SISO) identification was attempted using the L1/R1 and input and the vertical acceleration as output. This I/O pair was chosen because a shorter data segment was found where L1/R1 provided excitation when other surfaces remained relatively constant (t = 1265 to 1269 seconds). Also, it is known that L1/R1 collective deflection does not impart a significant pitch moment, therefore the pitch rate due to this input may not show significant amplitude. The vertical acceleration should display a more significant response. Figure 18 through Figure 23 below displays the time domain data.

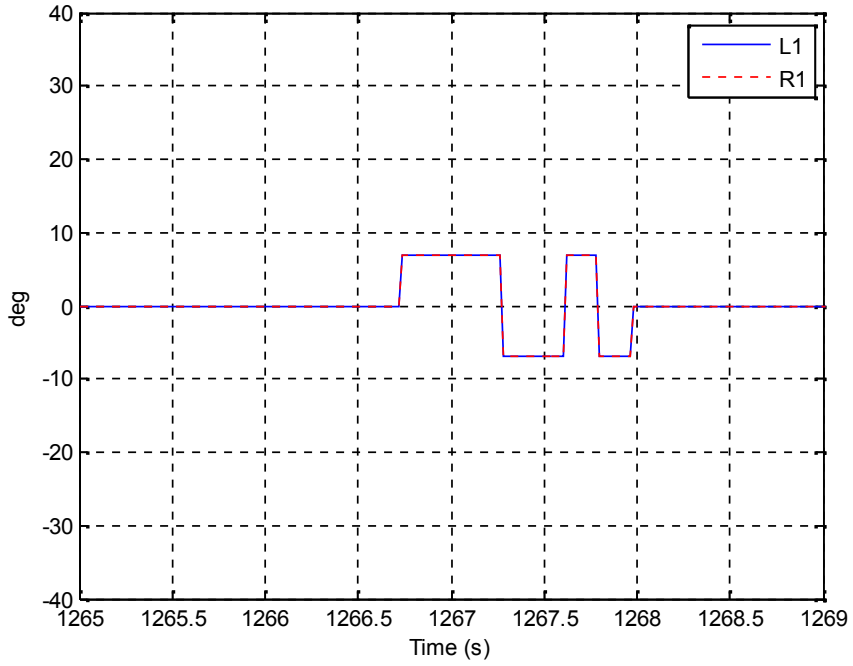

Figure 18: L1/R1 command.

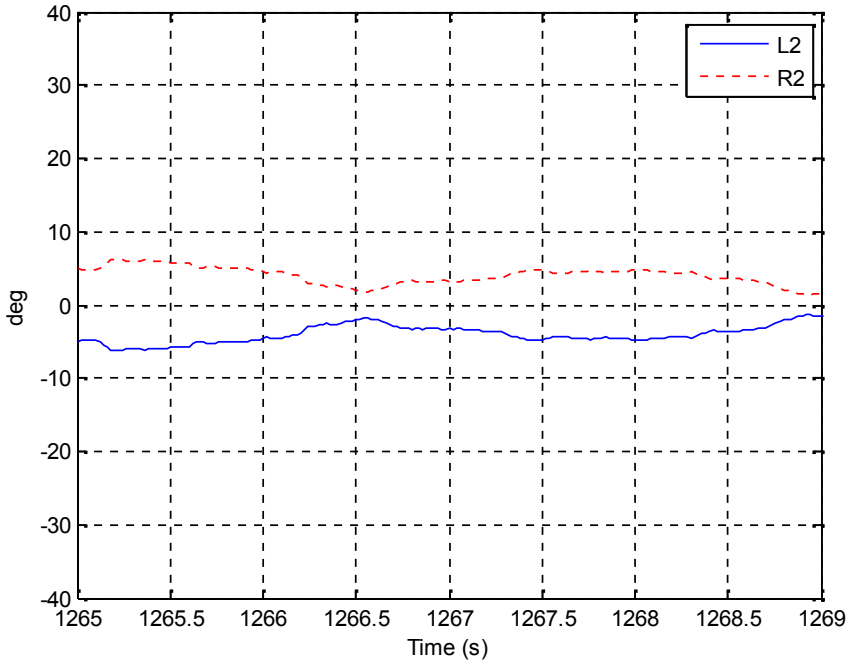

Figure 19: L2/R2 command.

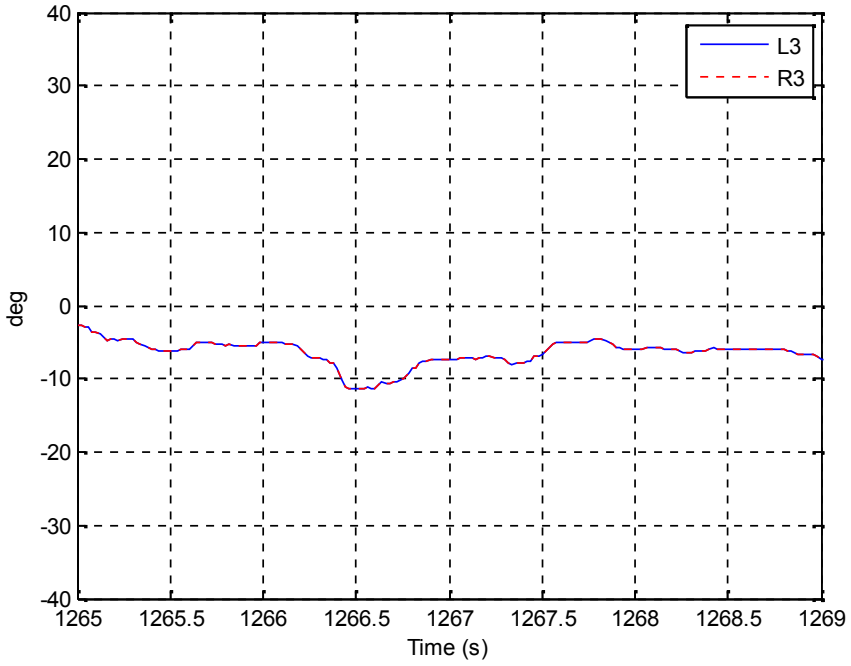

Figure 20: L3/R3 command.

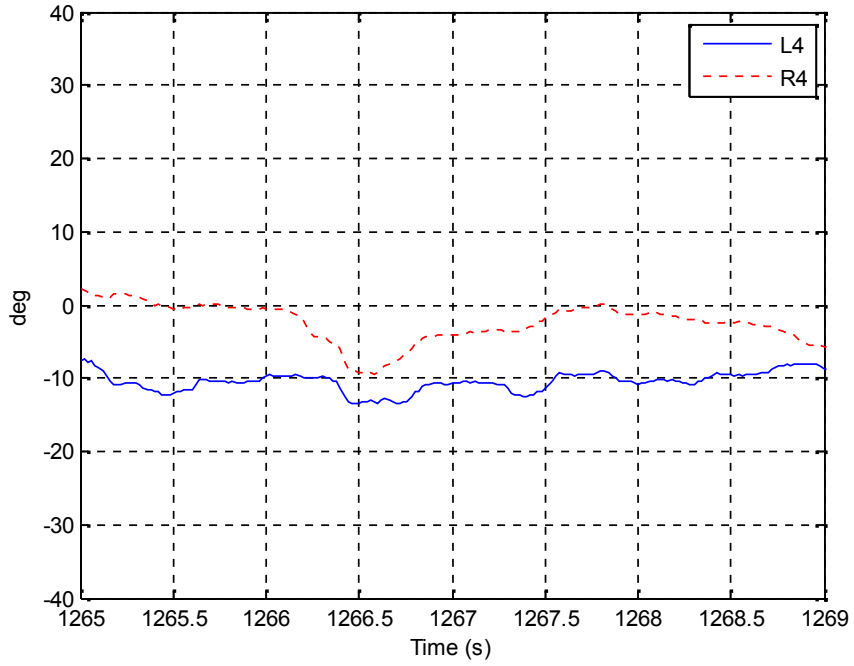

Figure 21: L4/R4 command.

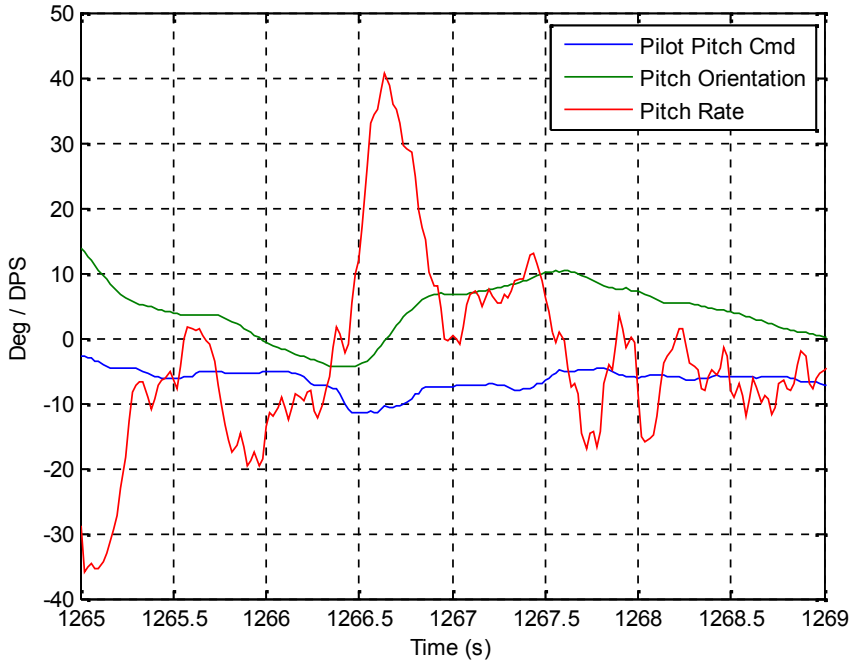

Figure 22: Pilot pitch command, pitch orientation, and pitch rate response.

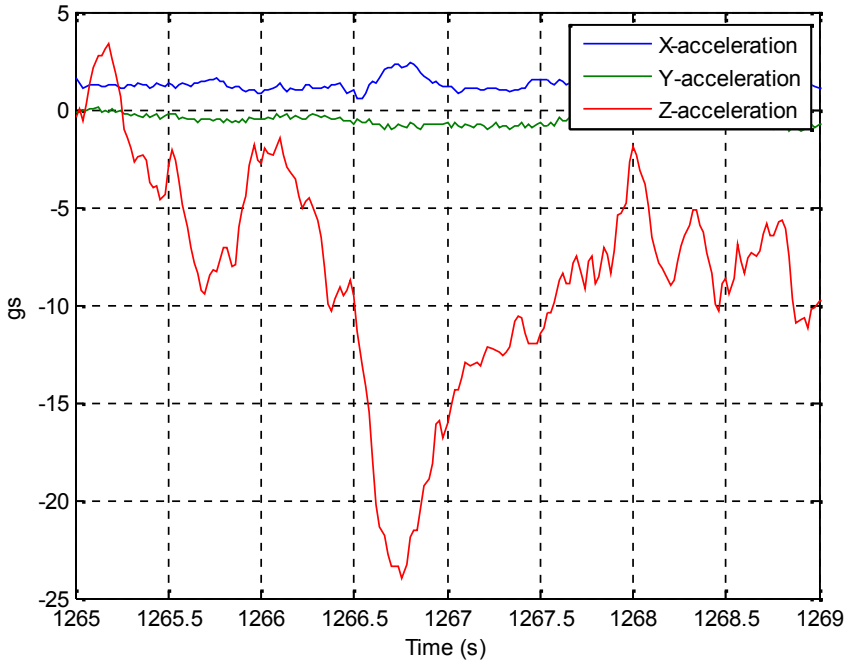

Figure 23: IMU acceleration response.

FREDA identification using L1 as input and az as output is shown in Figure 24 through Figure 26 below [FREDA settings: bin ratio = 1.07, bin size = 3, psdTaper = 0.05, zeroFill = 50 seconds).

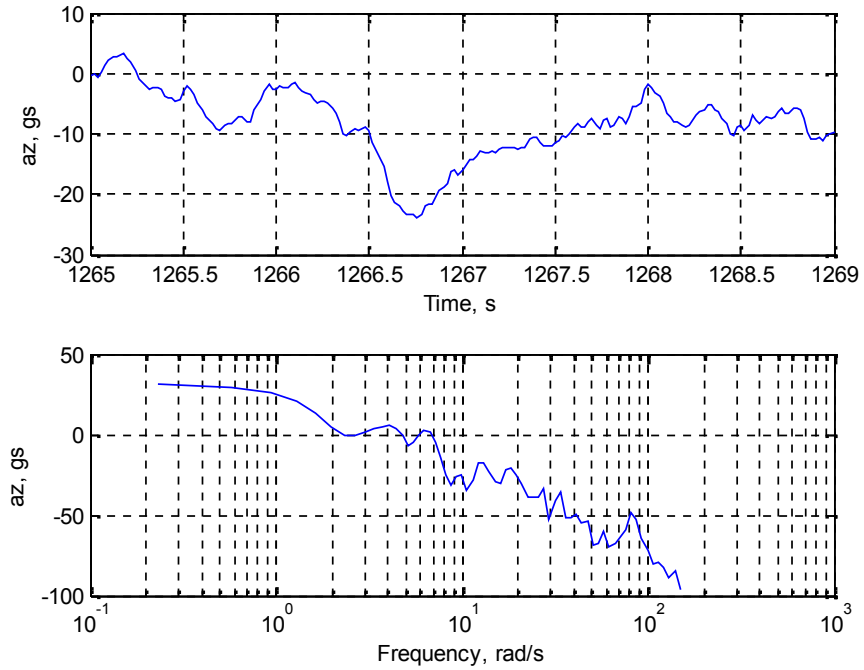

Figure 24: Output (az) PSD.

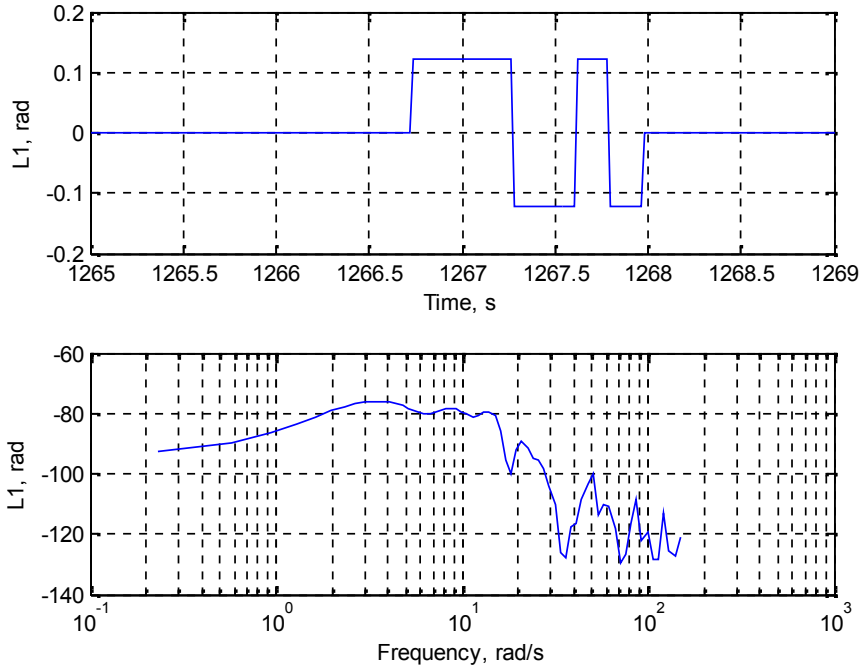

Figure 25: Input (L1) PSD.

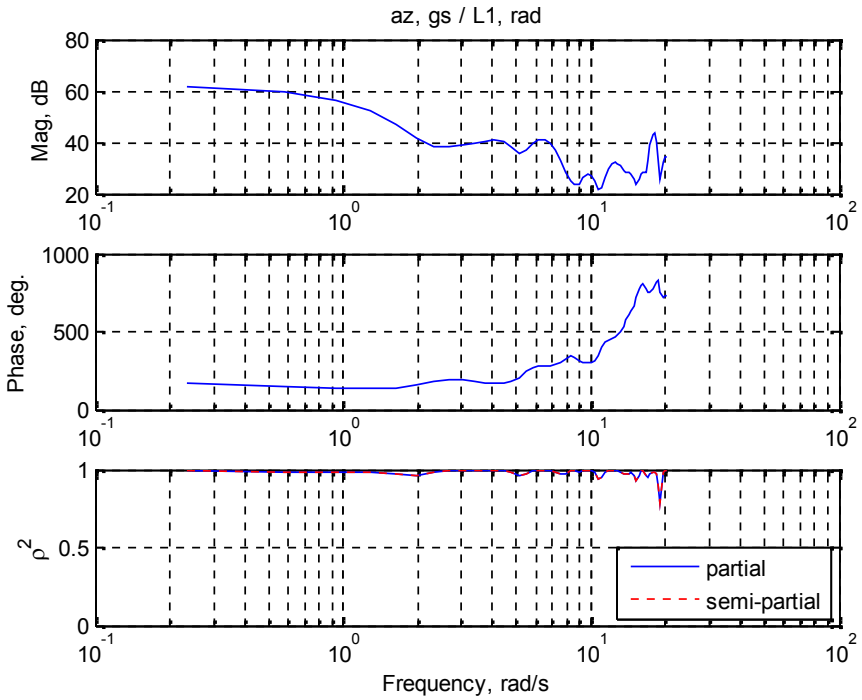

Figure 26: Identified frequency response (az/L1).

In the identified frequency response, there is a notable peak near ~6 - 6.5 rad/s. A SISO ID using the same settings was also performed using the pitch rate as output (Figure 27 and Figure 28). The same FREDA settings were used.

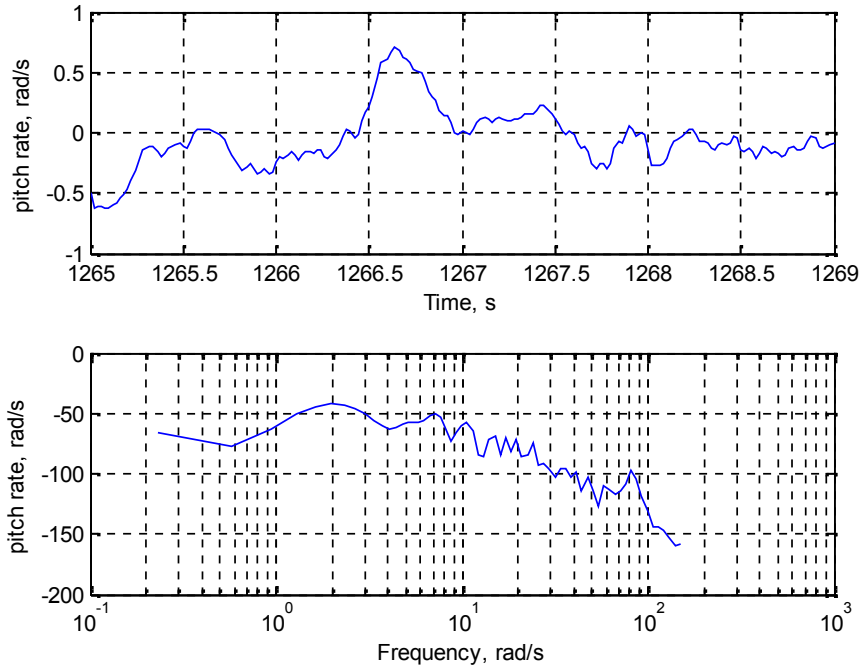

Figure 27: Output (q) PSD.

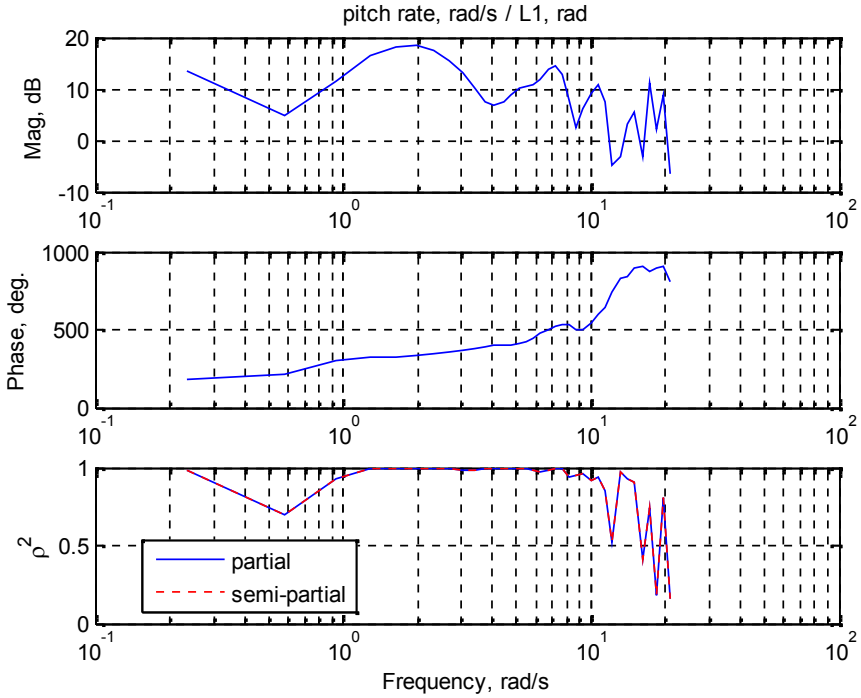

Figure 28: Identified frequency response (q/L1).

Again, a peak is noted near ~7 rad/s. The increase in Phase suggests lead, which is odd. It is noted that zero padding and windowing of data can influence the phase in this way and this may be investigated further.

2.2.2 L3/R3 excitation

The data segment from 1268.5 to 1272.5 was used for SISO ID. There are two 3-2-1-1 excitation commands to L3/R3 and this one represented a case where the other surfaces had minimal excitation. The time domain data is shown in Figure 29 through Figure 34.

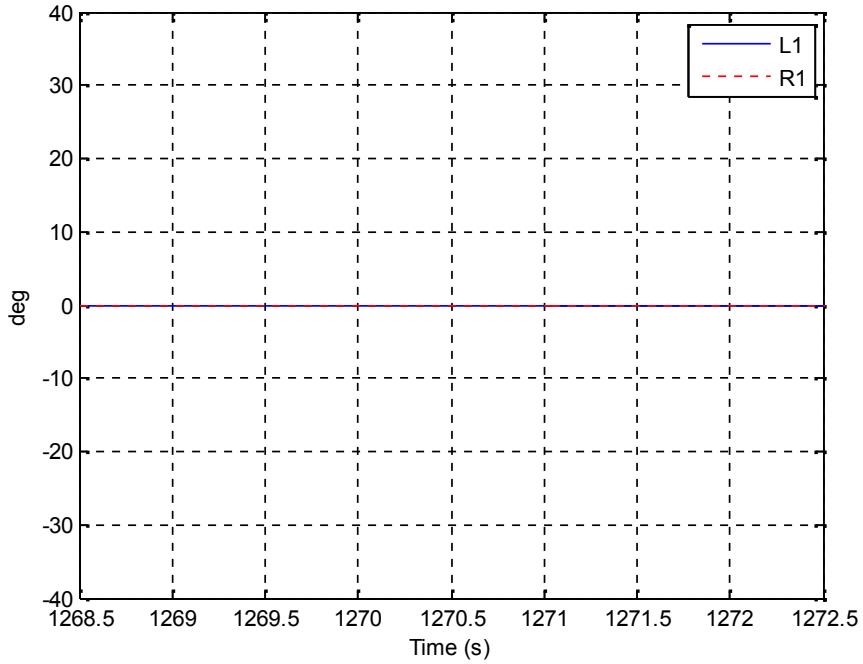

Figure 29: L1/R1 command.

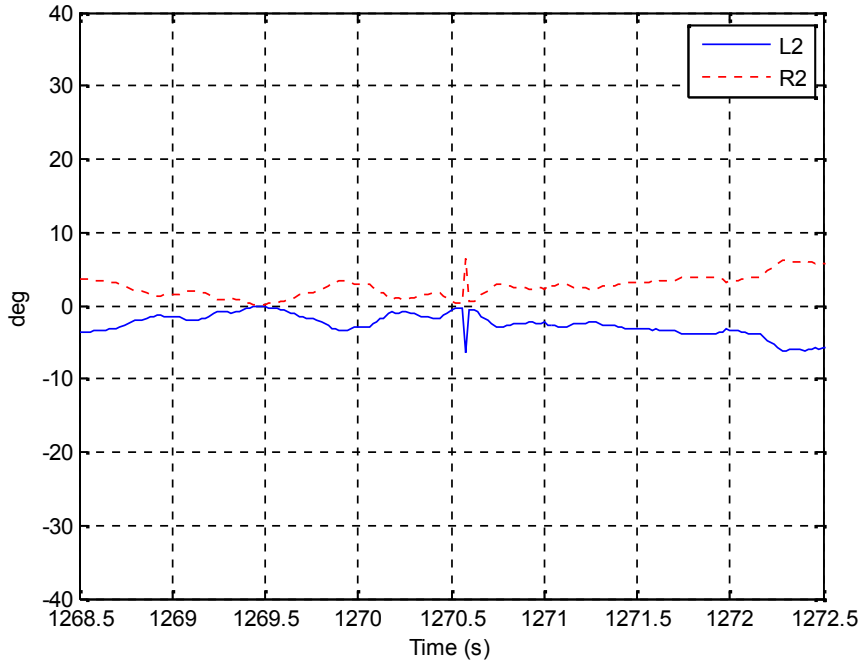

Figure 30: L2/R2 command.

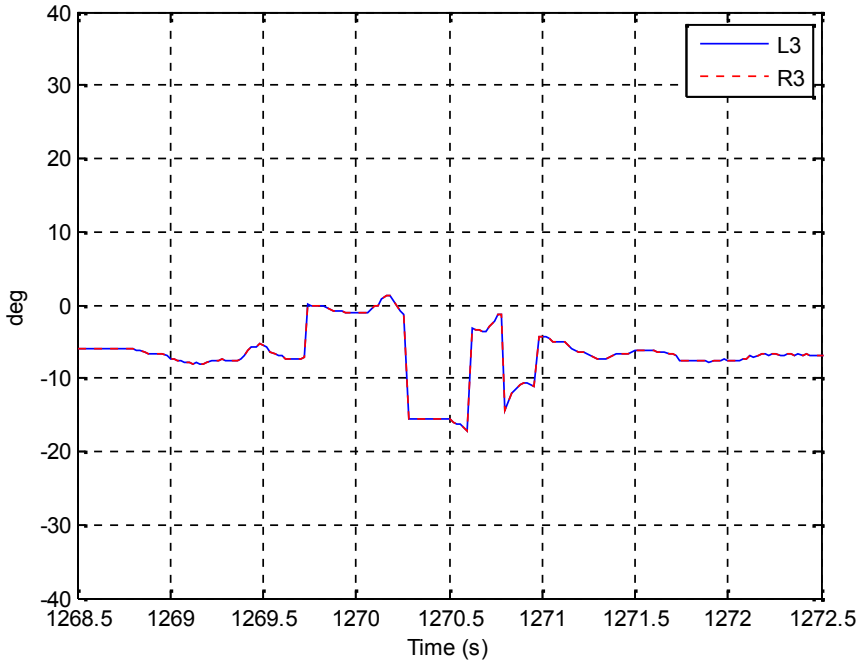

Figure 31: L3/R3 command.

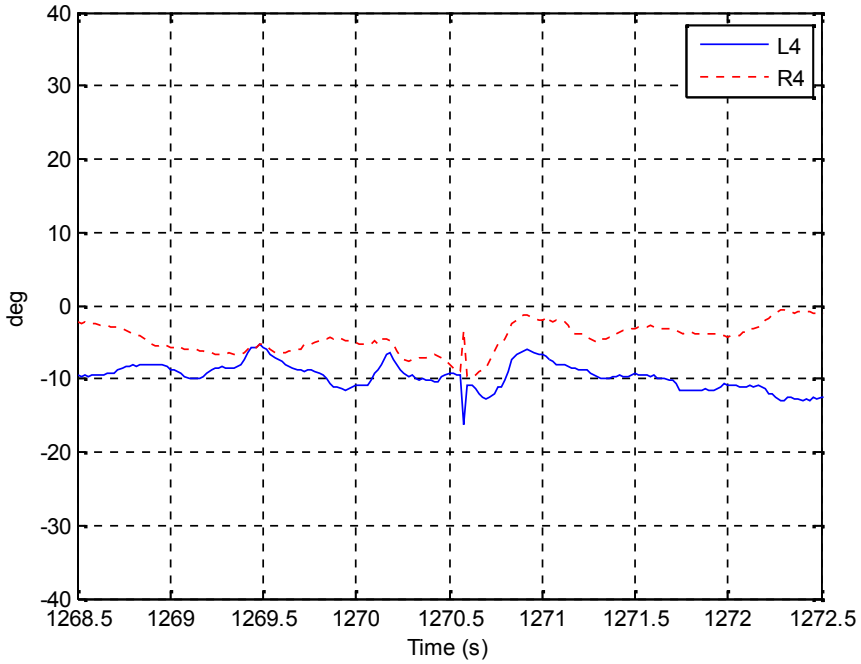

Figure 32: L4/R4 command.

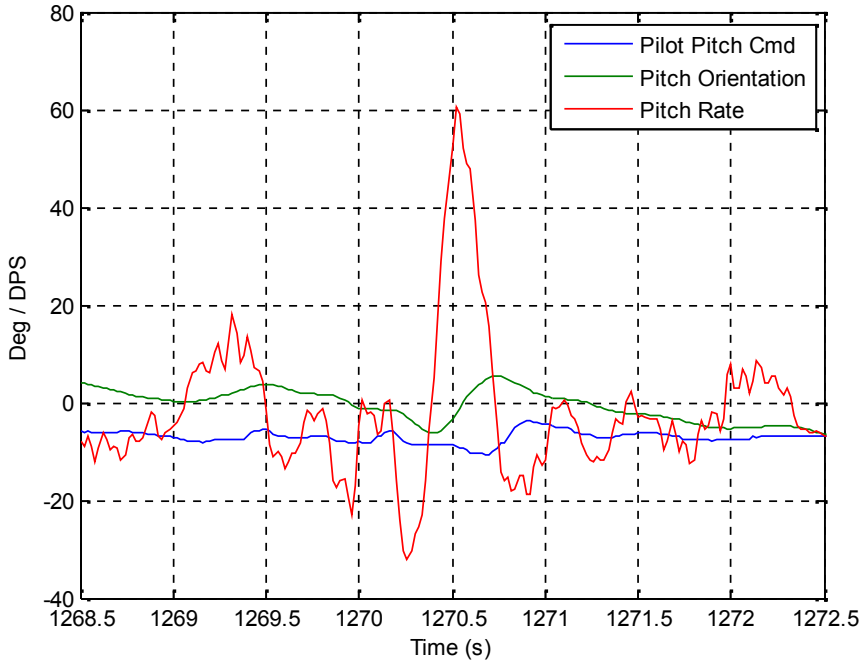

Figure 33: Pilot pitch command, pitch orientation, and pitch rate response.

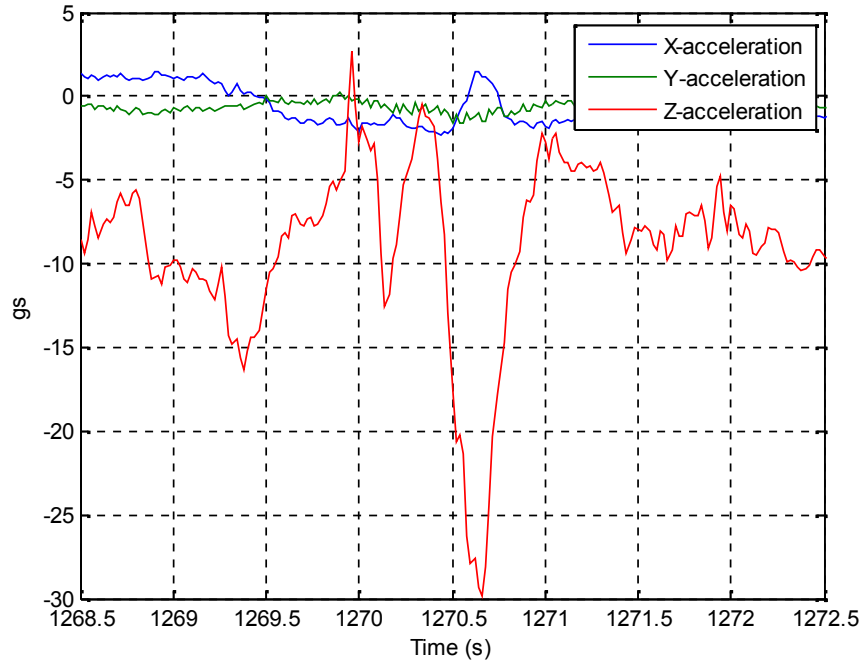

Figure 34: IMU acceleration response.

Identification was performed using L3 as input with az and q as output [FREDA settings: bin ratio = 1.07, bin size = 3, psdTaper = 0.05, zeroFill = 50 seconds).

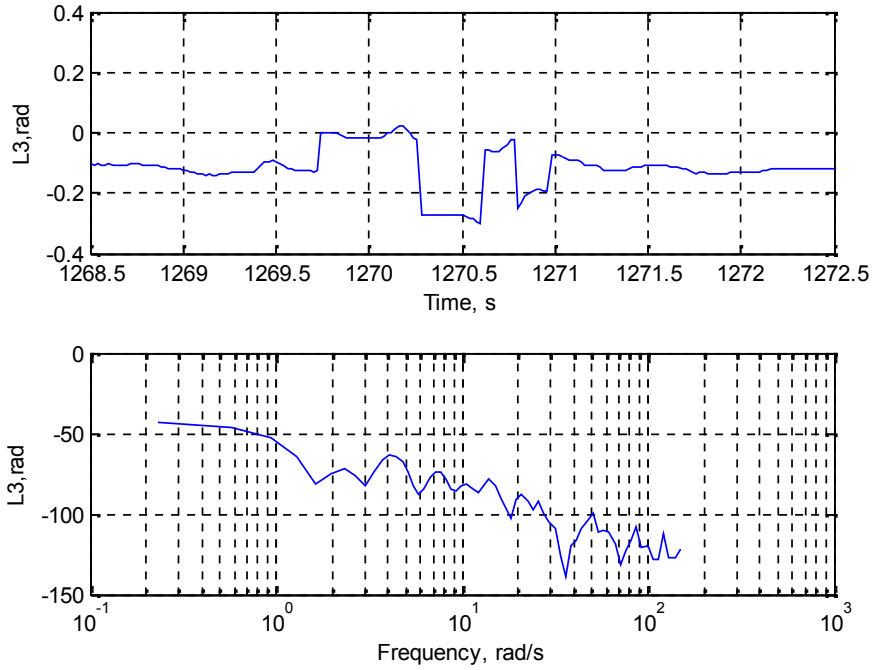

Figure 35: Input (L3) PSD.

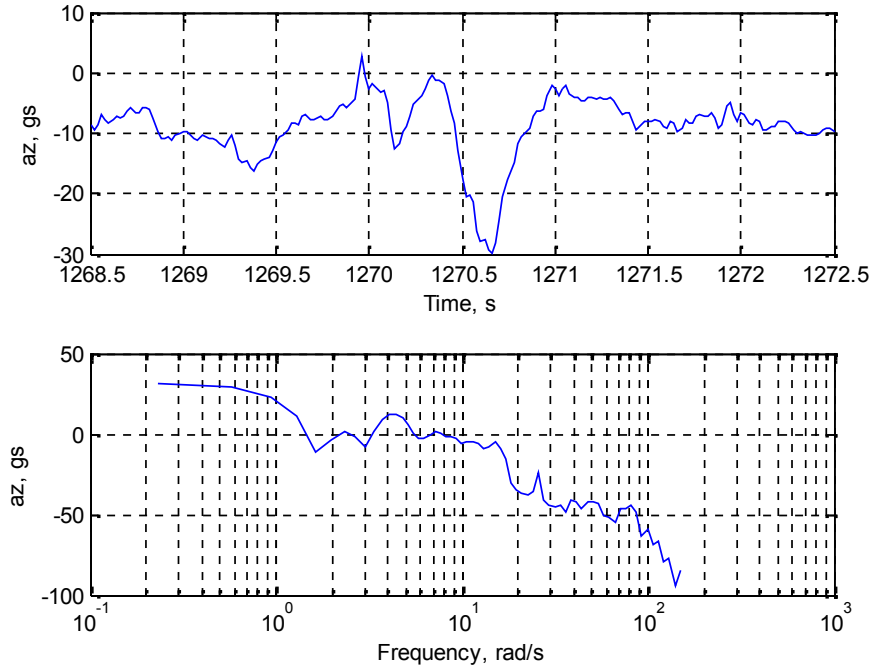

Figure 36: Output (az) PSD.

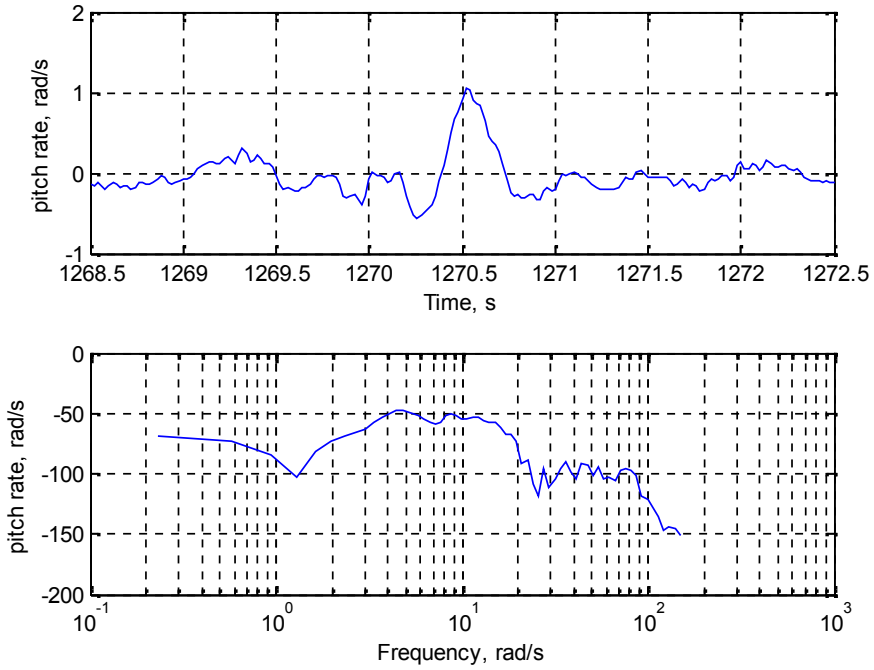

Figure 37: Output (q) PSD.

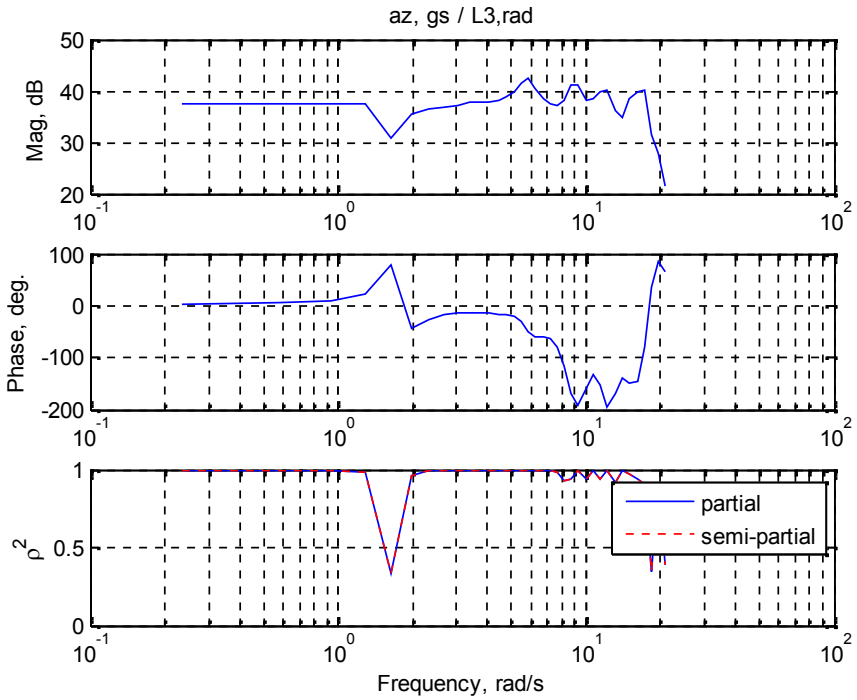

Figure 38: Identified frequency response (az/L3).

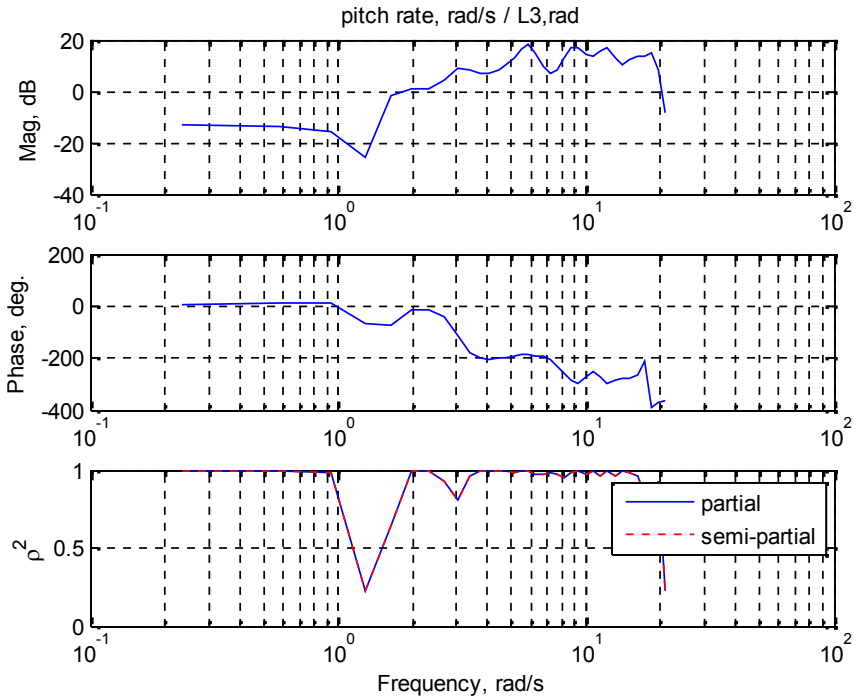

Figure 39: Identified frequency response (q/L3).

In both of these frequency responses, a peak is visible near ~5.5 rad/s. As compared to the L1 input cases above, the phase is also much more favorable.

2.3 MISO FREDA Identification

Identification was attempted using all 4 inputs (L1, L2, L3, L4) simultaneously. For this, the entire data segment shown in Section 1.2 was used. The identification of both systems with az and q output was performed. [FREDA settings: bin ratio = 1.07, bin size = 3, psdTaper = 0.05, zeroFill = 30 seconds].

NOTE: Following further analysis, as indicated later in this report, it was noted that signals L1, L2, L3, and L4 are correlated due to pilot input acting on multiple surface pairs. Analysis with an uncorrelated input set is shown in Appendix A.1. More FREDA results that utilized different data segments are documented in Appendices A.2, A.3, and A.4.

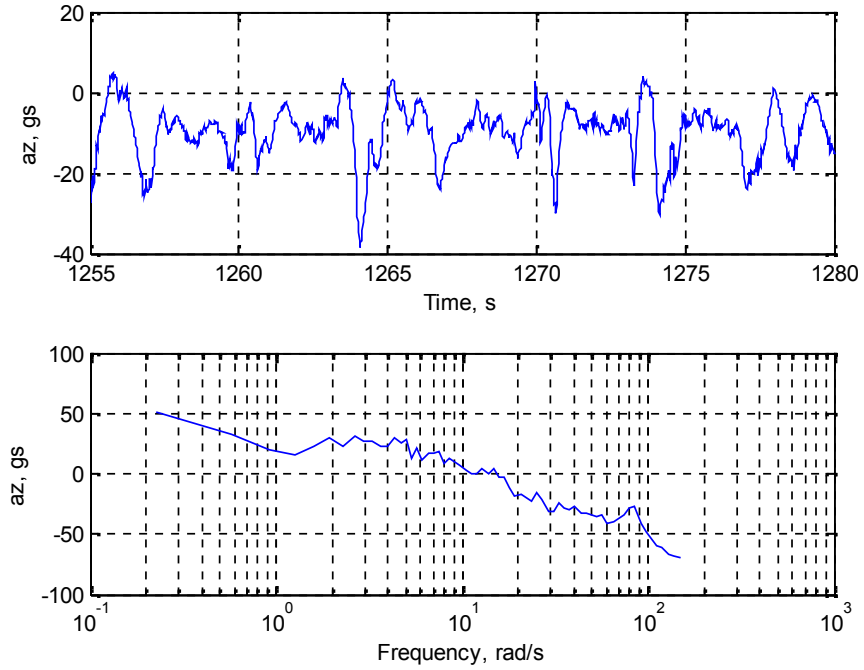

Figure 40: Output (az, gs) time history and resulting PSD.

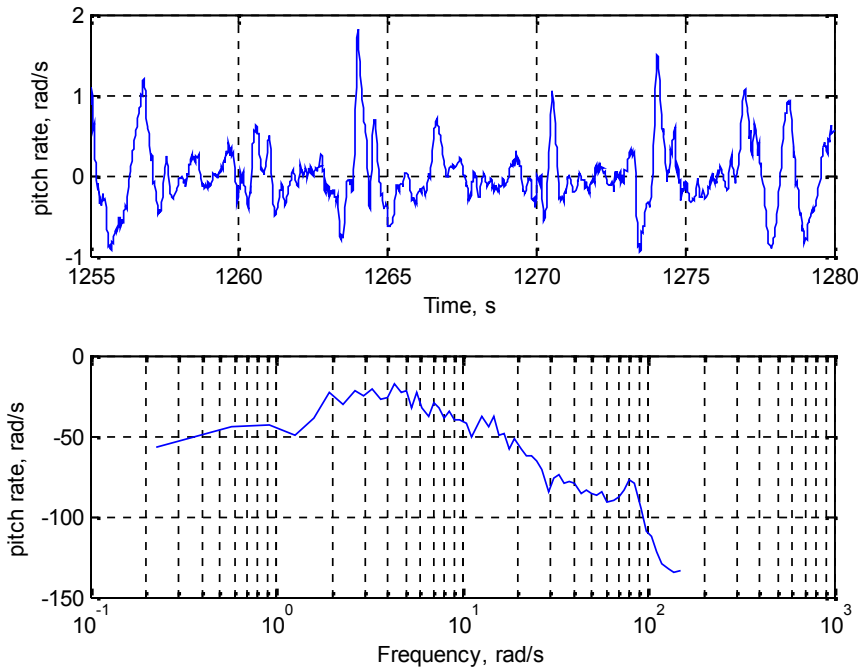

Figure 41: Output (pitch rate, rad/s) time history and resulting PSD.

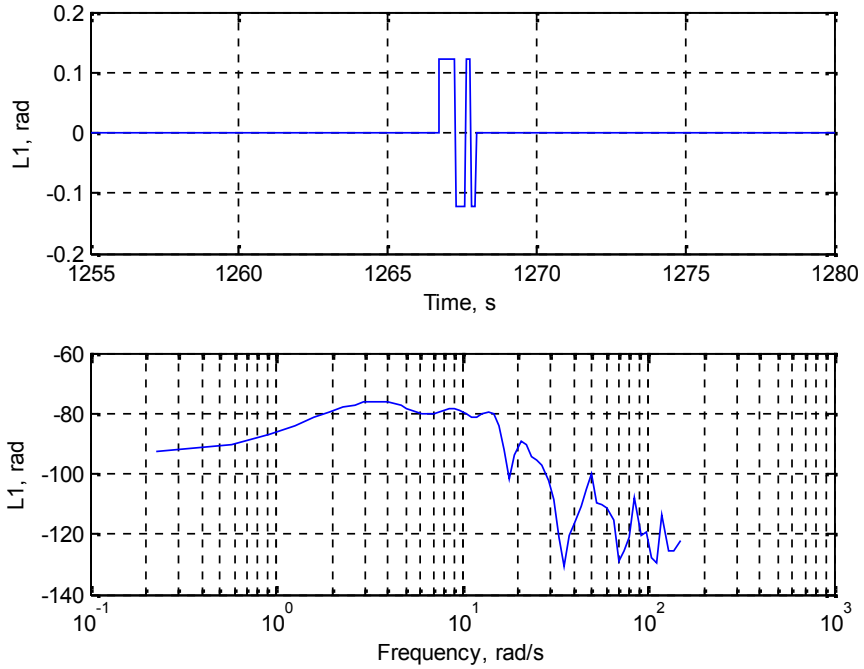

Figure 42: Input (L1, rad) time history and resulting PSD.

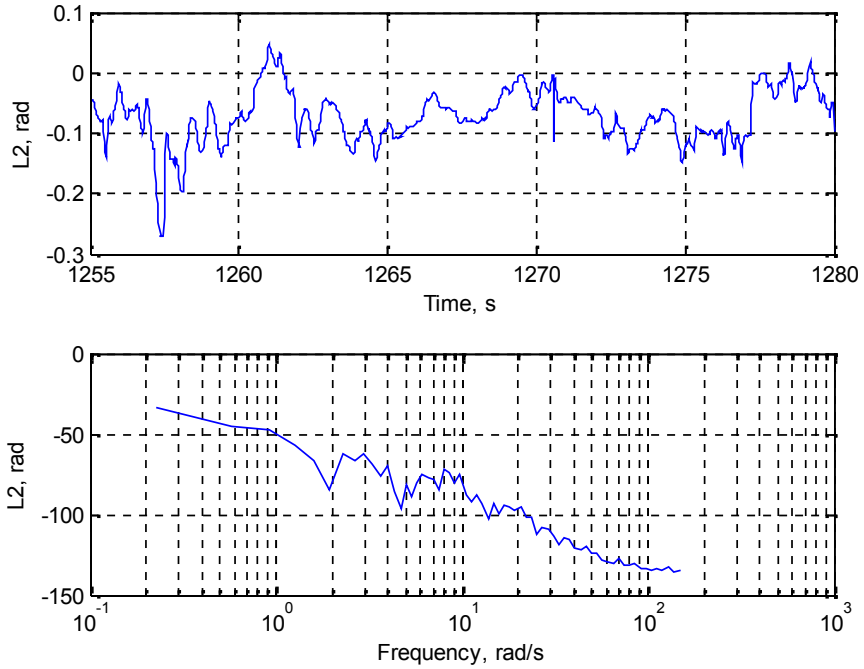

Figure 43: Input (L2, rad) time history and resulting PSD.

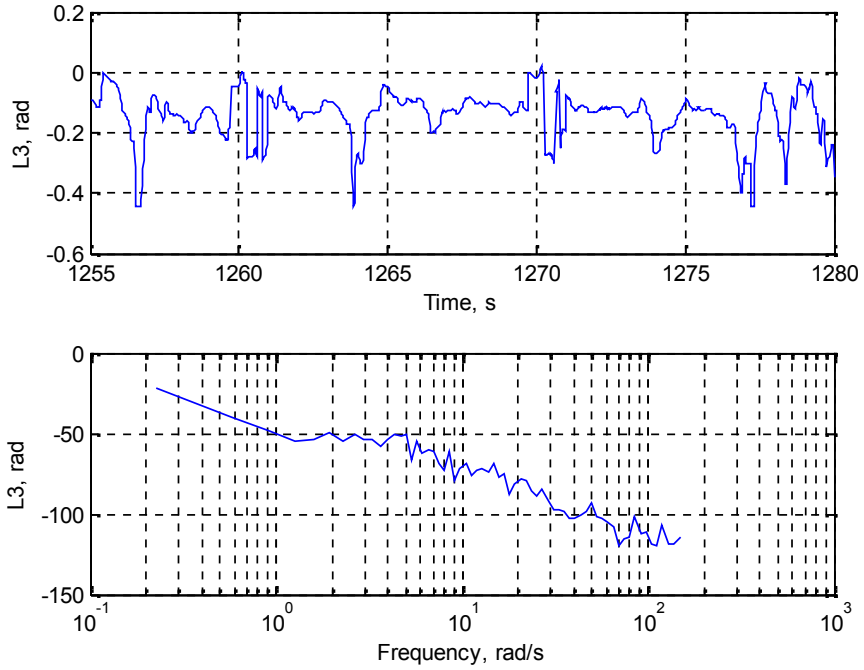

Figure 44: Input (L3, rad) time history and resulting PSD.

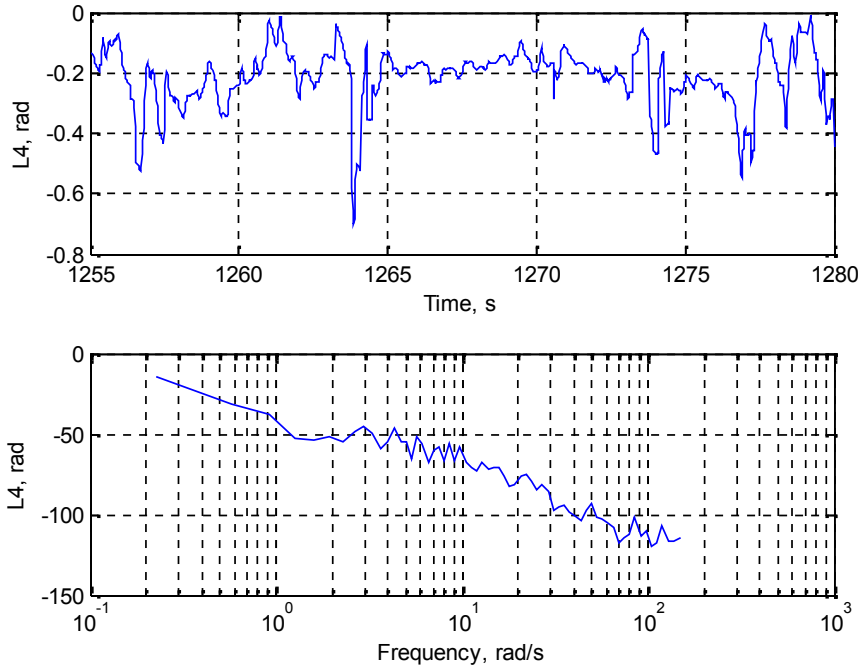

Figure 45: Input (L4, rad) time history and resulting PSD.

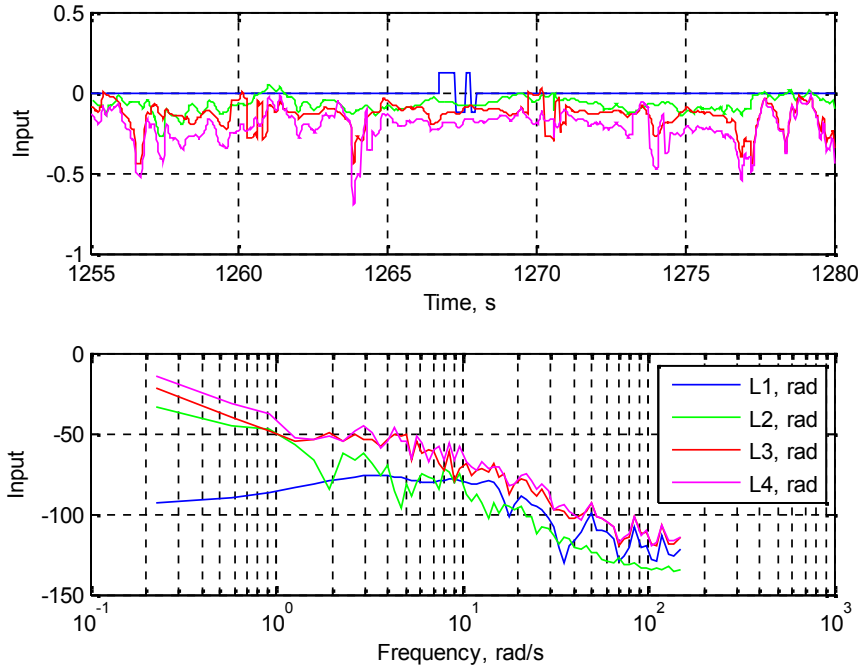

Figure 46: All inputs time histories and resulting PSDs.

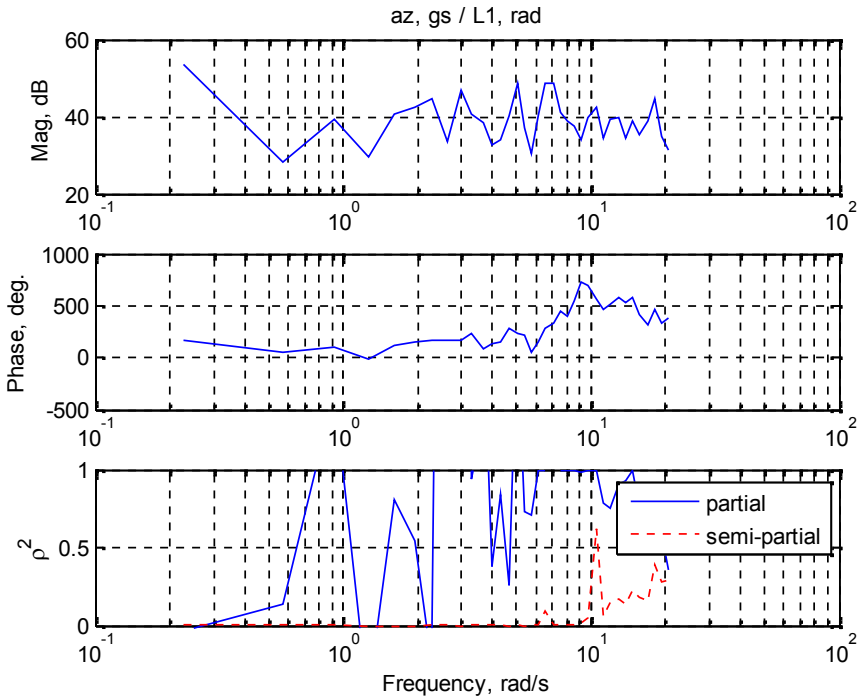

Figure 47: Identified frequency response: az, gs / L1, rad

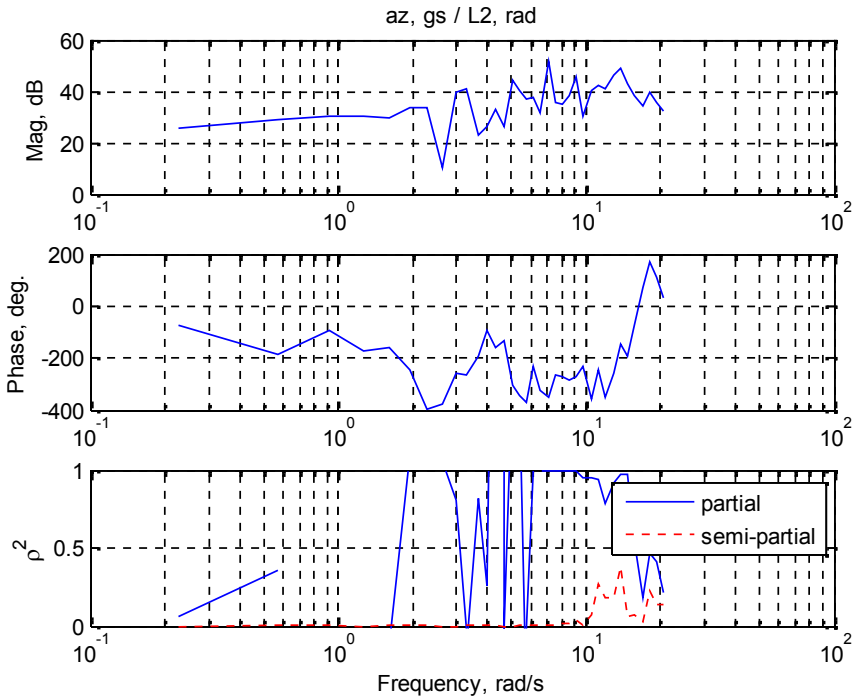

Figure 48: Identified frequency response: az, gs / L2, rad

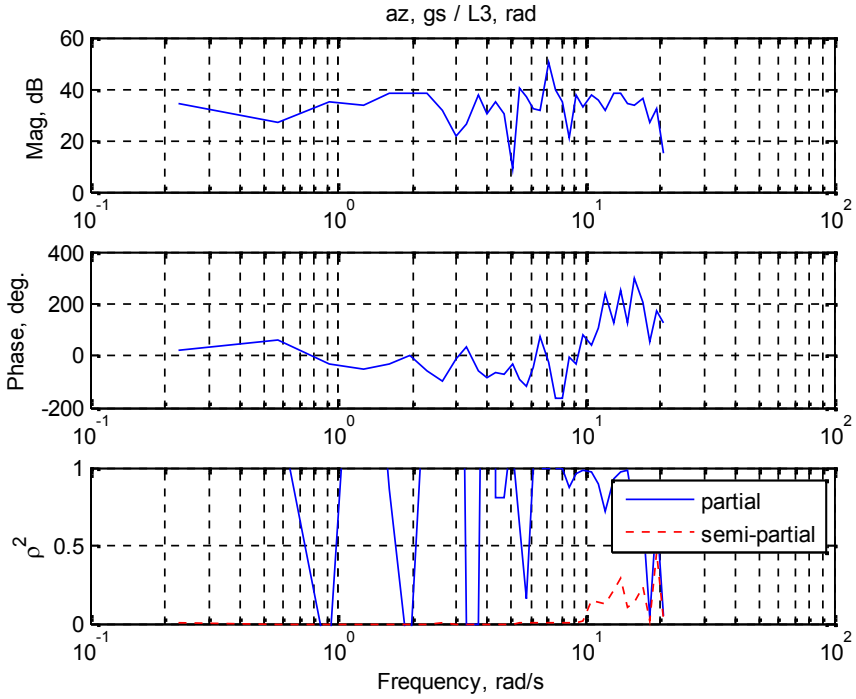

Figure 49: Identified frequency response: az, gs / L3, rad

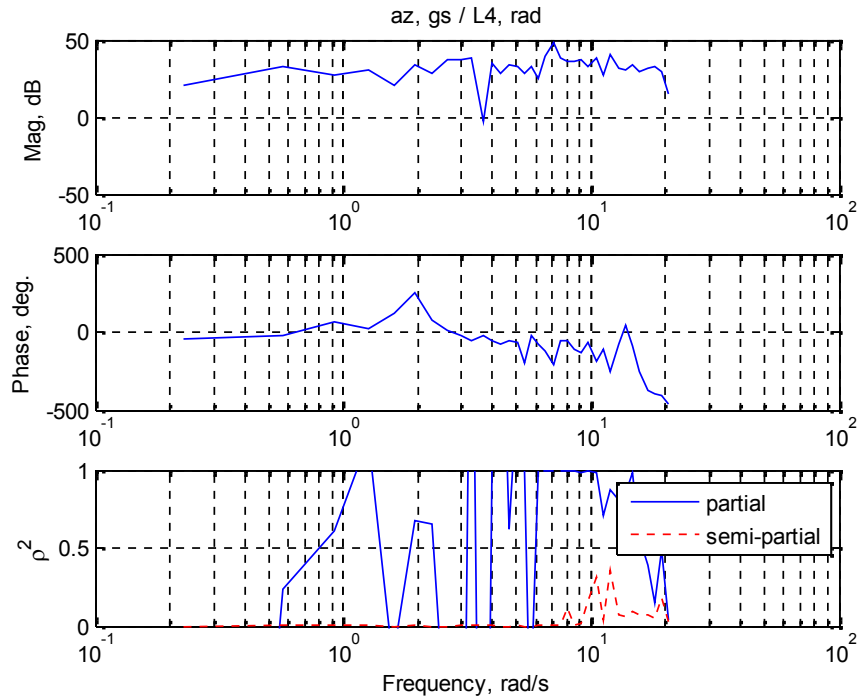

Figure 50: Identified frequency response: az, gs / L4, rad

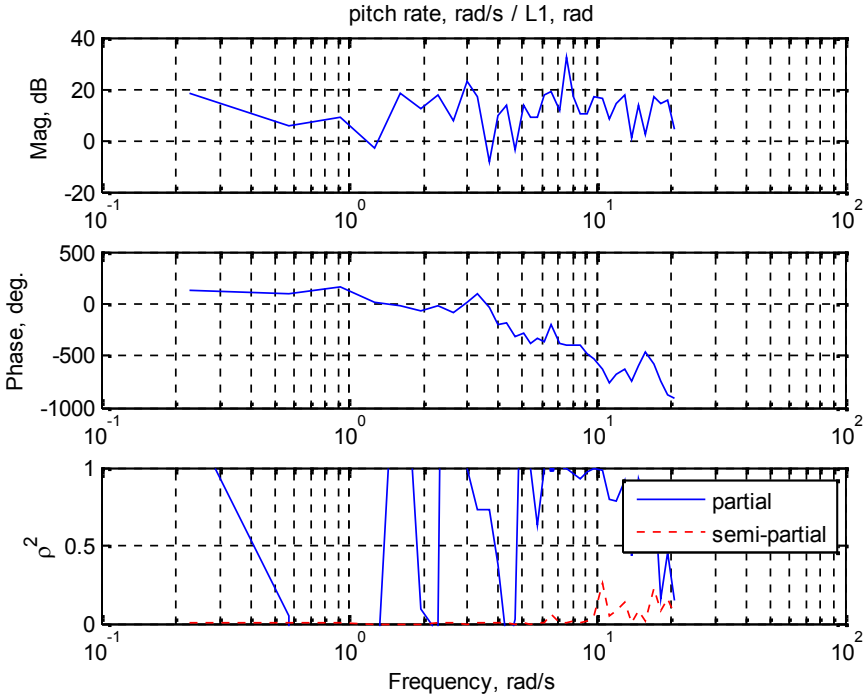

Figure 51: Identified frequency response: pitch rate, rad/s / L1, rad

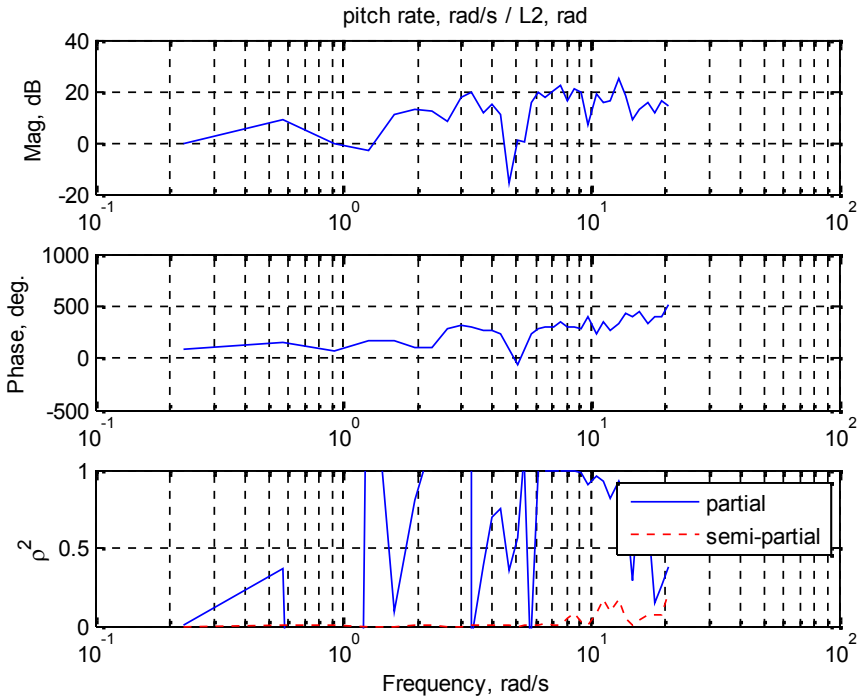

Figure 52: Identified frequency response: pitch rate, rad/s / L2, rad

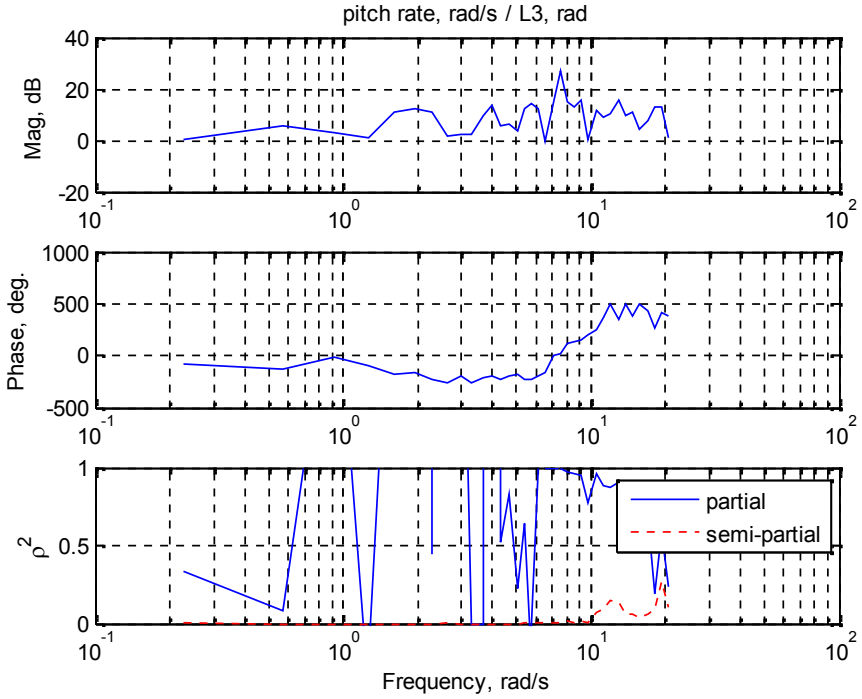

Figure 53: Identified frequency response: pitch rate, rad/s / L3, rad

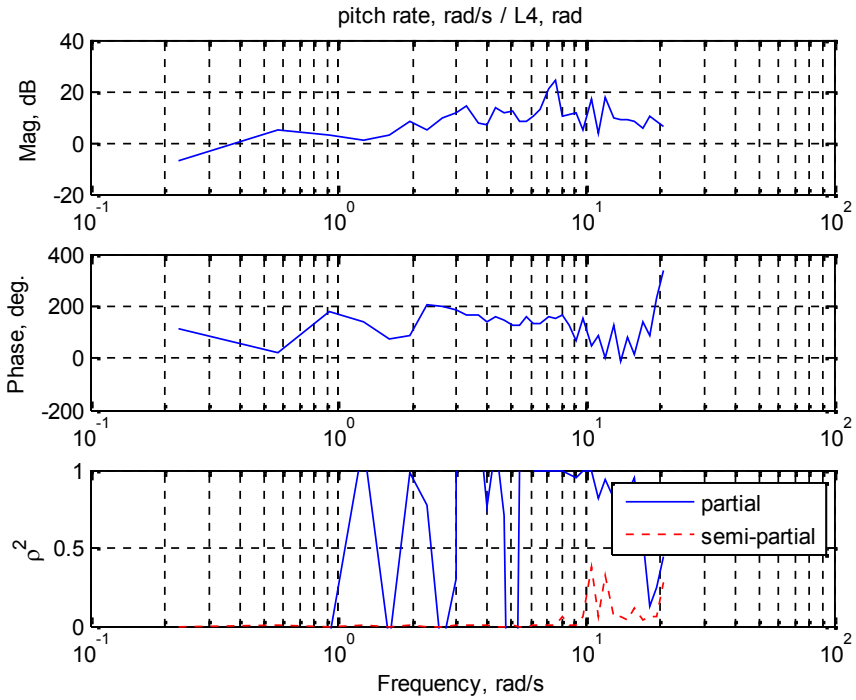

Figure 54: Identified frequency response: pitch rate, rad/s / L4, rad.

In most of these identified responses, there is a noted peak near ~7 rad/s.

2.4 MISO parameter identification for short period mode

SIDPAC[2] was used to identify a parametric model. The frequency domain equation error method was used (via the *fdoe.m* function). A parametric model was defined as a generic MISO transfer function with a common denominator (Eq. (1)). The transfer function numerator and denominator polynomial coefficients are optimized. The individual inputs also have variable time delay, which can also be defined as a free parameter. If desired, a single consistent time delay can be used which is applied to all inputs. The denominator and numerator orders can be user defined prior to optimization.

$$G(s) = \frac{1}{\Delta(s)}\begin{bmatrix} n_1(s)e^{-T_1 s} & n_2(s)e^{-T_2 s} & \cdots & n_{n_u}(s)e^{-T_{n_u} s} \end{bmatrix}$$

where,

$$\Delta(s) = s^n + a_{n-1}s^{n-1} + \ldots + a_0 \qquad (1)$$

$$n_i(s) = b_{i,m_i}s^{m_i} + b_{i,m_i-1}s^{m_i-1} + \ldots + b_{i,0}$$

The four uncorrelated longitudinal inputs L1 excite, L3 excite, L4 excite, and pilot pitch command were used with the measured pitch rate. The denominator was assumed 2nd order and each of the four numerators was assumed 1st order. This is equivalent to a short period approximation from each longitudinal "elevator-like" input (Eq. (2)).[3]

$$\frac{q}{\delta_e} = \frac{(M_\delta + Z_\delta M_{\dot{w}})s + (Z_\delta M_w - M_\delta Z_w)}{s^2 - (U_0 M_{\dot{w}} + Z_w + M_q)s + (M_q Z_w - U_0 M_w)} = K_{q/\delta_e}\frac{\left(s + 1/T_{\theta_2}\right)}{\left(s^2 + 2\zeta_{sp}\omega_{sp}s + \omega_{sp}^2\right)} \qquad (2)$$

The complete time series shown in Section 1.1 was used. Both input and output time domain data were windowed using a cosine-tapered window with a taper fraction of 5%. For the frequency domain equation error method, 50 linearly distributed frequencies from 0.1 to 20 rad/s were used. A single time delay applied to all inputs was used as it is assumed that the time delay for all control surfaces is dominated by the communication delay and this should be a relatively consistent value independent of the control surface being actuated. The initial guess for all parameters was set to zero. Results are shown in Figure 55 through Figure 57 below.

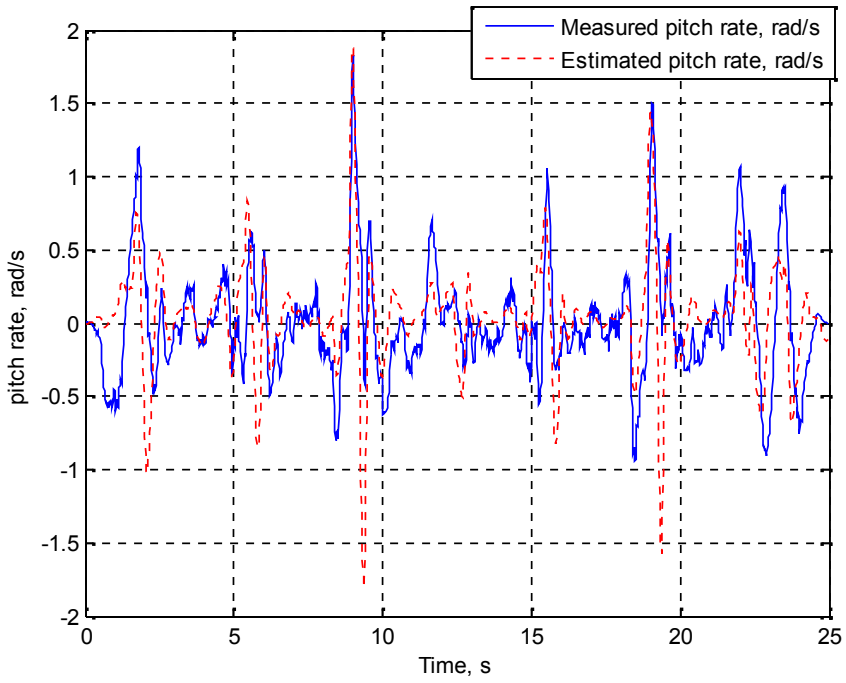

Figure 55: Measured and estimated time domain pitch rate (2nd order system model).

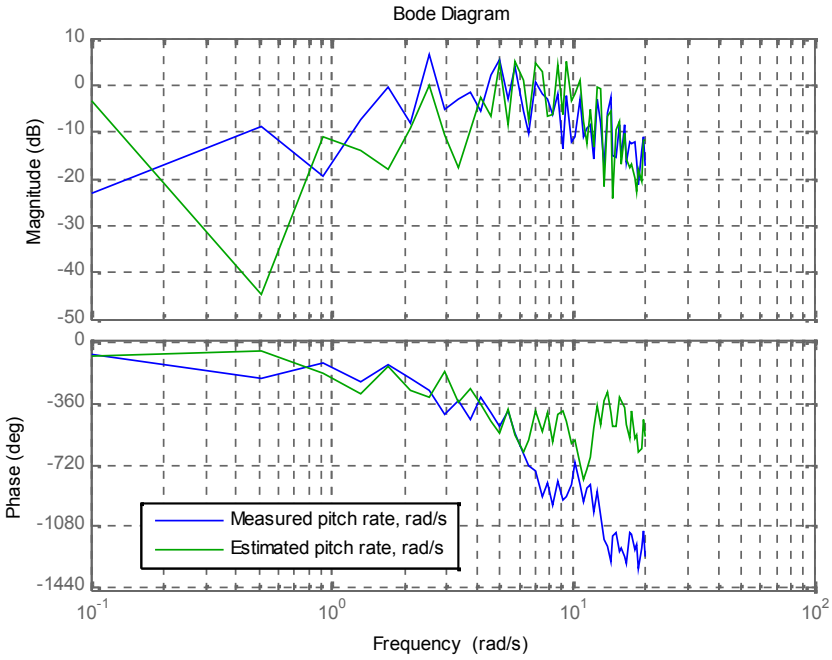

Figure 56: Measured and estimated frequency domain pitch rate (2nd order system model).

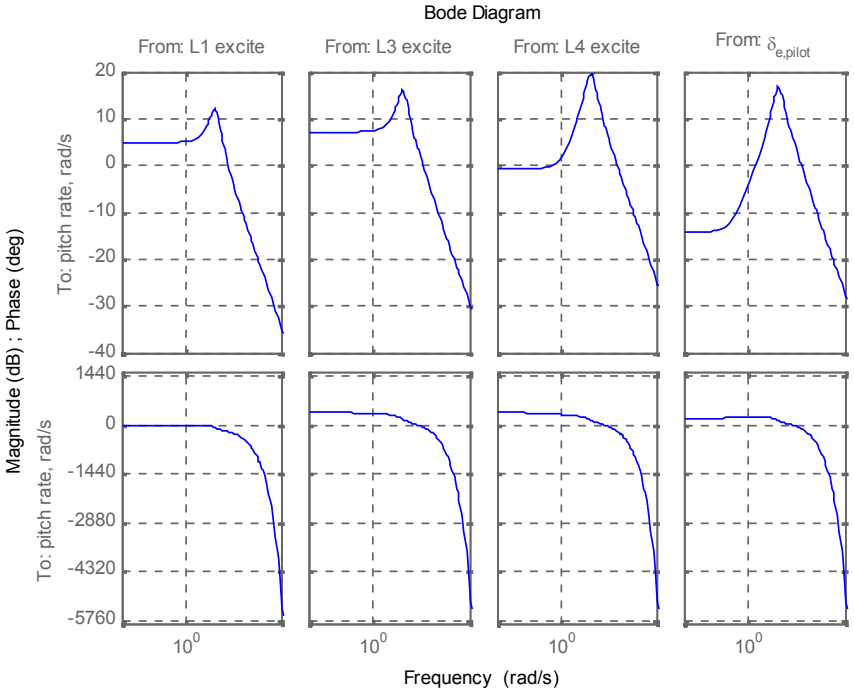

Figure 57: Estimated Transfer Function Bode Plots – pitch rate output (2nd order system model).

The estimated transfer functions are shown below.

$$\frac{q}{¢_{L1,excite}} = \frac{18.61(7.108)}{[0.3507,8.651]} e^{(-0.0845s)} \qquad \frac{q}{¢_{L3,excite}} = \frac{-33.27(-5.129)}{[0.3507,8.651]} e^{(-0.0845s)}$$

$$\frac{q}{¢_{L4,excite}} = \frac{-58.51(-1.173)}{[0.3507,8.651]} e^{(-0.0845s)} \qquad \frac{q}{¢_{e,pilot}} = \frac{-42.71(0.3401)}{[0.3507,8.651]} e^{(-0.0845s)}$$

The same procedure was applied but using the vertical acceleration as output. The model was again assumed 2nd order but this time the numerator order was also assumed 2nd order, rather than 1st order.

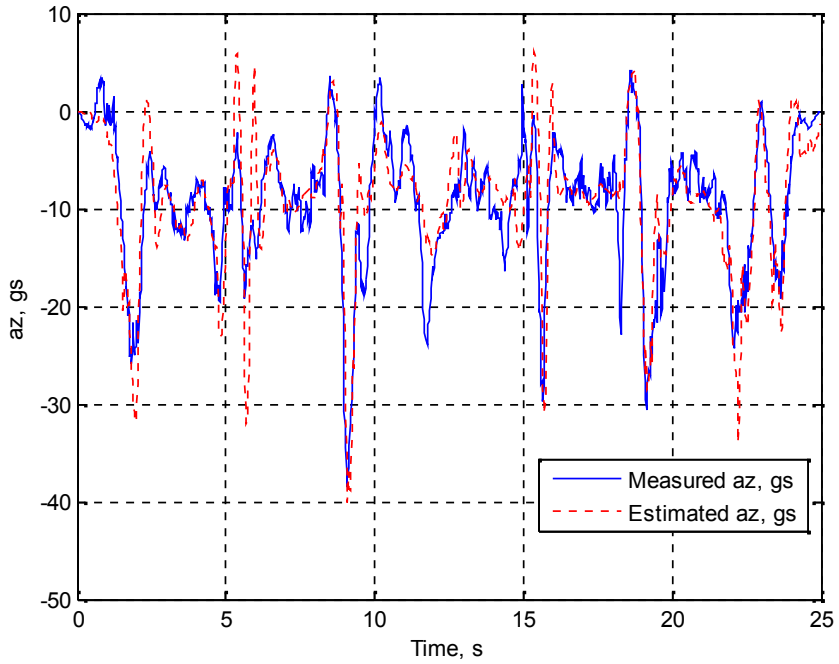

Figure 58: Measured and estimated time domain vertical acceleration (2nd order system model).

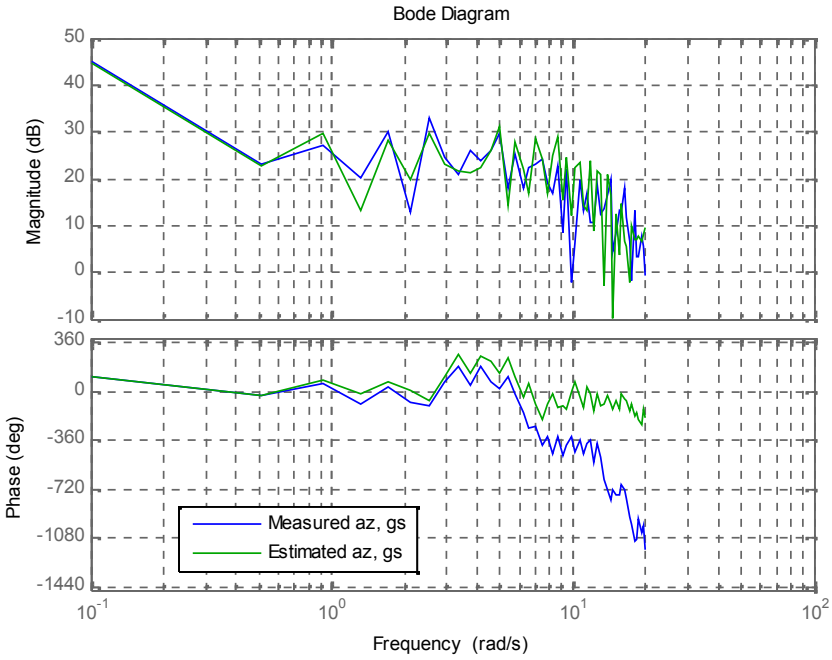

Figure 59: Measured and estimated frequency domain vertical acceleration (2nd order system model).

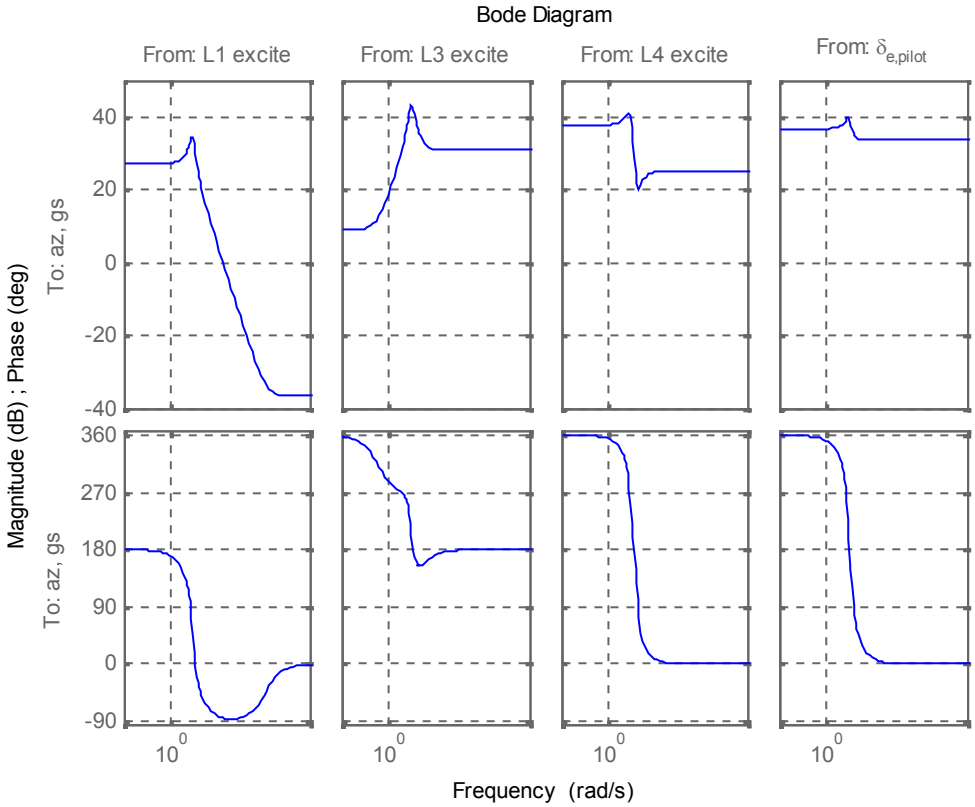

Figure 60: Estimated Transfer Function Bode Plots - vertical acceleration output (2nd order system model).

The estimated transfer functions are shown below.

$$\frac{a_z}{¢_{L1,excite}} = \frac{0.01499(-10.35)(1.257e+004)}{[0.3016,9.218]} e^{(-0s)} \qquad \frac{a_z}{¢_{L3,excite}} = \frac{-35.08(-0.3285)(20.84)}{[0.3016,9.218]} e^{(-0s)}$$

$$\frac{a_z}{¢_{L4,excite}} = \frac{17.84[-0.2458,19.21]}{[0.3016,9.218]} e^{(-0s)} \qquad \frac{a_z}{¢_{e,pilot}} = \frac{48.88[-0.4752,10.92]}{[0.3016,9.218]} e^{(-0s)}$$

The optimized time delay was negative for this case. Since that is not physically possible, the time delay was set to zero. For both output cases, the estimated short period mode is similar in both frequency and damping ratio.

Comparison to the Analytical Model

The identification results were compared to the draft Fenrir model. From this model, the three transfer functions from L1, L3 and L4 to pitch rate q were extracted. A 2nd order short period approximation was then determined from these transfer functions, see below.

$$\frac{q}{¢_{L1}} = \frac{0.7974(95.29)}{[0.6582,9.023]} \quad \frac{q}{¢_{L3}} = \frac{-45.45(6.725)}{[0.6582,9.023]} \quad \frac{q}{¢_{L4}} = \frac{-66.98(7.197)}{[0.6582,9.023]}$$

In parallel, the identified results were used to extract the equivalent systems using Eq. (3) shown in Section 3.2 below.* The Bode plots of the analytical model (DKS) and estimated model (Estimated) are compared in Figure 61 below (the time delay is ignored in the Bode plot of the estimated model).

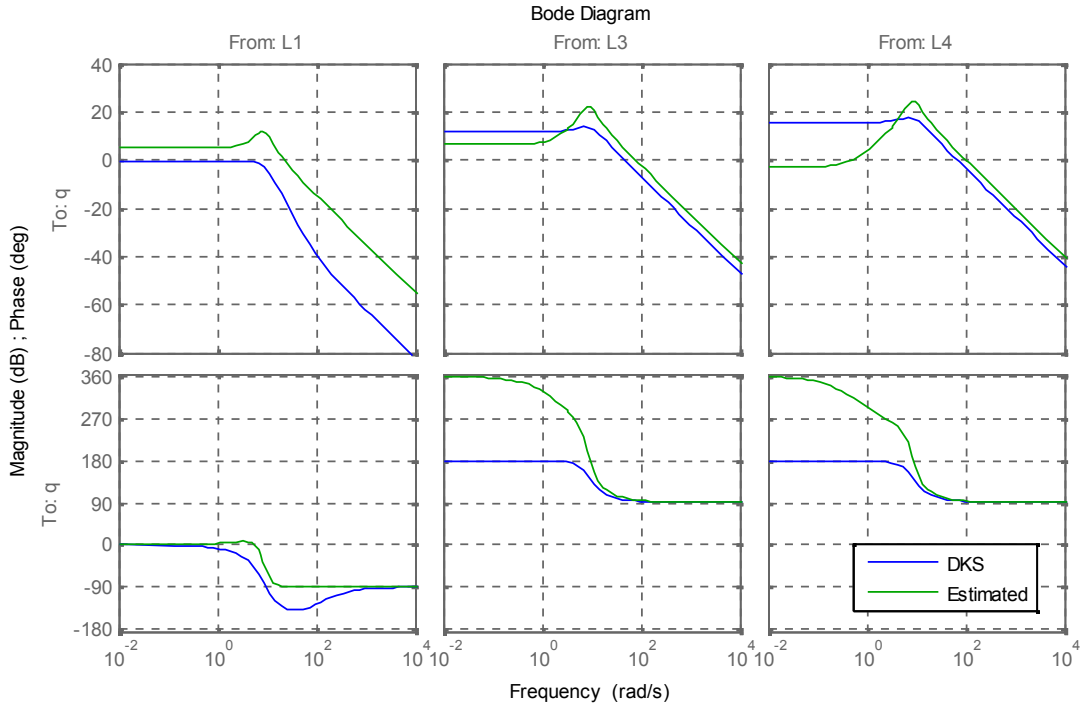

Figure 61: Comparison of analytical (DKS) and estimated models.

The DC gains have opposite sign of the estimated model when considering inputs L3 and L4! This warrants further investigation. Another identification attempt was run assuming no time delay (Figure 62 through Figure 64).

* It is assumed that $q/¢_{a,pilot}$ is 0.

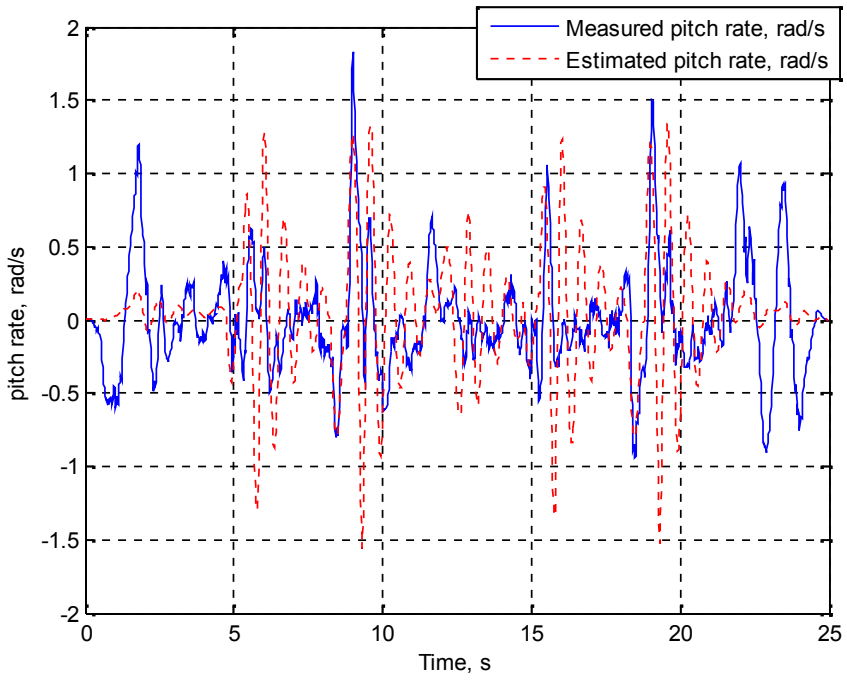

Figure 62: Measured and estimated time domain pitch rate (2nd order system model, no time delay).

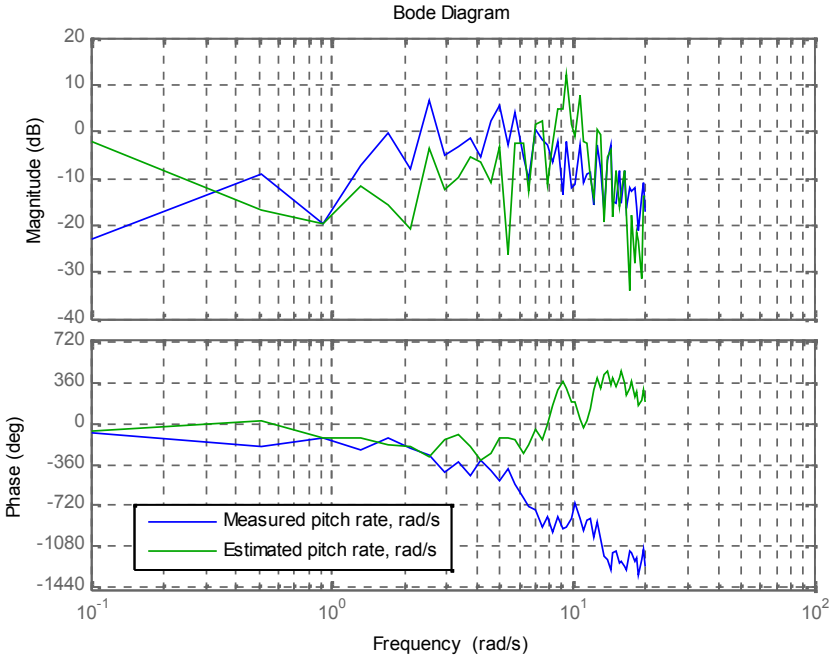

Figure 63: Measured and estimated frequency domain pitch rate (2nd order system model, no time delay).

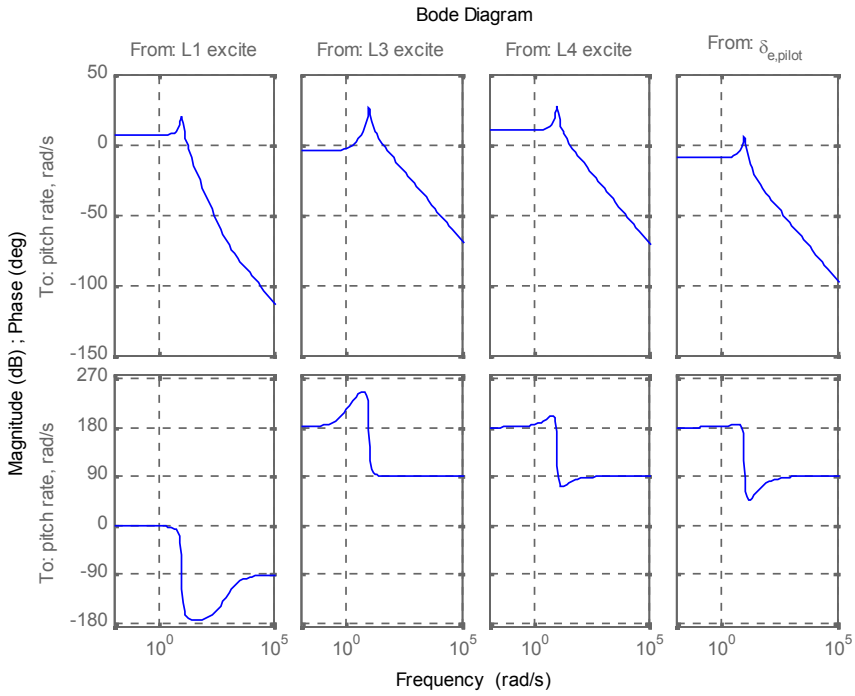

Figure 64: Estimated Transfer Function Bode Plots – pitch rate output (2nd order system model, no time delay).

These estimated transfer functions assuming no time delay are shown below:

$$\frac{q}{¢_{L1,excite}} = \frac{0.2501(770.3)}{[0.09893, 9.56]} \qquad \frac{q}{¢_{L3,excite}} = \frac{-35.97(1.499)}{[0.09893, 9.56]}$$

$$\frac{q}{¢_{L4,excite}} = \frac{-31.36(9.105)}{[0.09893, 9.56]} \qquad \frac{q}{¢_{e,pilot}} = \frac{-1.491(21.2)}{[0.09893, 9.56]}$$

The short period mode is estimated with a higher frequency but with a much lower damping ratio. Comparison of this estimated model to the analytical model is shown in Figure 65 below.

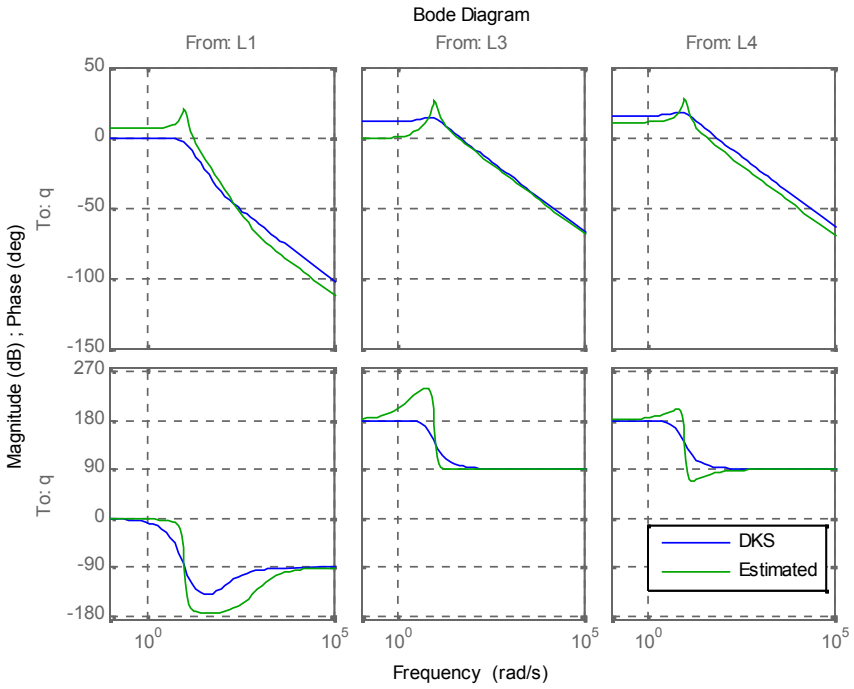

Figure 65: Comparison of analytical (DKS) and estimated model with no time delay.

When no time delay is assumed, the DC gains now match in sign. However, the low estimated damping ratio is not reassuring and the time and frequency domain comparisons are not as good (compare Figure 62 and Figure 63 to Figure 55 and Figure 56).

3.0 SYSTEM IDENTIFICATION USING TIME DOMAIN-BASED METHODS

3.1 Initial Identification Attempt

A MIMO ID was attempted using GRA. A new data set was selected that included a set of excitation for each of the 3 surface pairs (1266 to 1275 seconds). Only inputs L1, L3, and L4 were used with az and q as outputs (note that L2 was not used).

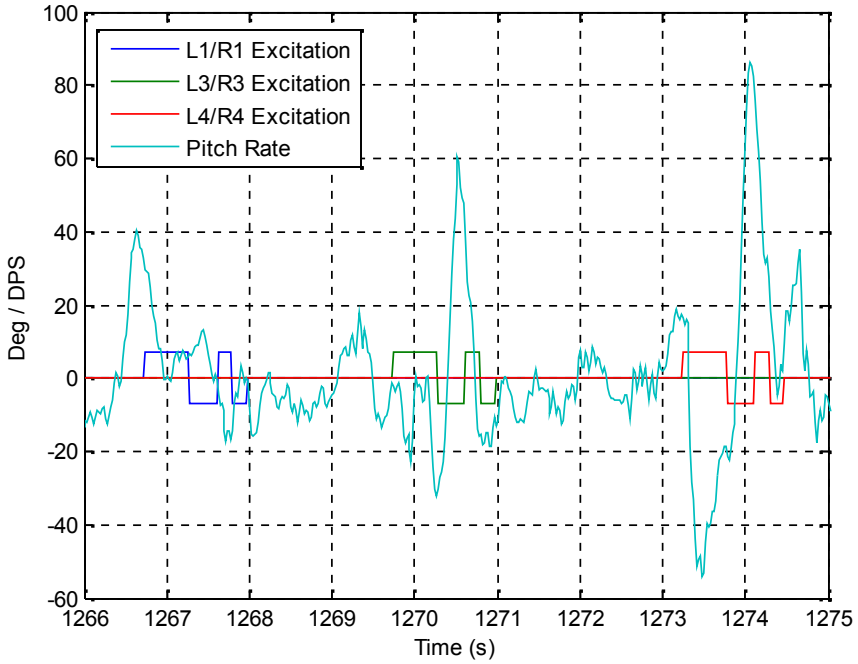

Figure 66: Excitation and pitch rate signals for selected data segment.

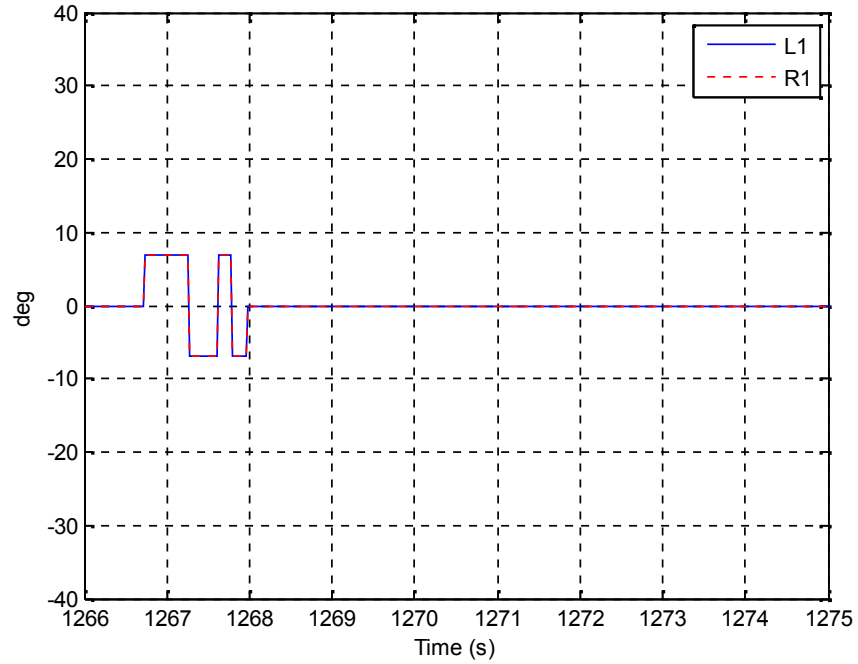

Figure 67: L1/R1 for selected data segment.

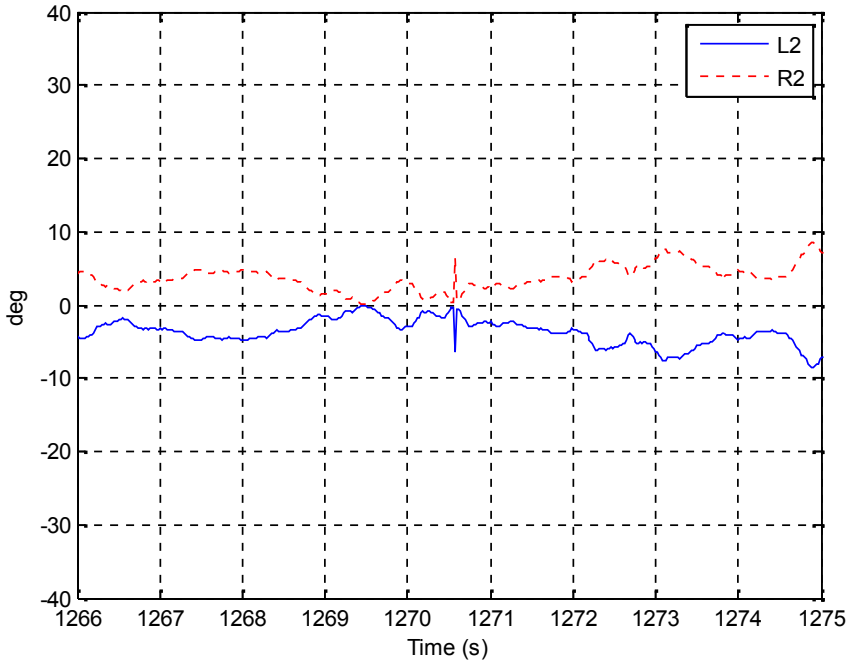

Figure 68: L2/R2 for selected data segment.

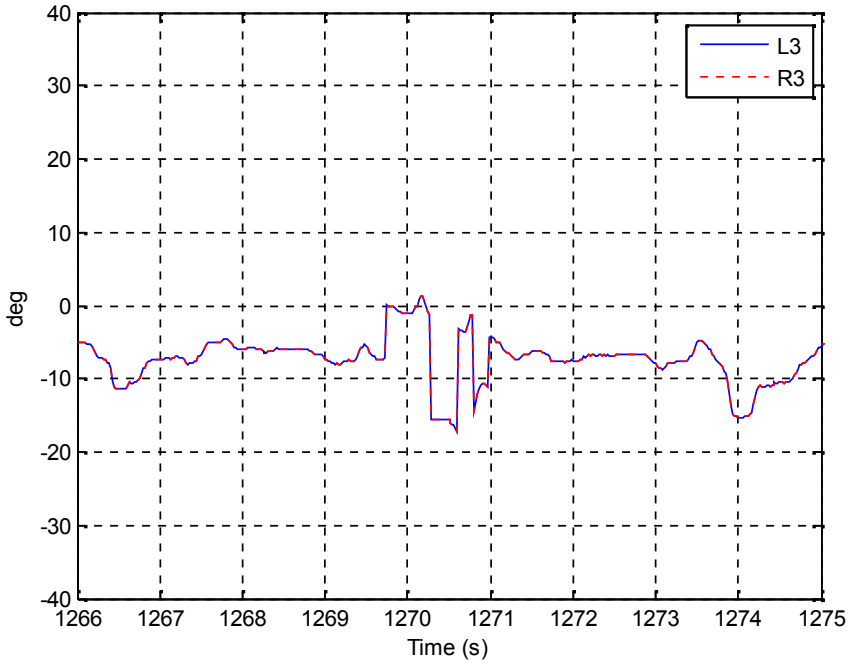

Figure 69: L3/R3 for selected data segment.

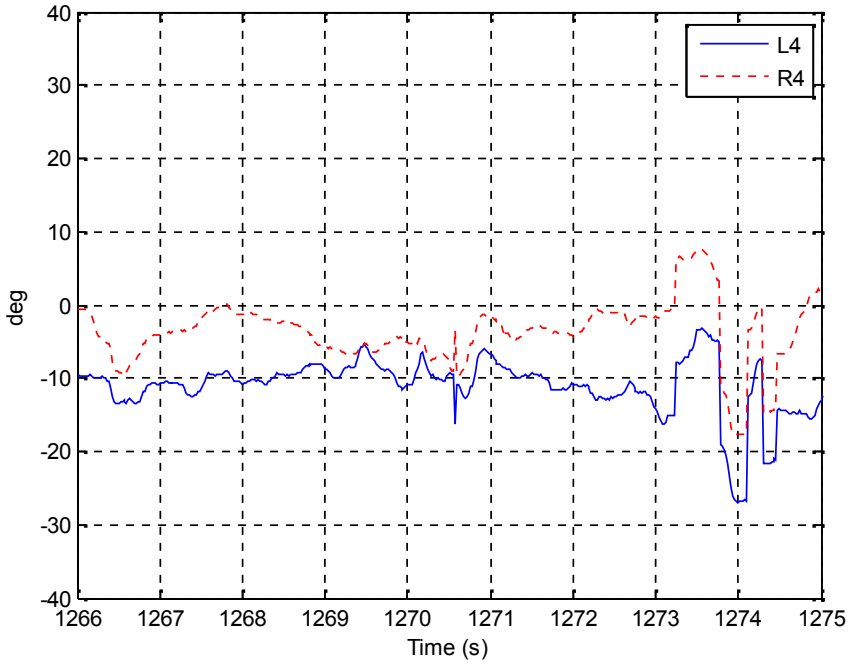

Figure 70: L3/R3 for selected data segment.

The GRA settings used were:

```
GRA settings:
option.ne = 6;
option.max_order = 20;
option.selector = 'off';
option.correlation = 'off';
option.forgetting = 'off';
option.oscatype = 'std';
```

GRA results are shown below.

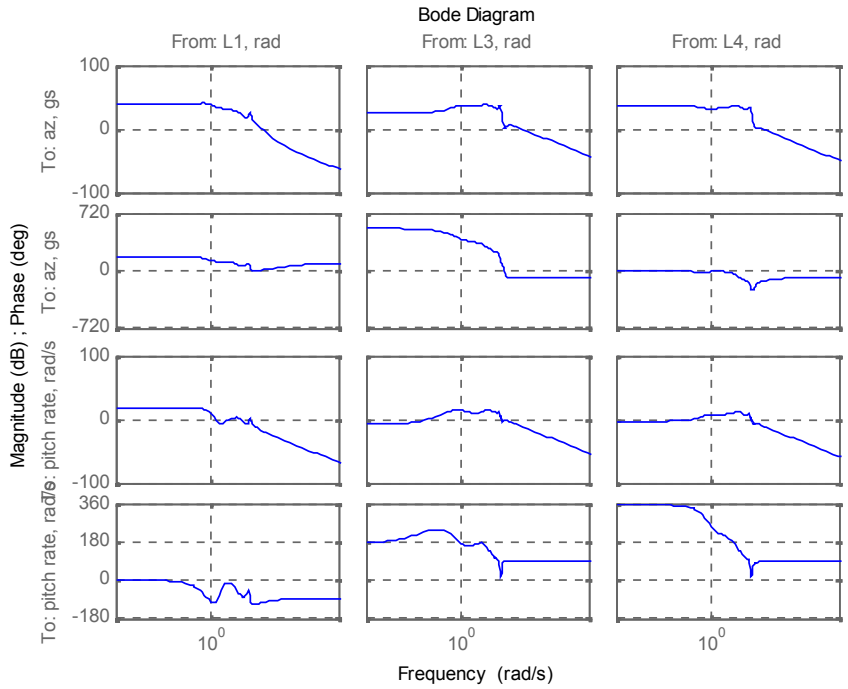

Figure 71: identified model from GRA.

The identified system poles are shown below.

Eigenvalue	Damping	Frequency
-9.38e-001 + 1.61e+001i	5.80e-002	1.62e+001
-9.38e-001 - 1.61e+001i	5.80e-002	1.62e+001
-2.87e+000 + 6.29e+000i	4.15e-001	6.91e+000
-2.87e+000 - 6.29e+000i	4.15e-001	6.91e+000
-4.61e-001 + 5.28e-001i	6.58e-001	7.00e-001
-4.61e-001 - 5.28e-001i	6.58e-001	7.00e-001

These results are indicating two poles near 7 rad/s with 0.4 and 0.7 damping ratio. This is in the neighborhood of the short period mode identified from the draft Fenrir model (9.02 rad/s with 0.658 damping ratio). It is noted that these results were sensitive to the GRA settings used, notably the max_order parameter.

3.2 Refined Identification

After running the above identification, it was noted that the inputs being used are correlated. This is due to the pilot input being sent to multiple surface pairs. An uncorrelated input set can be defined that consists of the independent pilot commands (elevator and aileron), and the excitation signals to L1/R1, L3/R3, and L4/R4. Another ID attempt was made using these 5 uncorrelated input signals. The entire data segment shown in in Section 1.0 was used. For reference, the PSDs of these input signals are shown below. Identification using this set can be performed and the systems from individual surface pairs can be extracted from the identified model using the relations in Eq. (3).

$$\frac{q}{¢_{L1}}(s) = \frac{q}{¢_{L1,excite}}(s)$$

$$\frac{q}{¢_{L2}}(s) = \frac{q}{¢_{a,pilot}}(s)$$

$$\frac{q}{¢_{L3}}(s) = \frac{q}{¢_{e,pilot}}(s) + \frac{q}{¢_{L3,excite}}(s) \tag{3}$$

$$\frac{q}{¢_{L4}}(s) = \frac{q}{¢_{e,pilot}}(s) + \frac{q}{¢_{a,pilot}}(s) + \frac{q}{¢_{L4,excite}}(s)$$

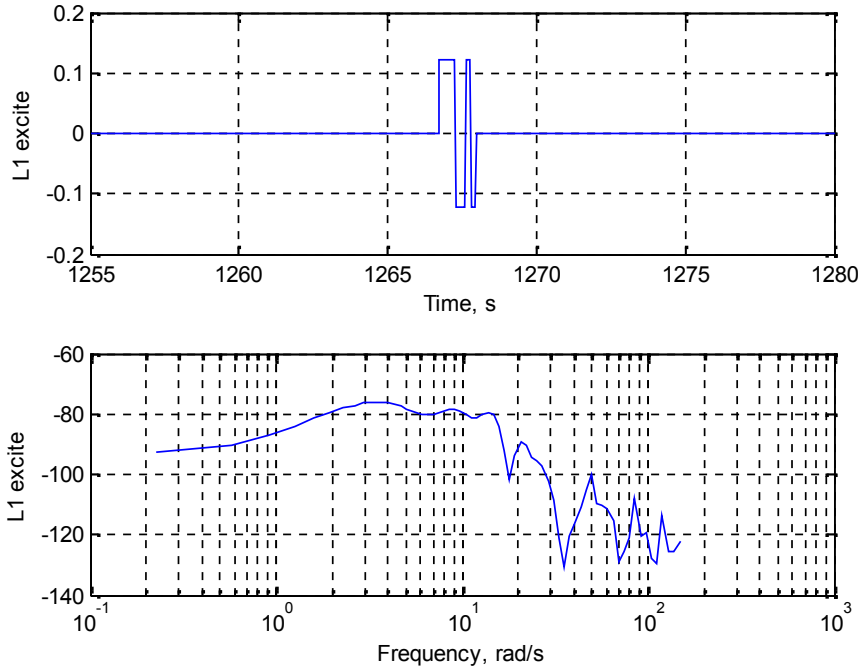

Figure 72: Input (L1 excite) time history and resulting PSD.

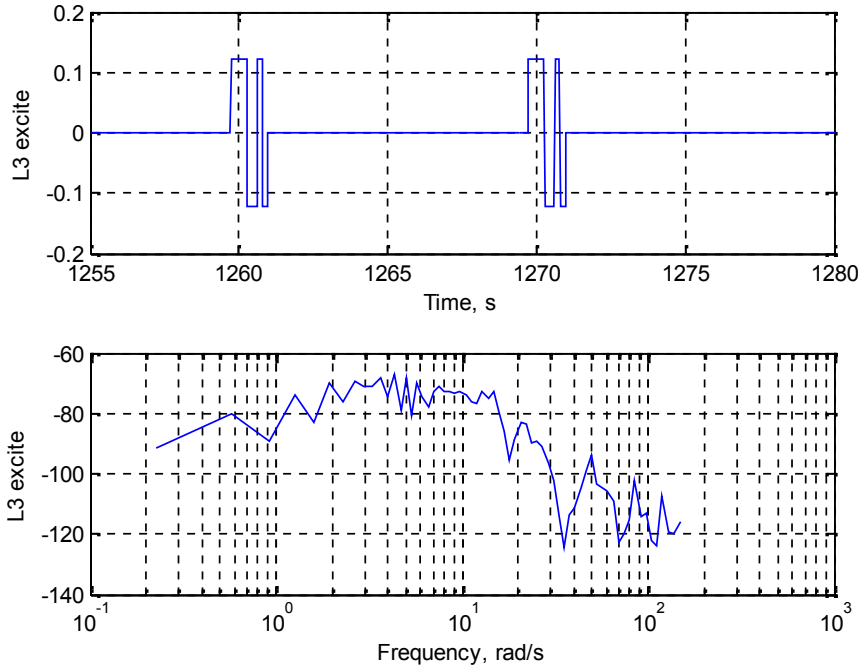

Figure 73: Input (L3 excite) time history and resulting PSD.

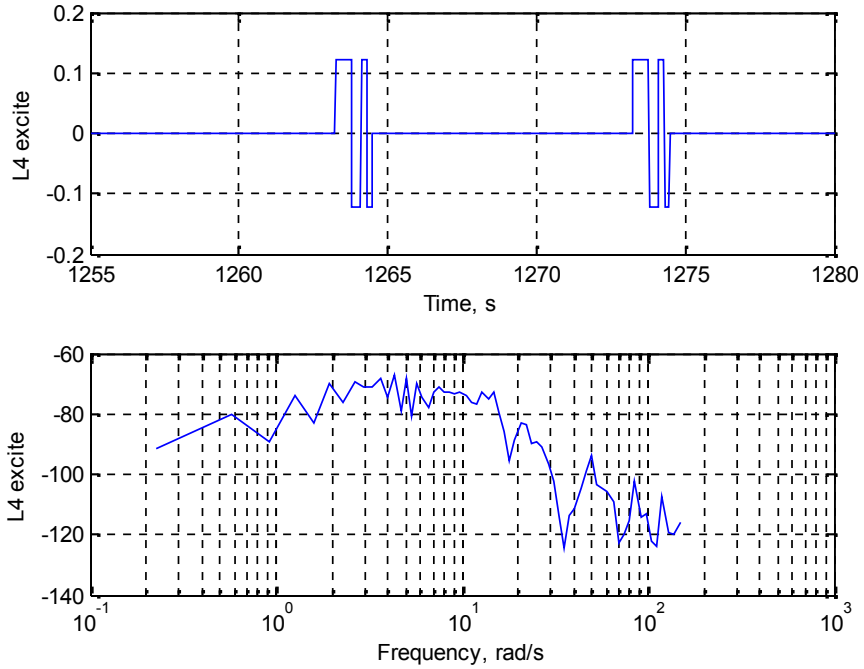

Figure 74: Input (L4 excite) time history and resulting PSD.

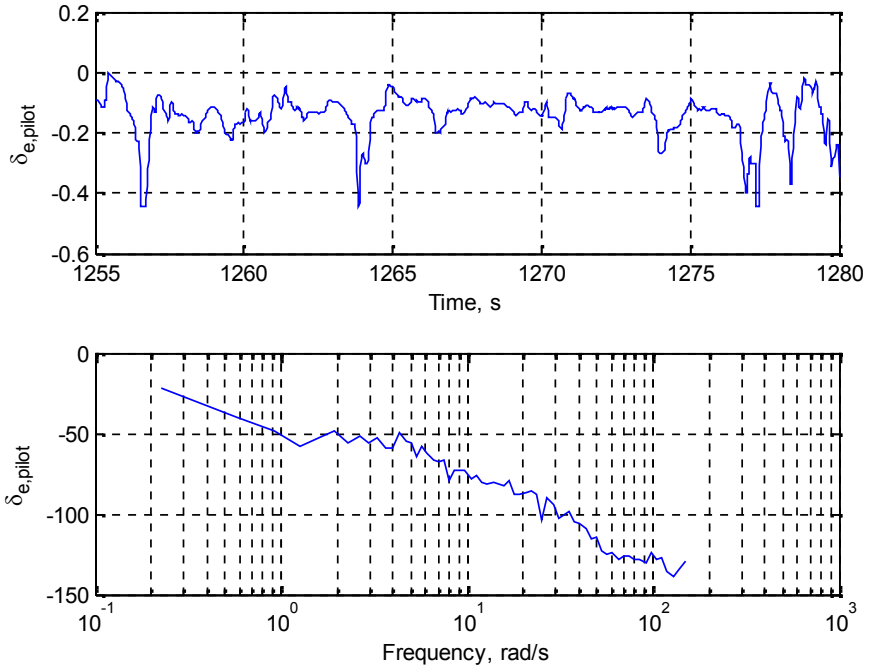

Figure 75: Input ¢$_{e,pilot}$ time history and resulting PSD.

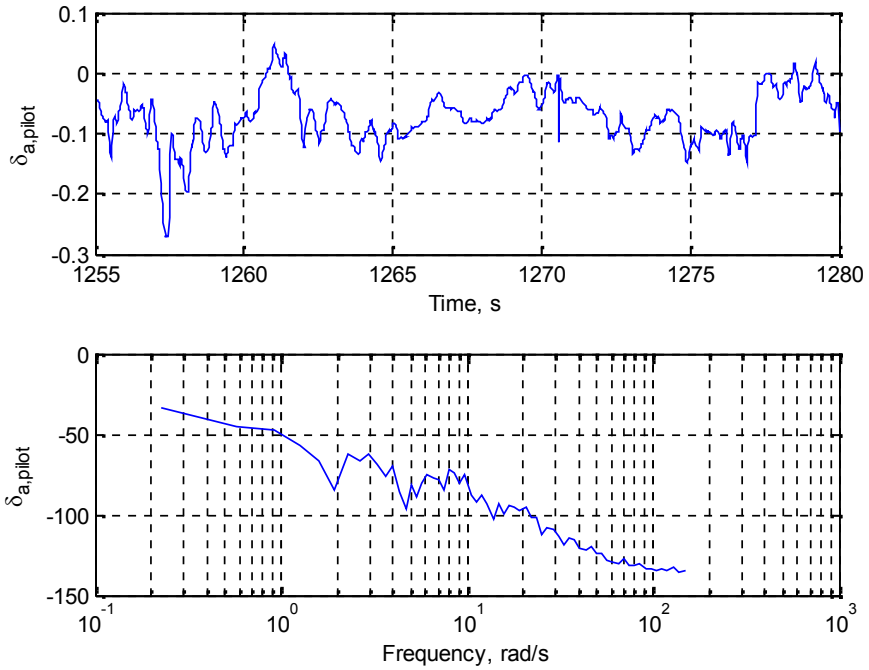

Figure 76: Input ¢$_{a,pilot}$ time history and resulting PSD.

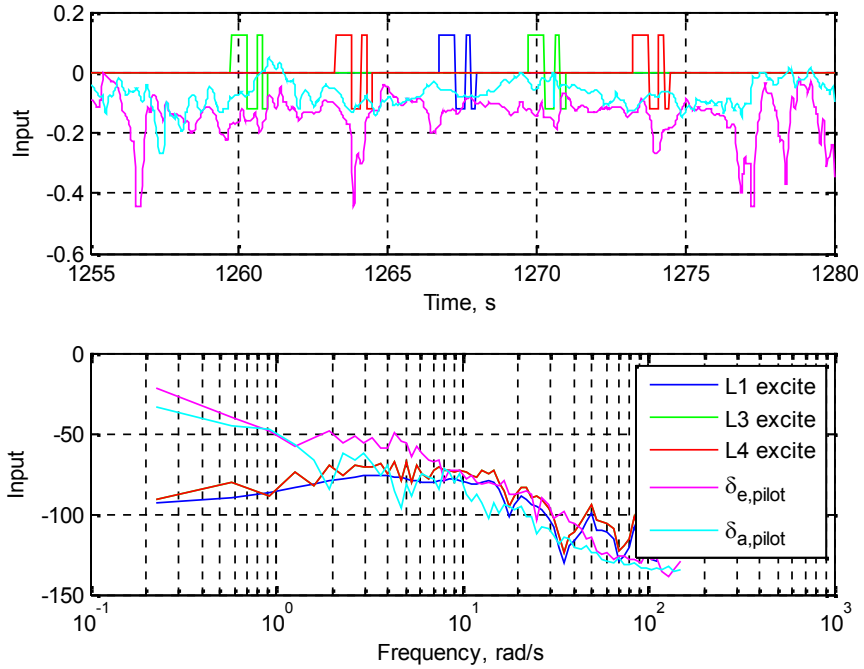

Figure 77: All inputs time histories and resulting PSDs.

It is noted that the pilot commands have much higher energy in the lower frequency range. The GRA settings used were:

```
ne = 6;
option.ne = ne;
option.max_order = 20;
option.selector = 'off';
option.correlation = 'off';
option.forgetting = 'off';
option.oscatype = 'std';
```

The identified system poles were:

Eigenvalue	Damping	Frequency
-1.22e+000 + 1.53e+001i	7.96e-002	1.54e+001
-1.22e+000 - 1.53e+001i	7.96e-002	1.54e+001
-2.20e+000 + 5.55e+000i	3.68e-001	5.97e+000
-2.20e+000 - 5.55e+000i	3.68e-001	5.97e+000
-4.42e-001 + 8.56e-001i	4.59e-001	9.64e-001
-4.42e-001 - 8.56e-001i	4.59e-001	9.64e-001

The pole identified near 6 rad/s with a damping ratio of 0.368 is likely the short period. The identified frequency response is shown in Figure 78.

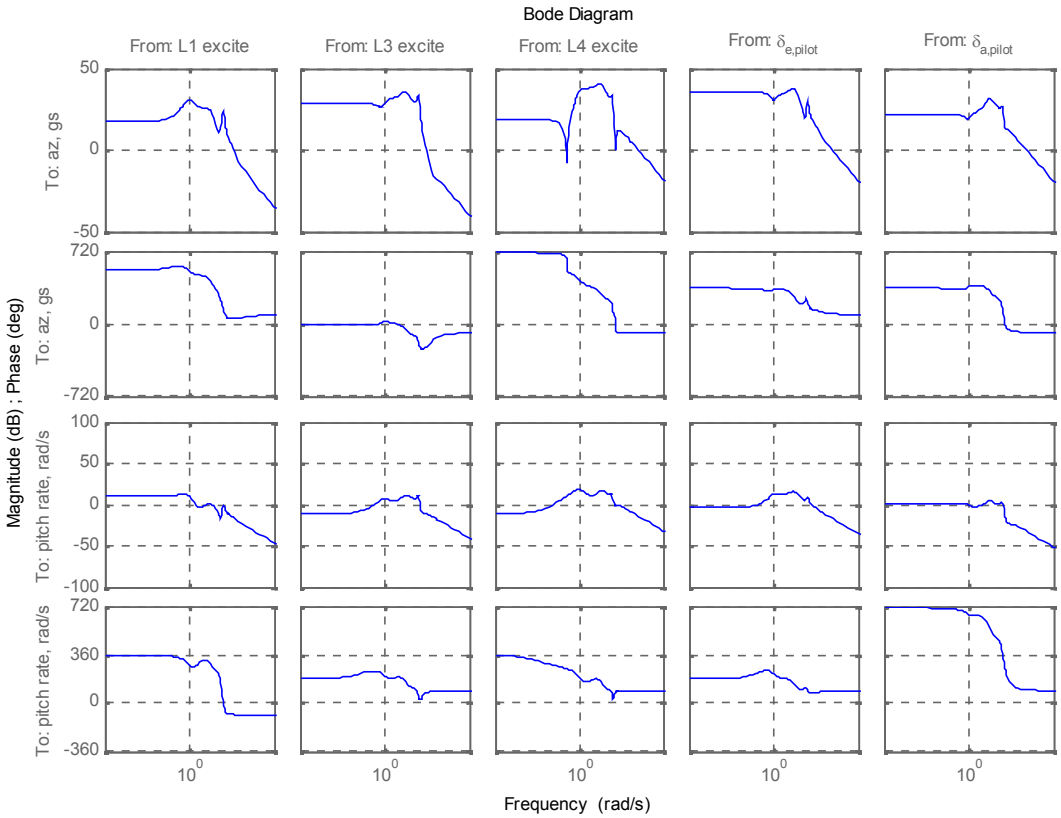

Figure 78: GRA-identified frequency response using the uncorrelated inputs.

If the pilot roll command is eliminated from the input data, the identified system poles remain relatively unchanged. It is known that this flight consisted of much more pitch excitation, so this is not surprising. For reference, the FREDA identification using this data set is displayed in Appendix A.1. A direct comparison of both identified models in the frequency domain is shown in Figure 79 below.

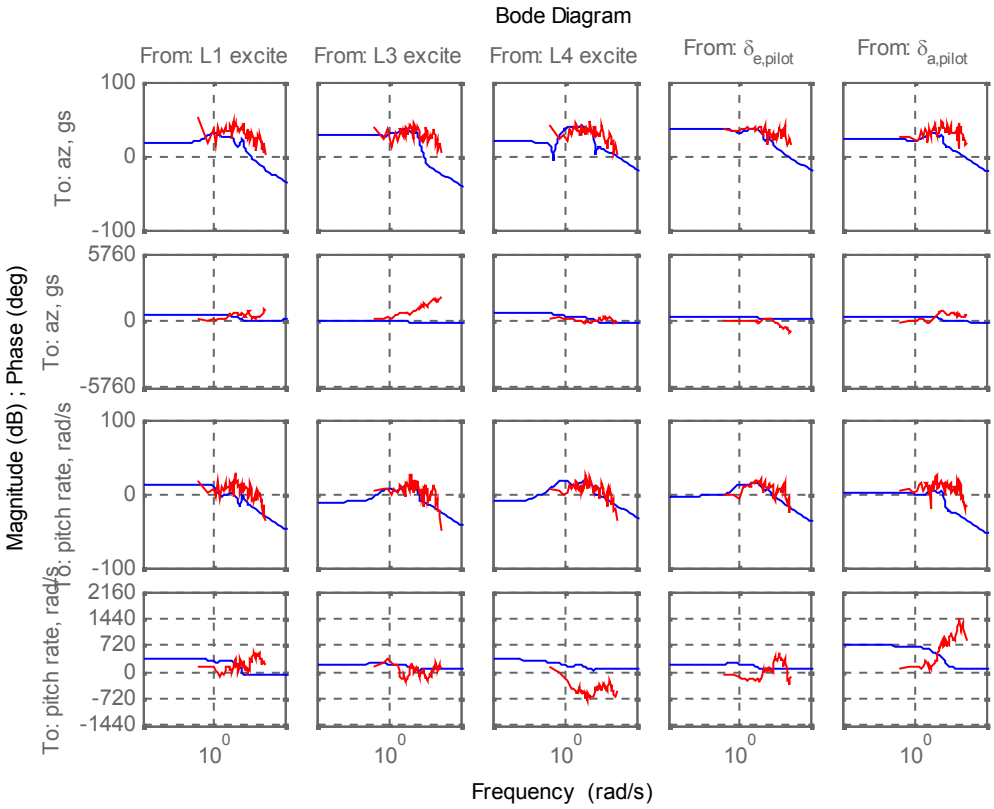

Figure 79: Comparison of FREDA (red) and GRA (blue) results using same I/O data set.

This comparison is not very good. The FREDA results show a phase increase for many of the I/O pairs, which is odd. It is noted that zero padding and windowing can cause this effect.

More FREDA results that utilized different data segments are documented in Appendices A.2, A.3, and A.4.

4.0 CONCLUSIONS

- A notable result from this analysis is that a peak near 6 rad/s was identified in many different data segments using both the FREDA frequency and GRA time domain identification approaches (see results in Section 3.2, Appendices A.2 and A.3). This suggests that the short period mode is located here. This is reasonable, as the draft Fenrir model indicates a short period at 9.02 rad/s, which is in the neighborhood. The GRA identification estimated a damping ratio for this mode to be 0.368 which is also reasonable.
- Using SIDPAC parameter ID, a short period mode was identified near 9 rad/s with a damping ratio of ~0.3 (Section 2.4). This value differs from 6 rad/s (which was suggested by both FREDA and GRA) but it is closer to the estimated value taken from the draft model (μ = 9.02 rad/s, ¸ = 0.658).
- Using SIDPAC, including the time delay in the model as a free parameter had a significant impact on the results. Particularly, the short period mode damping ratio was estimated much lower if no time delay was assumed. Also, the time delay shows a better match when comparing time and frequency domain data. However, when the time delay is assumed, some of the system DC gain values have opposite sign of the analytical model.

- SIDPAC is more flexible as it allows the user to define a parametric model of any desired form. The drawback is that the optimization has many local minima, making the initial guess critical. GRA does not suffer from this local minima problem but the identified model is a completely general state space model. A combination of GRA (for the initial guess) and SIDPAC (for refinement) may be a good approach to identification.
- The phugoid mode is expected to be very low in frequency making it very difficult and probably not possible to identify from these data.
- Excitation commands were issued to symmetric surface pairs to target longitudinal dynamics. Identification of lateral dynamics was not attempted since there is not sufficient excitation of these dynamics as planned.
- It is recommended to conduct a future flight test where only a single excitation input is issued rather than three separate inputs as done here. In addition, it is recommended to use the pilot pitch command (which is routed to multiple pairs). This will facilitate SISO identification since only a single input will be exciting the aircraft in the longitudinal axes. A single axis SISO identification case such as this will serve as a valuable baseline for future ID studies. A similar but separate test should be conducted for lateral-directional dynamics using the pilot roll command.
- Following baseline identification as described above, future tests can use excitation inputs at all surfaces simultaneously (orthogonal multi-sine, pseudo random, or something similar). The baseline case can be used for validation. If successful for identification, tests with multiple simultaneous excitations such as this are very valuable as they provide persistent excitation from all inputs for the maximum time possible (the entire test).

APPENDIX A. ADDITIONAL FREQUENCY DOMAIN IDENTIFICATION

A.1 FULL RUN USING UNCORRELATED INPUTS

FREDA Settings:

```
st.useSmoothing = 1;
st.psdTaper=0.05;
st.binRatio=1.07;
st.binSize=3;
st.zeroFill=30;
```

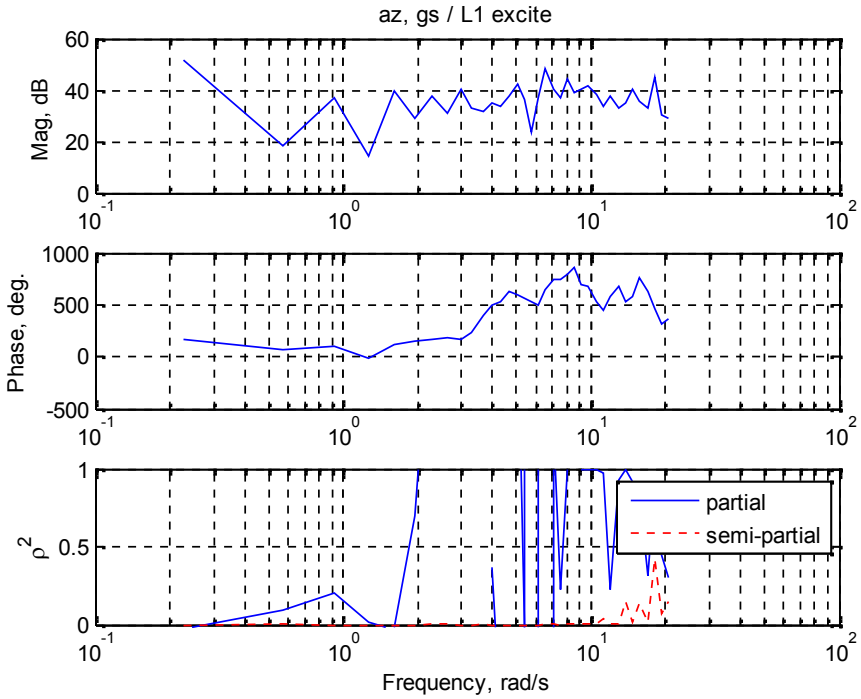

Figure 80: Identified frequency response: az, gs / L1 excite.

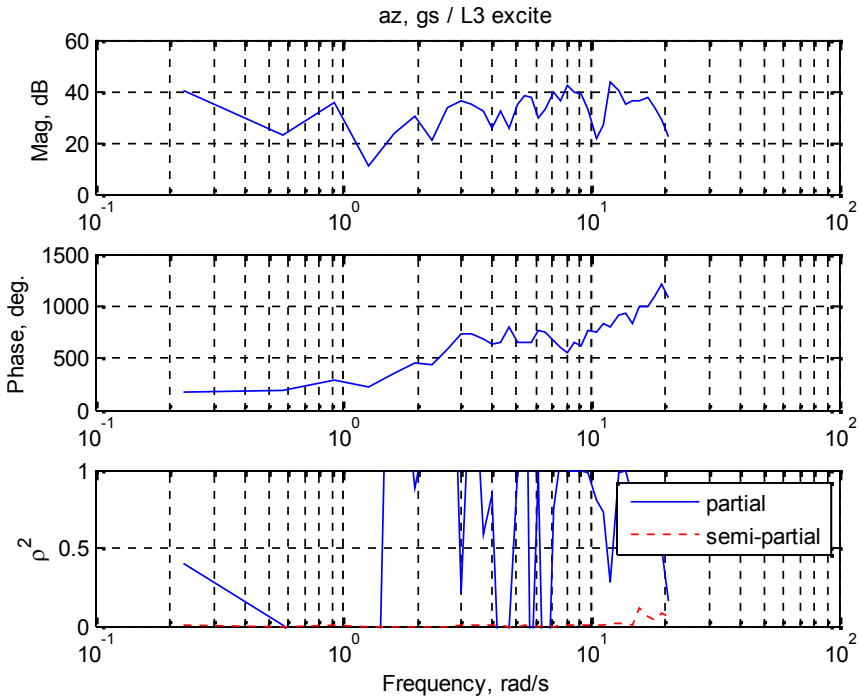

Figure 81: Identified frequency response: az, gs / L3 excite.

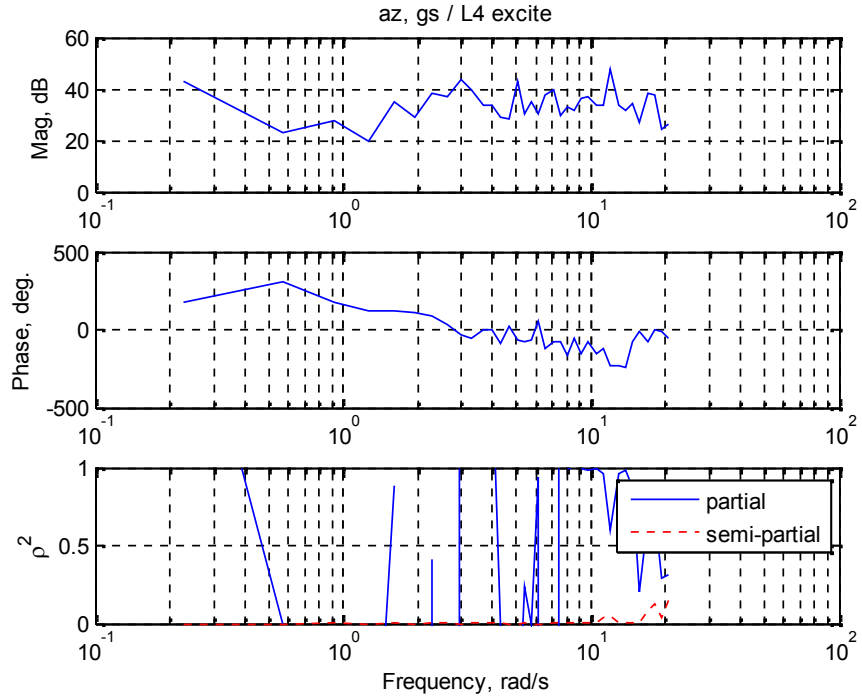

Figure 82: Identified frequency response: az, gs / L4 excite.

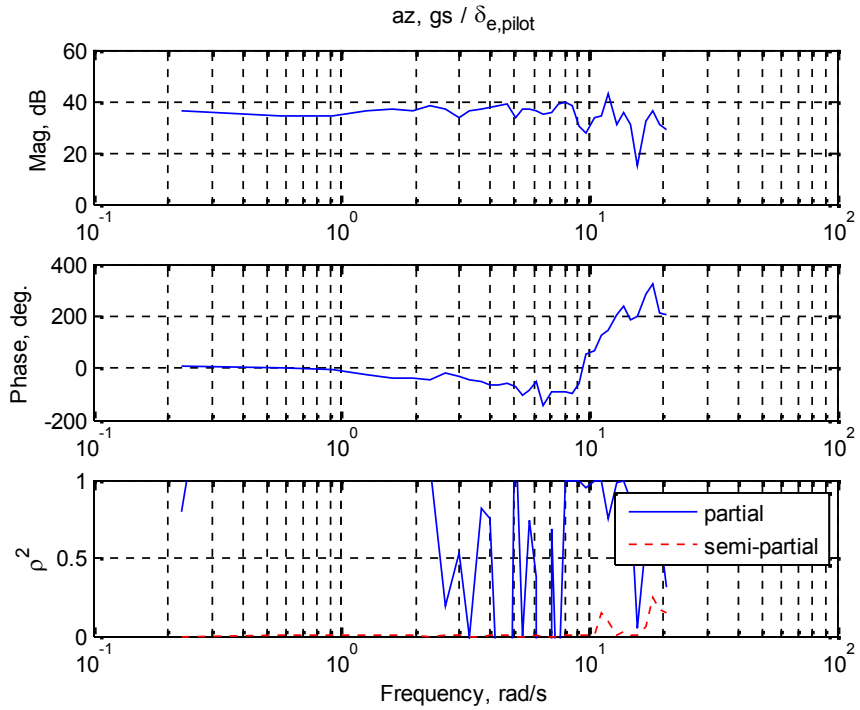

Figure 83: Identified frequency response: az, gs / \delta_{e,pilot}.

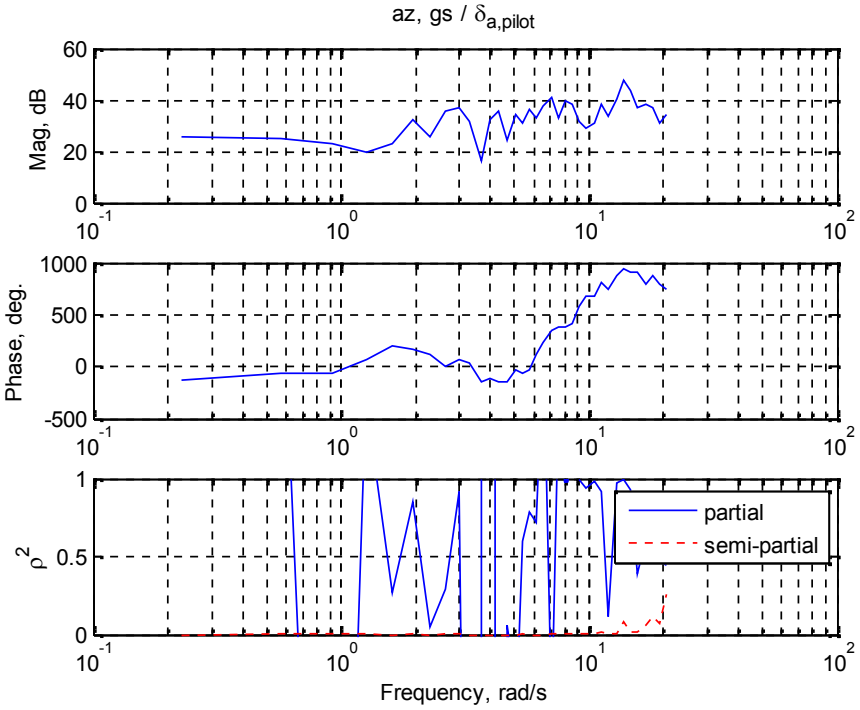

Figure 84: Identified frequency response: az, gs / \delta_{a,pilot}.

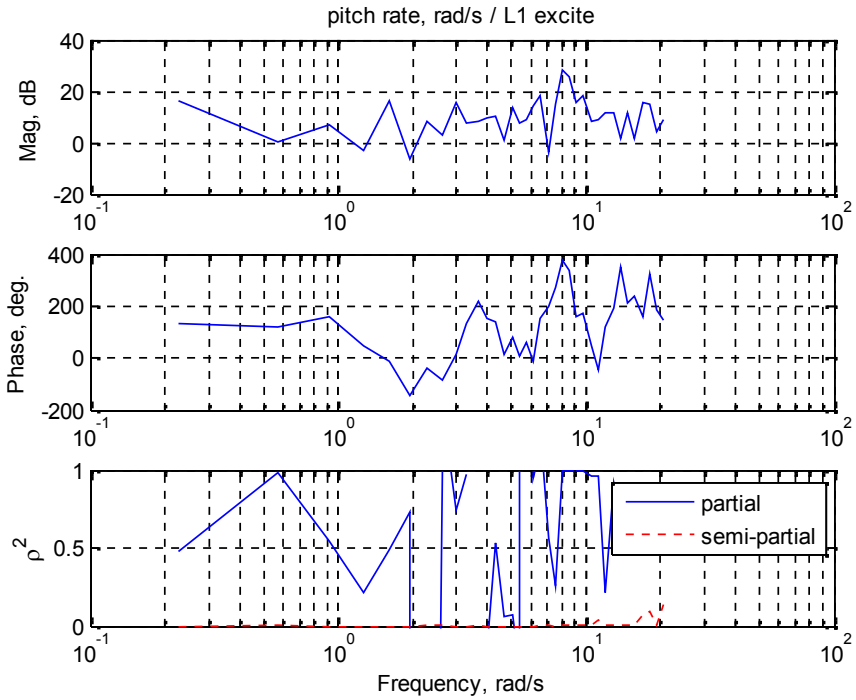

Figure 85: Identified frequency response: pitch rate, rad/s / L1 excite.

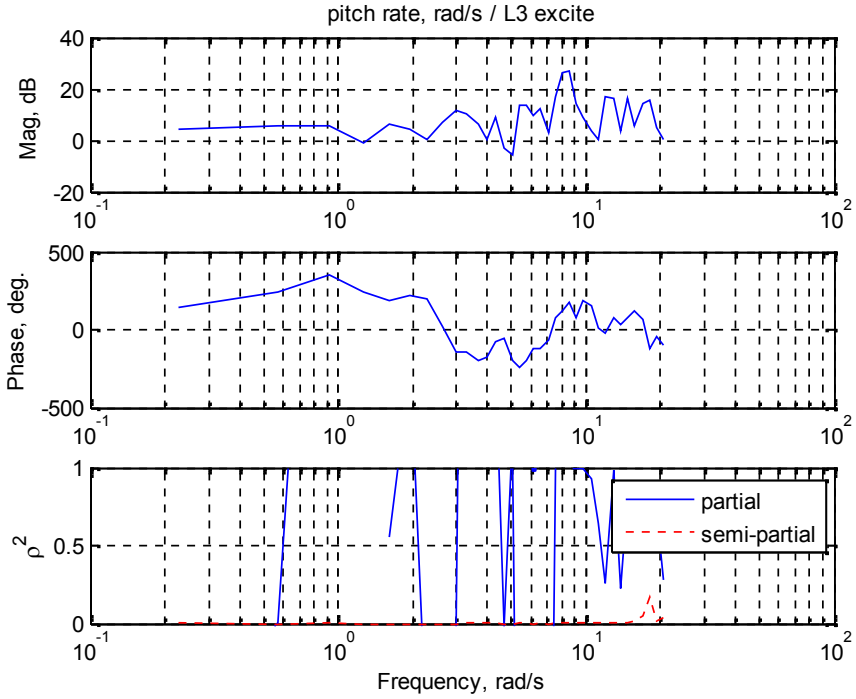

Figure 86: Identified frequency response: pitch rate, rad/s / L3 excite.

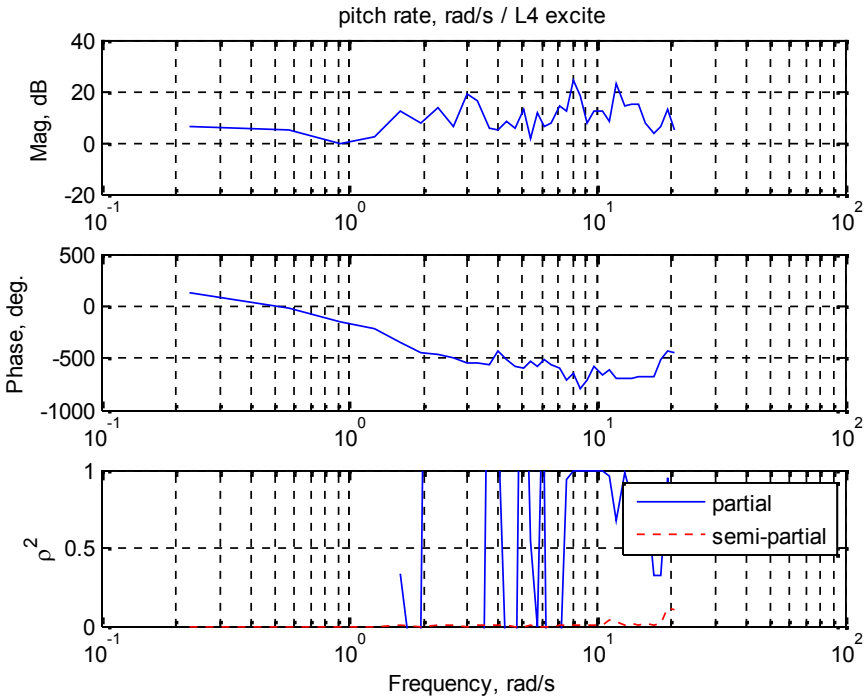

Figure 87: Identified frequency response: pitch rate, rad/s / L4 excite.

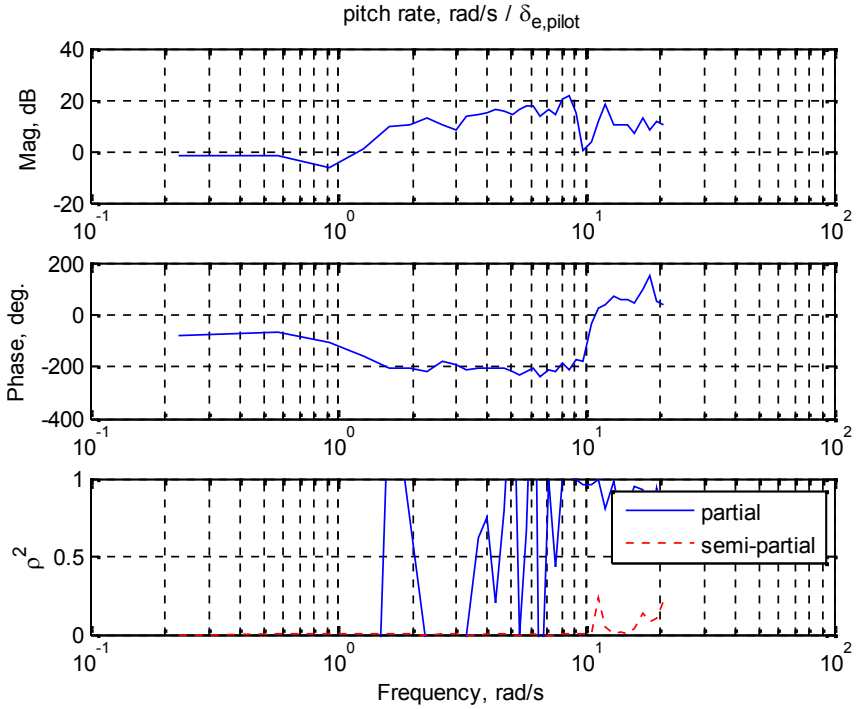

Figure 88: Identified frequency response: pitch rate, rad/s / \delta_{e,pilot}.

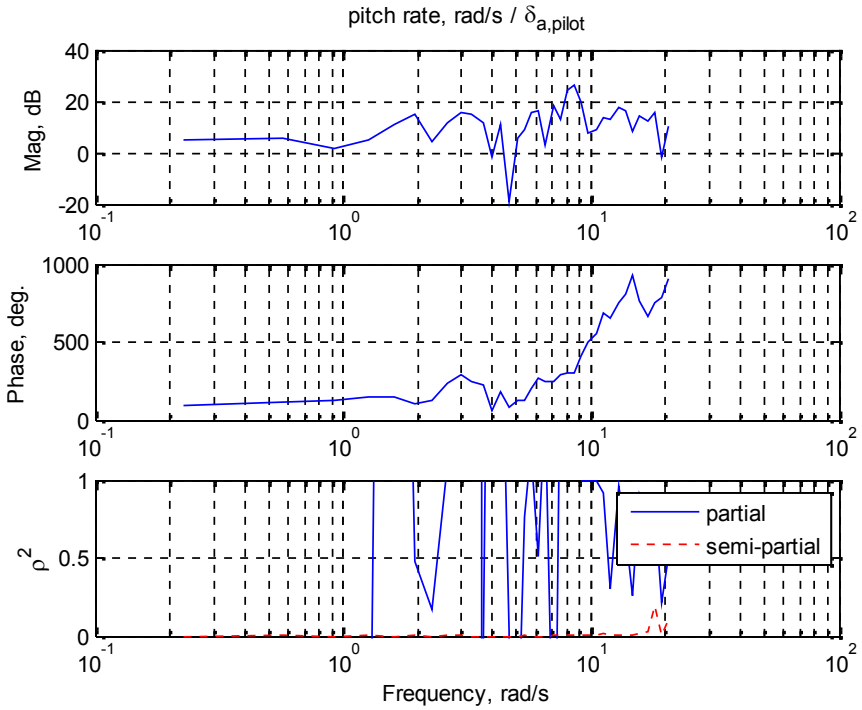

Figure 89: Identified frequency response: pitch rate, rad/s / \delta_{a,pilot}.

A.2 1ST L1/R1 EXCITATION

The data segment from 1265 to 1269 was used. Considering data correlation, inputs considered were L1/R1 excitation, pitch command from pilot and roll command from pilot. L3/R3 excitation and L4/R4 excitation are zero so they were eliminated.

FREDA Settings:

```
st.psdTaper=0.05; % taper fraction
st.binRatio=1.01; % bin ratio
st.binSize=3; % average at least this many points
st.zeroFill=30; % seconds of zero fill
```

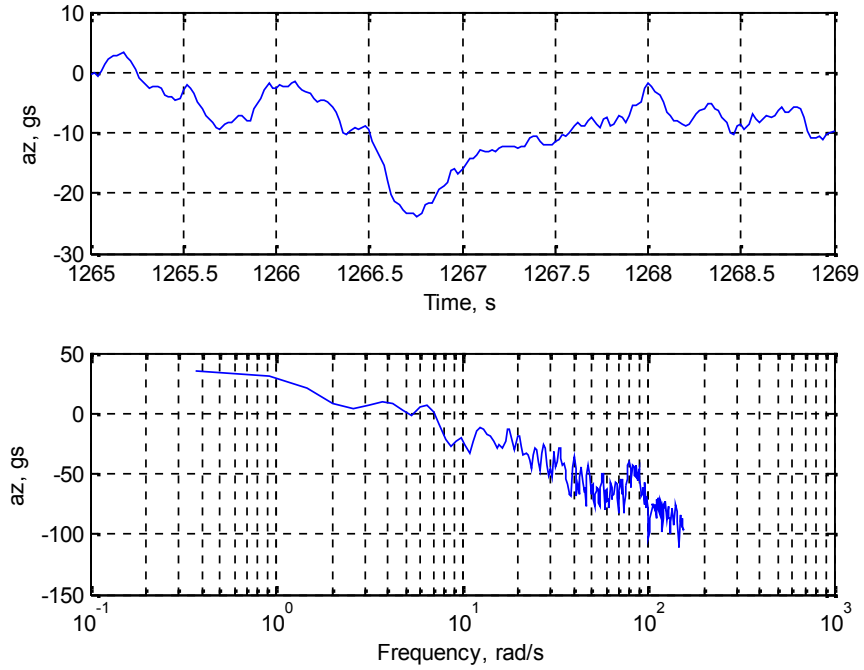

Figure 90: Output (az, gs) time history and resulting PSD.

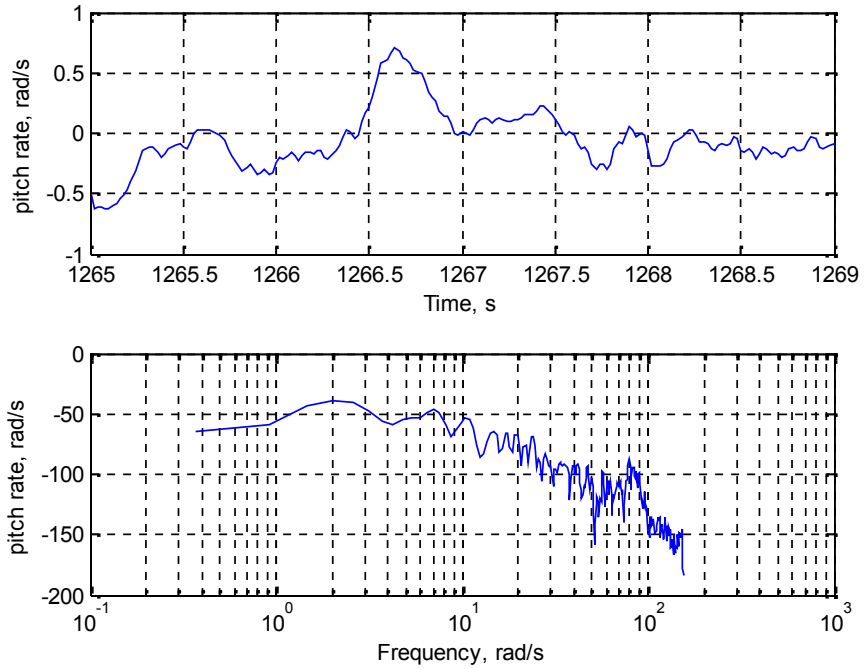

Figure 91: Output (pitch rate, rad/s) time history and resulting PSD.

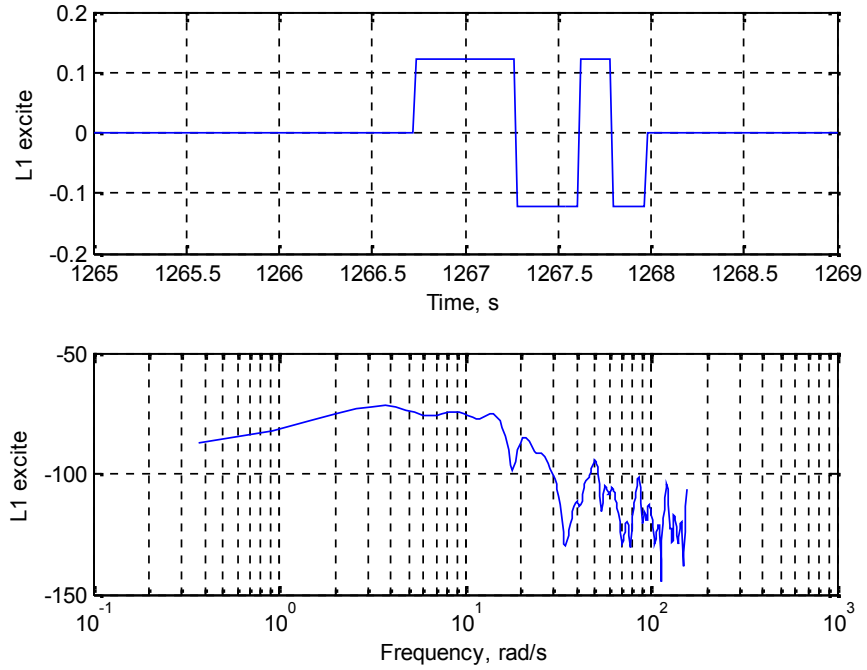

Figure 92: Input (L1 excite) time history and resulting PSD.

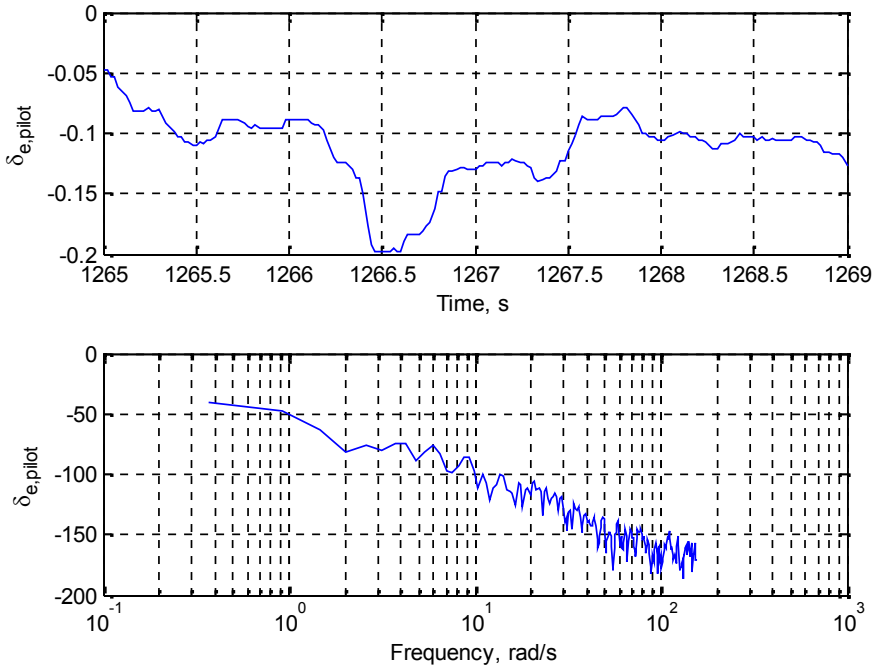

Figure 93: Input (\delta_{e,pilot}) time history and resulting PSD.

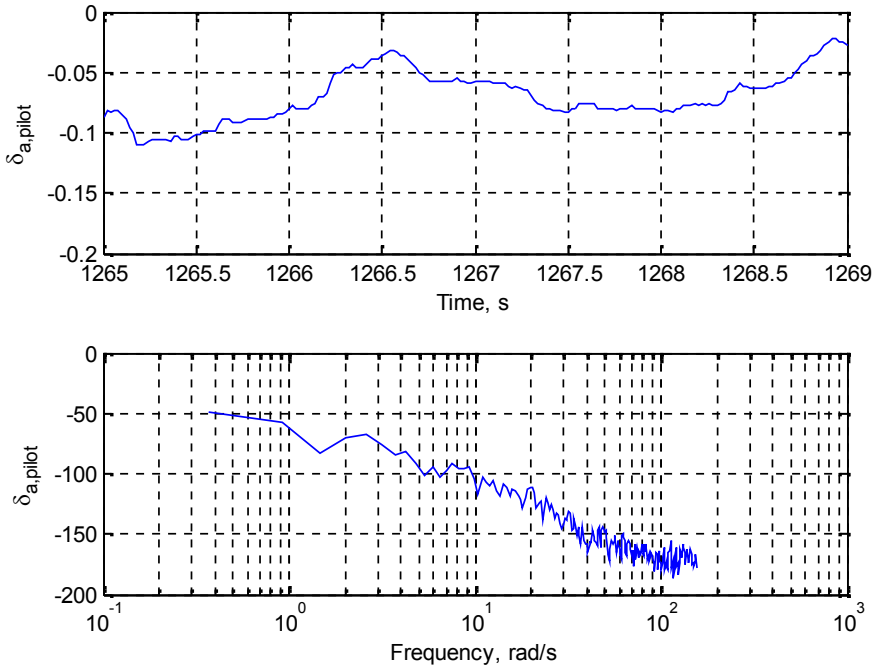

Figure 94: Input (\delta_{a,pilot}) time history and resulting PSD.

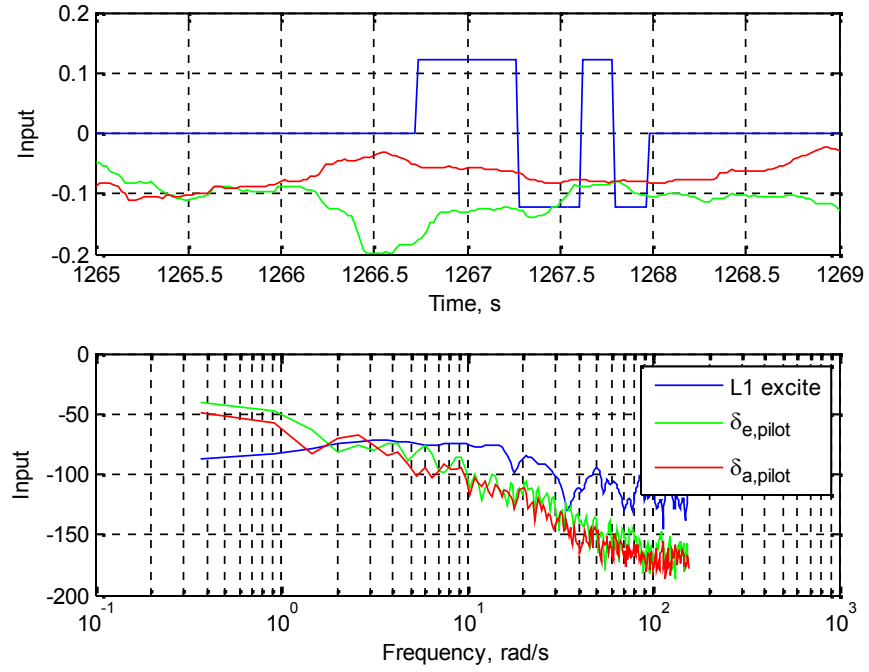

Figure 95: All inputs time histories and resulting PSDs.

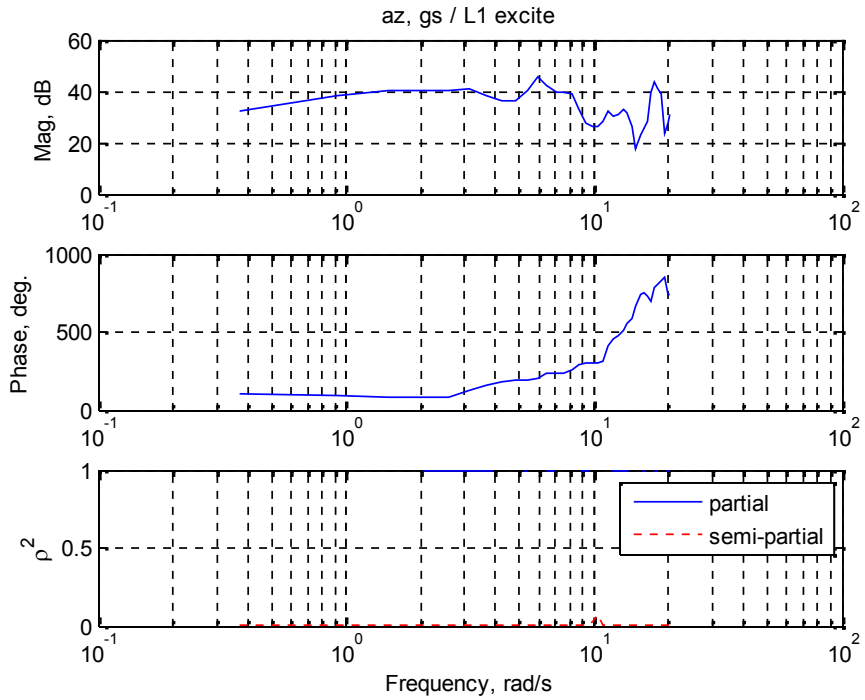

Figure 96: Identified frequency response: az, gs / L1 excite.

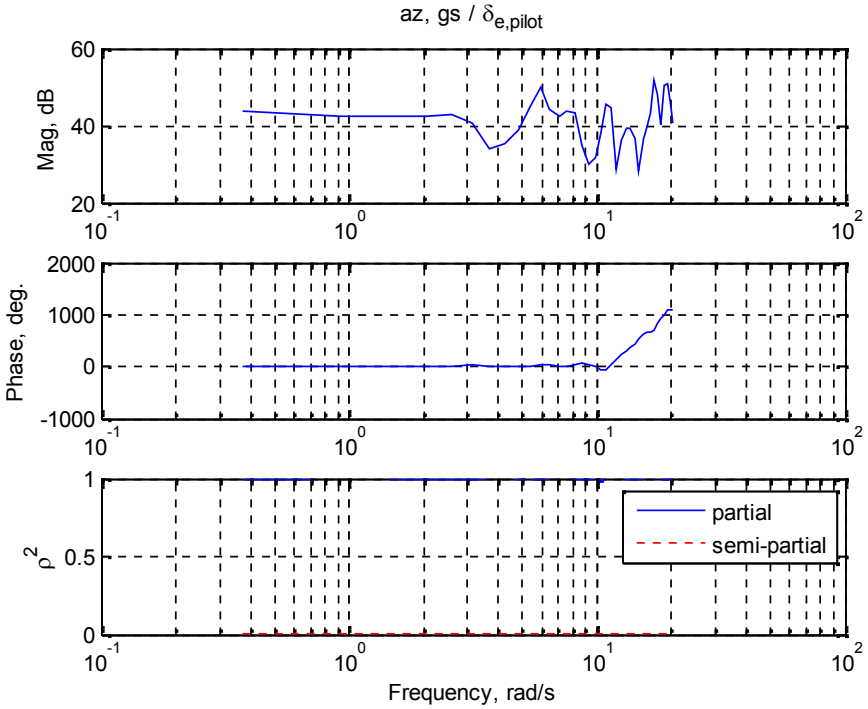

Figure 97: Identified frequency response: az, gs / \delta_{e,pilot}.

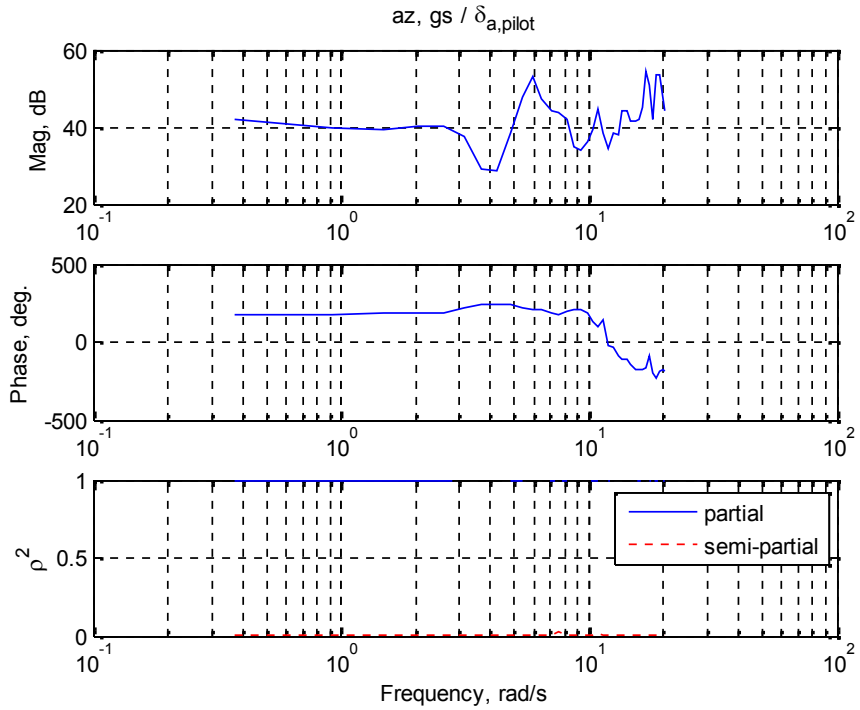

Figure 98: Identified frequency response: az, gs / \delta_{a,pilot}.

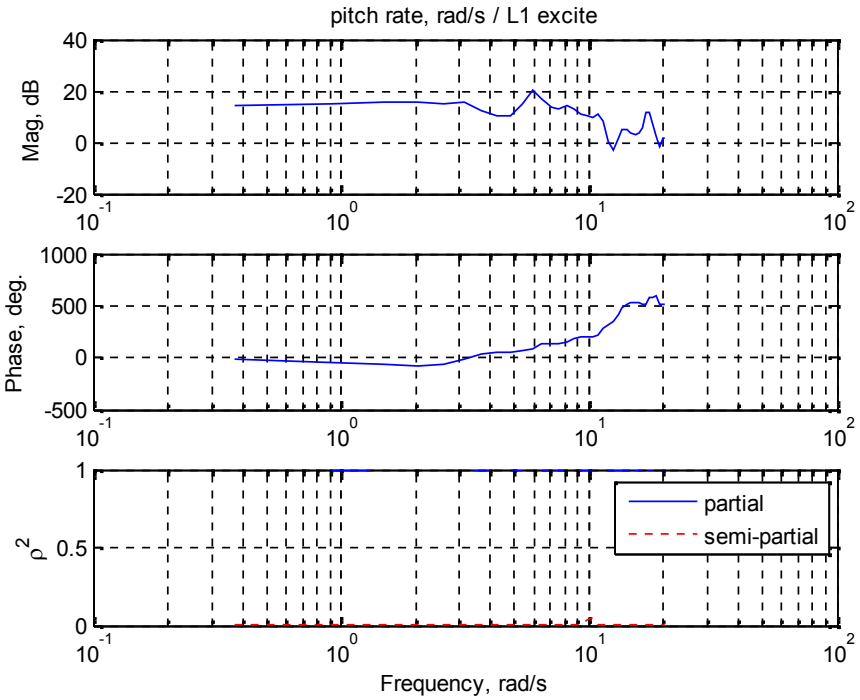

Figure 99: Identified frequency response: pitch rate, rad/s / L1 excite.

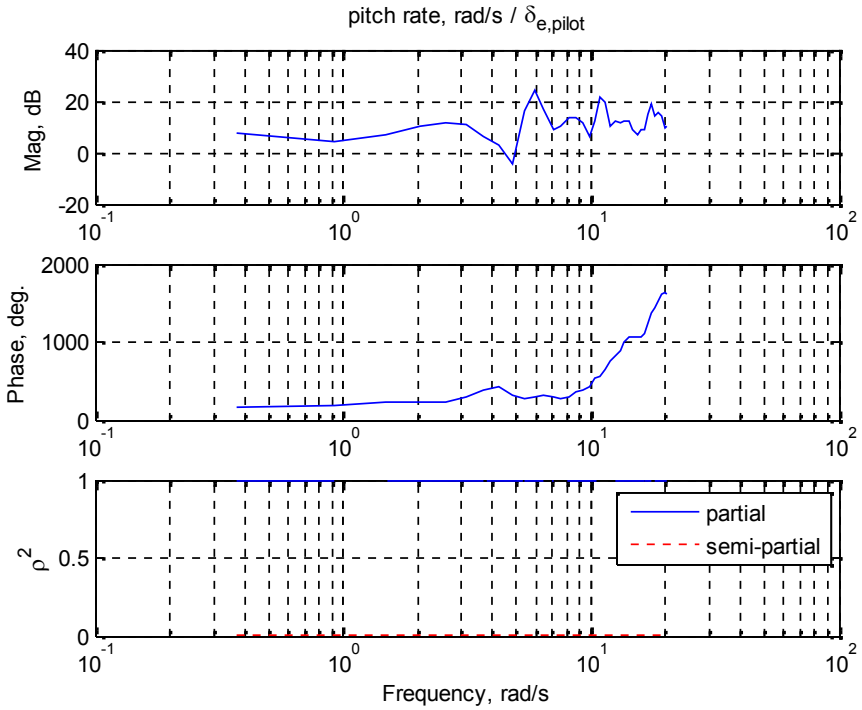

Figure 100: Identified frequency response: pitch rate, rad/s / \delta_{e,pilot}.

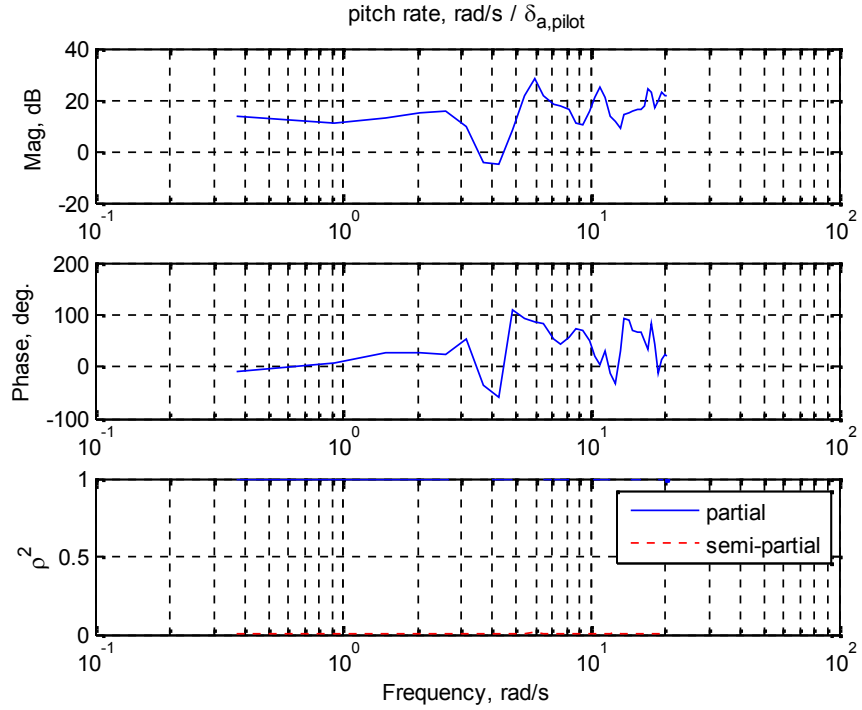

Figure 101: Identified frequency response: pitch rate, rad/s / \delta_{a,pilot}.

There is a notable peak near ~6 rad/s in many of these responses. This is notable when considering L1 input since that input has the most energy in the frequency range of interest.

A.3 2ND L3/R3 EXCITATION

The data segment from 1268.5 to 1272.5 was used. Considering data correlation, inputs considered were L3/R3 excitation, pitch command from pilot and roll command from pilot. L1/R1 excitation and L4/R4 excitation are zero so they were eliminated.

FREDA settings:

```
st.useSmoothing = 1;
st.psdTaper=0.05;
st.binRatio=1.01;
st.binSize=3;
st.zeroFill=30;
```

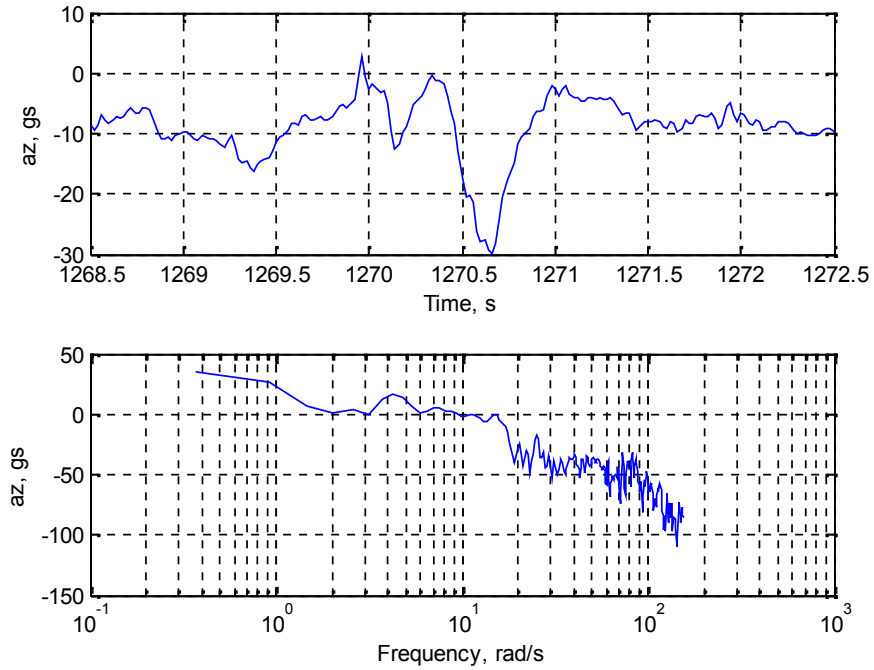

Figure 102: Output (az, gs) time history and resulting PSD.

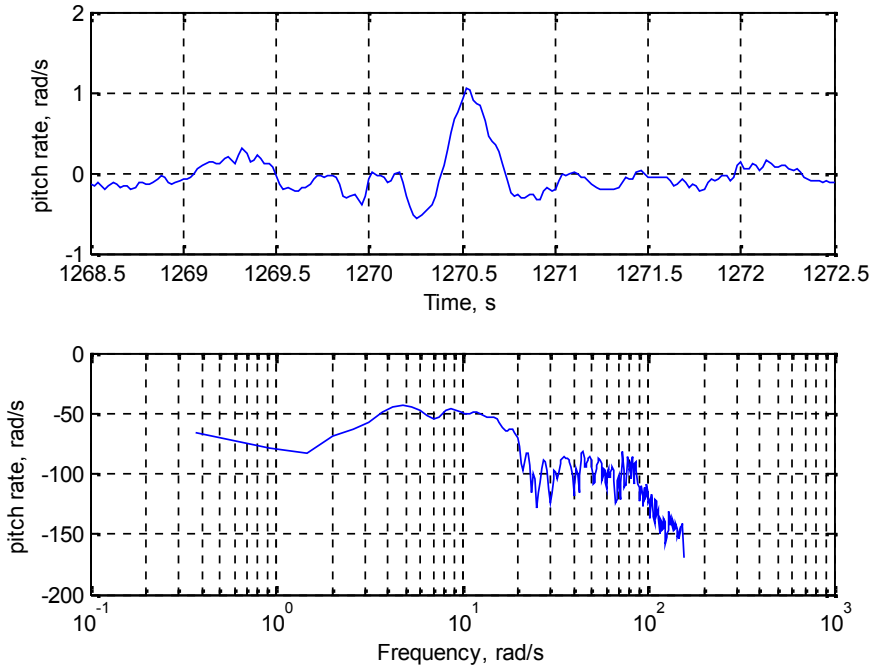

Figure 103: Output (pitch rate, rad/s) time history and resulting PSD.

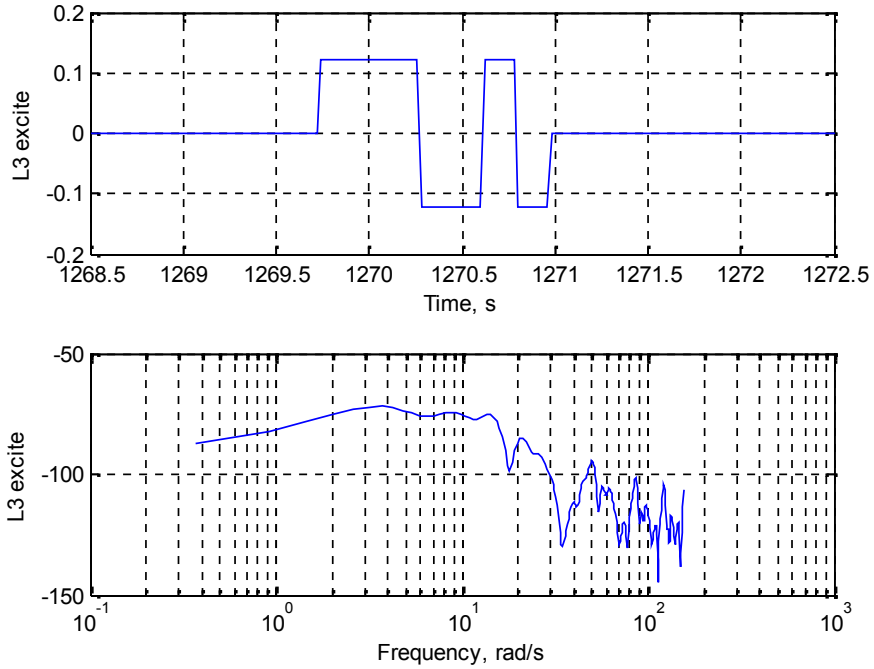

Figure 104: Input (L3 excite) time history and resulting PSD.

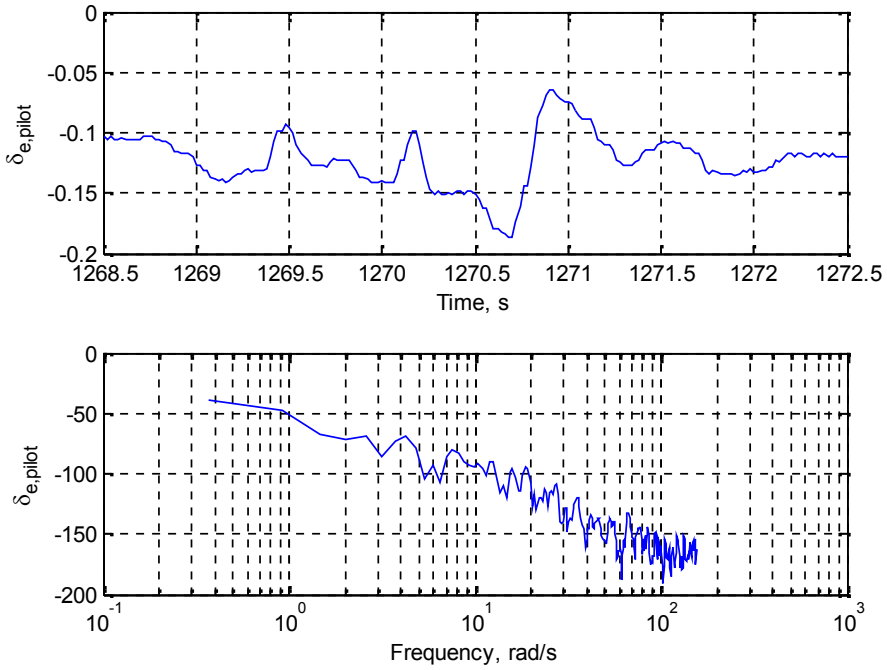

Figure 105: Input (\delta_{e,pilot}) time history and resulting PSD.

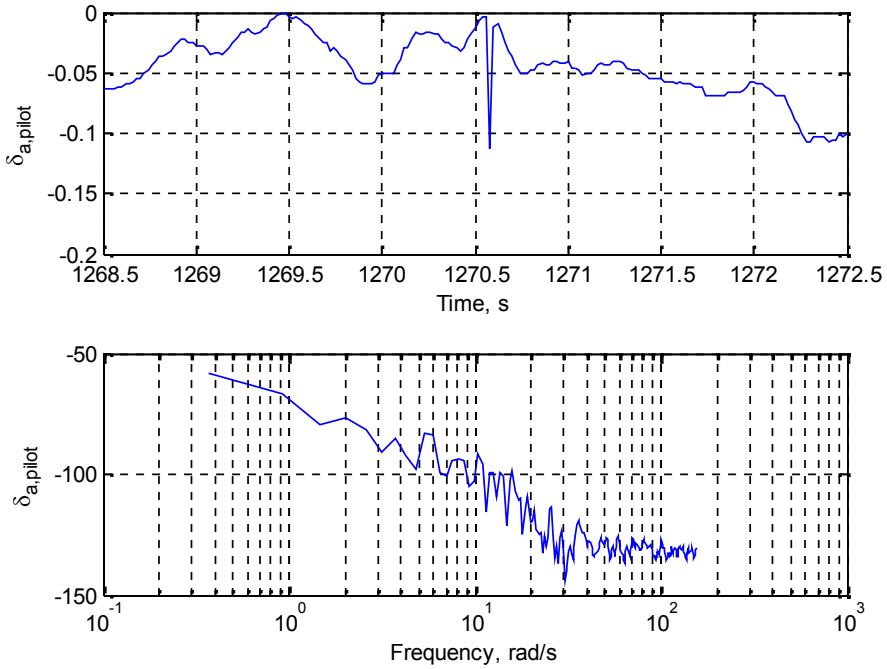

Figure 106: Input (\delta_{a,pilot}) time history and resulting PSD.

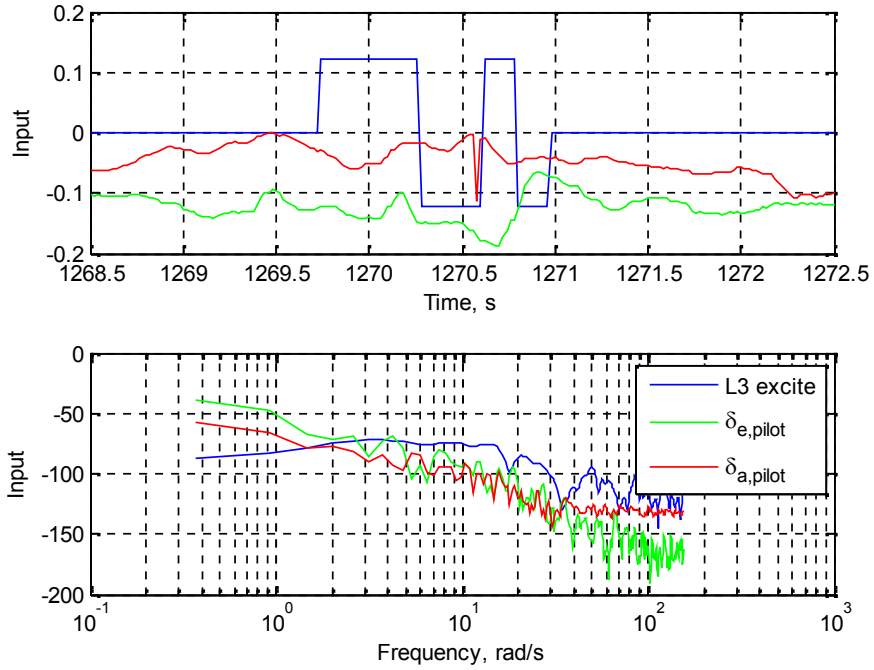

Figure 107: All inputs time histories and resulting PSDs.

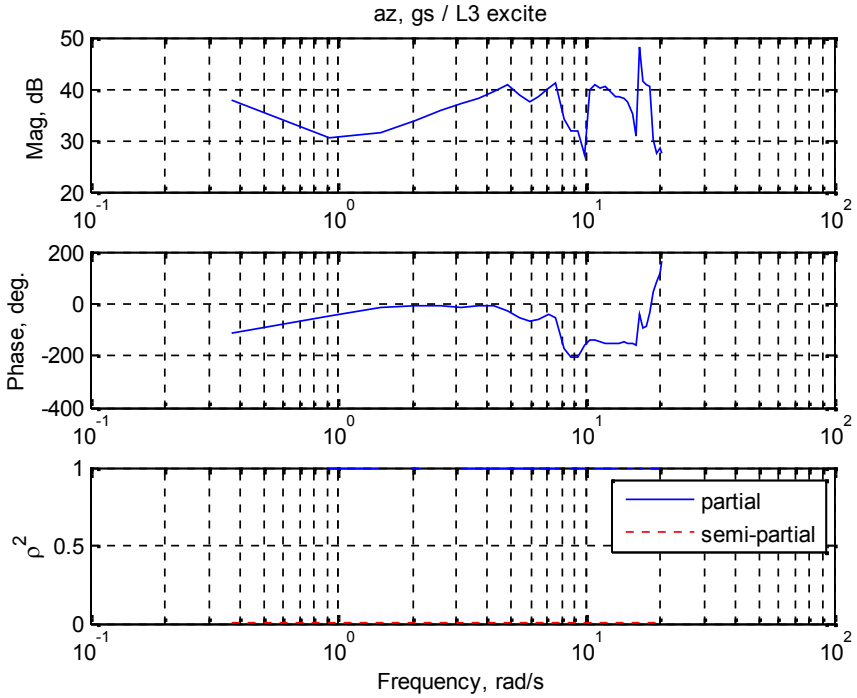

Figure 108: Identified frequency response: az, gs / L3 excite.

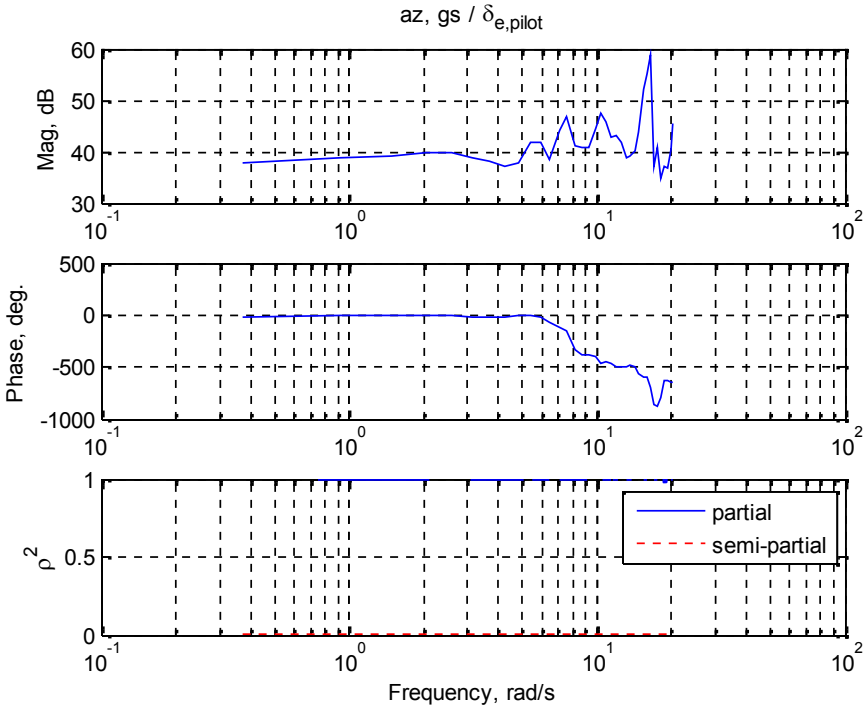

Figure 109: Identified frequency response: az, gs / \delta_{e,pilot}.

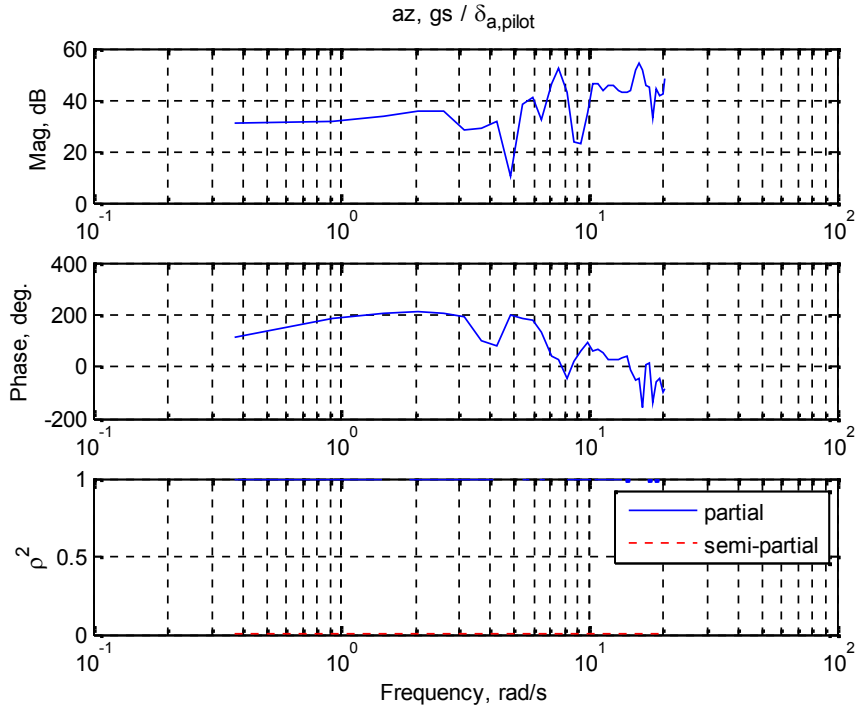

Figure 110: Identified frequency response: az, gs / \delta_{a,pilot}.

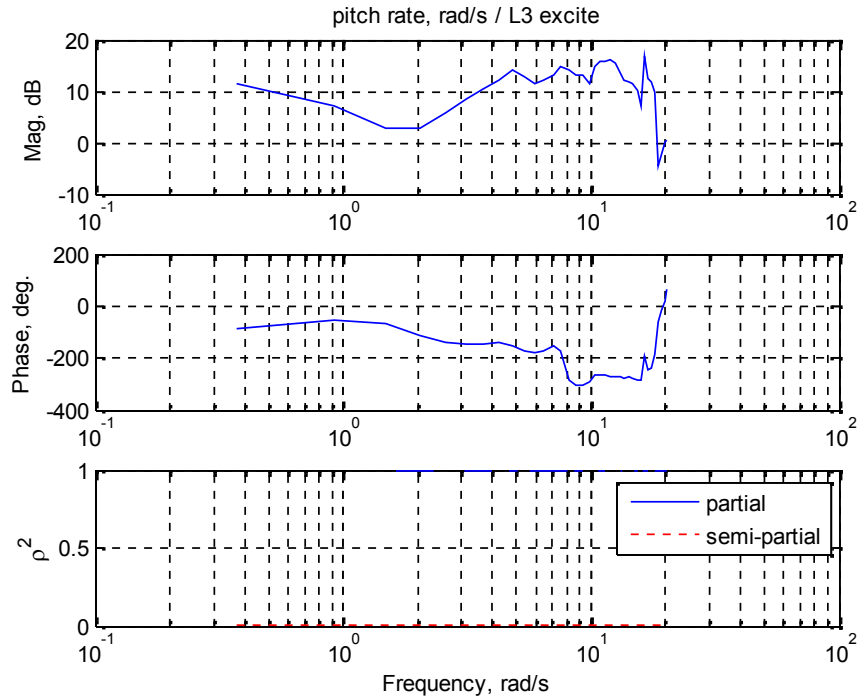

Figure 111: Identified frequency response: pitch rate, rad/s / L3 excite.

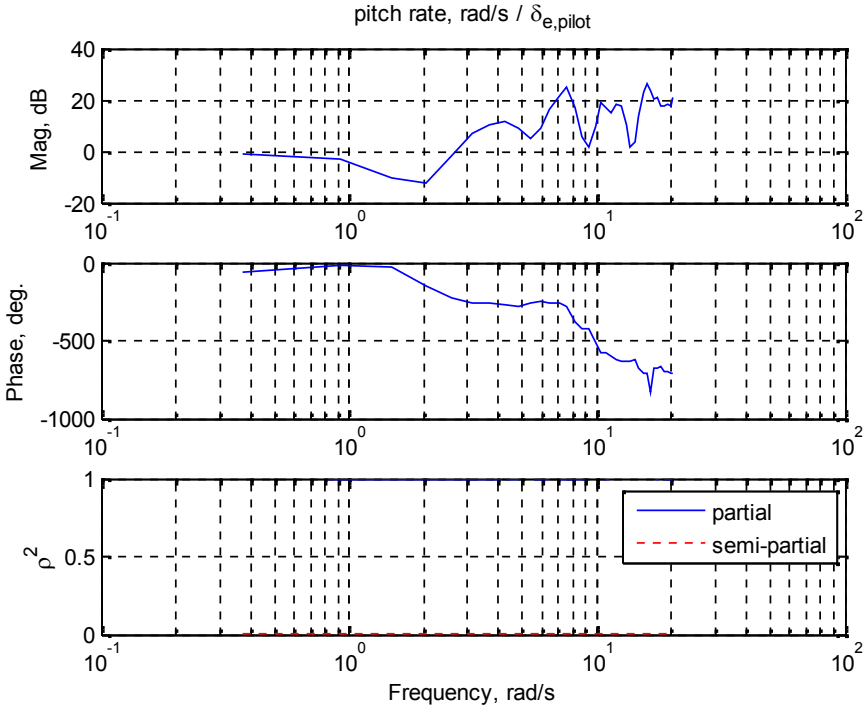

Figure 112: Identified frequency response: pitch rate, rad/s / \delta_{e,pilot}.

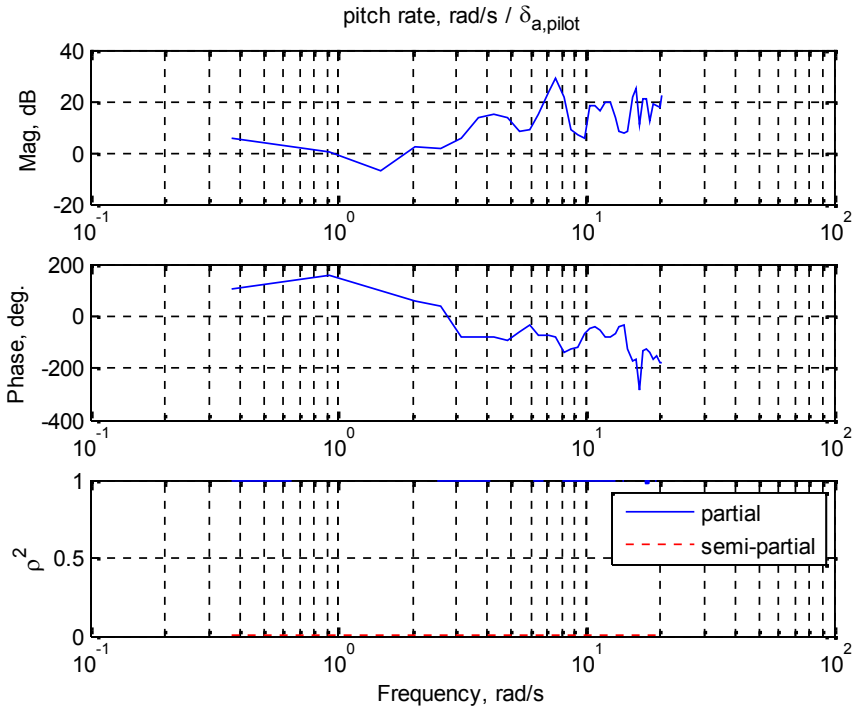

Figure 113: Identified frequency response: pitch rate, rad/s / \delta_{a,pilot}.

A.4 1ST L4/R4 EXCITATION

The data segment from 1262 to 1266 was used. Considering data correlation, inputs considered were L4/R4 excitation, pitch command from pilot and roll command from pilot. L1/R1 excitation and L3/R3 excitation are zero so they were eliminated.

FREDA settings:

```
st.psdTaper=0.05; % taper fraction
st.binRatio=1.01; % bin ratio
st.binSize=3; % average at least this many points
st.zeroFill=30; % seconds of zero fill
```

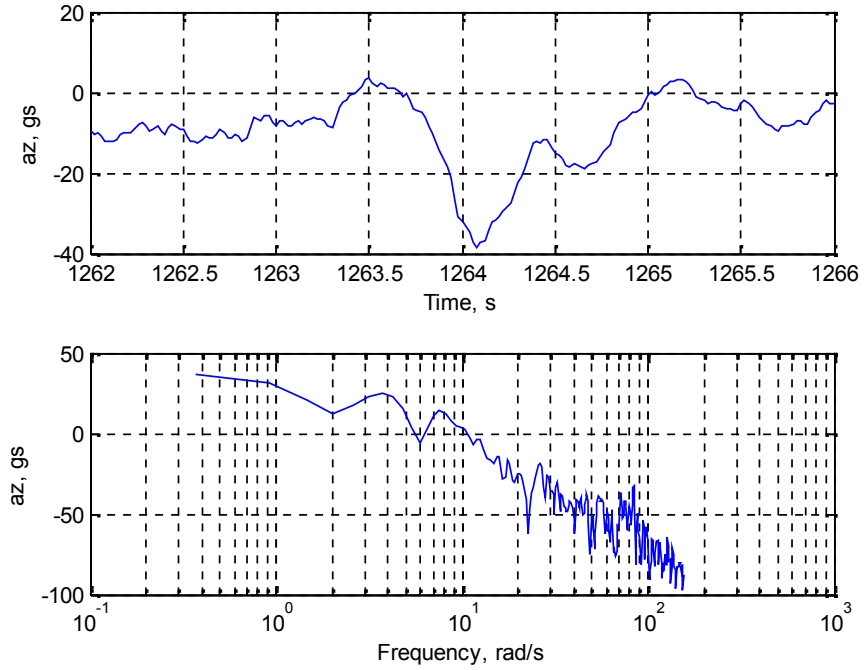

Figure 114: Output (az, gs) time history and resulting PSD.

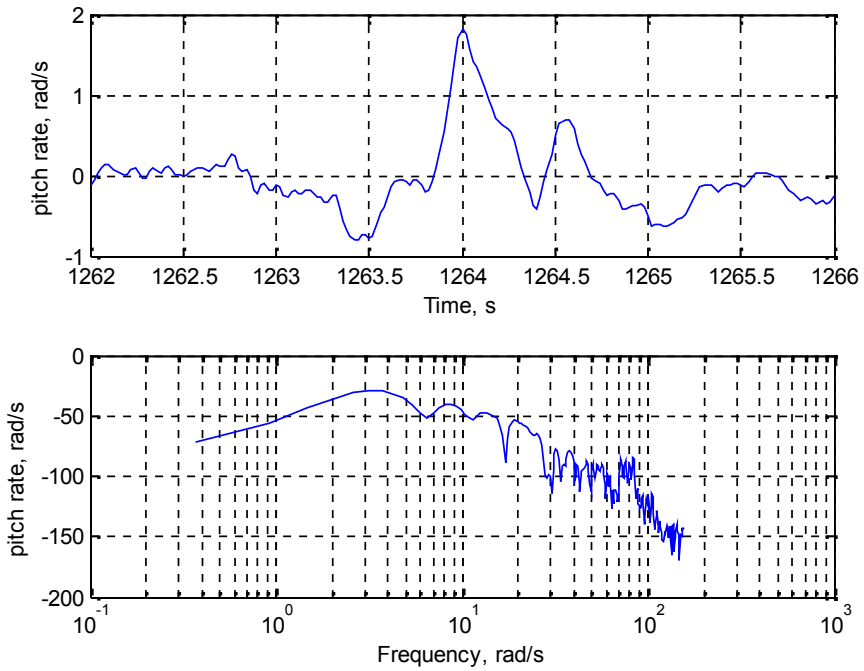

Figure 115: Output (pitch rate, rad/s) time history and resulting PSD.

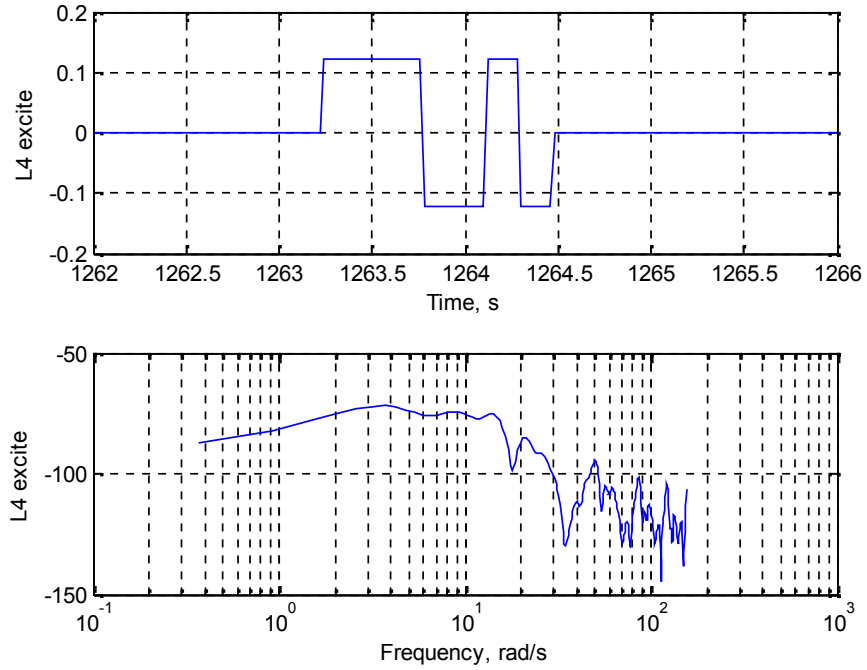

Figure 116: Input (L4 excite) time history and resulting PSD.

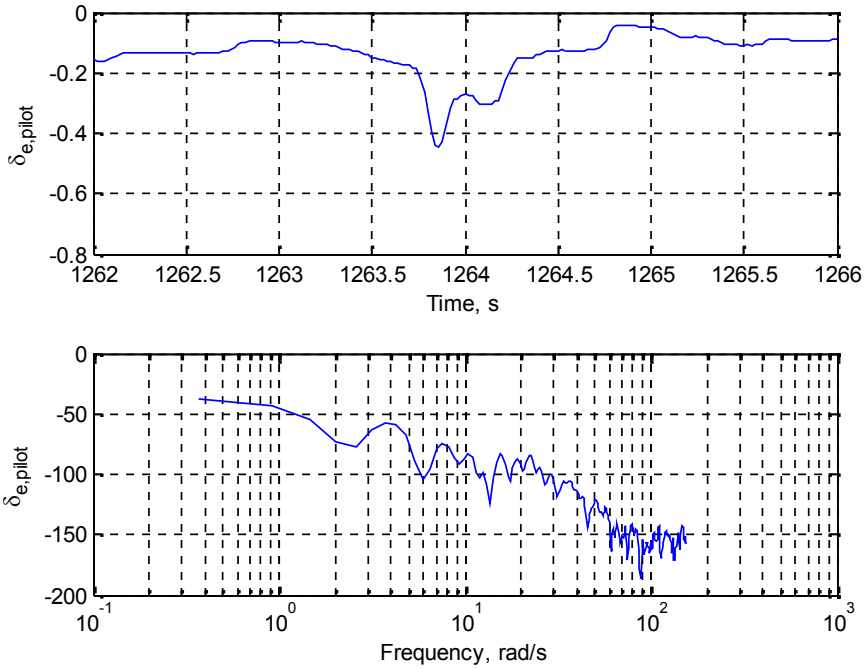

Figure 117: Input (\delta_{e,pilot}) time history and resulting PSD.

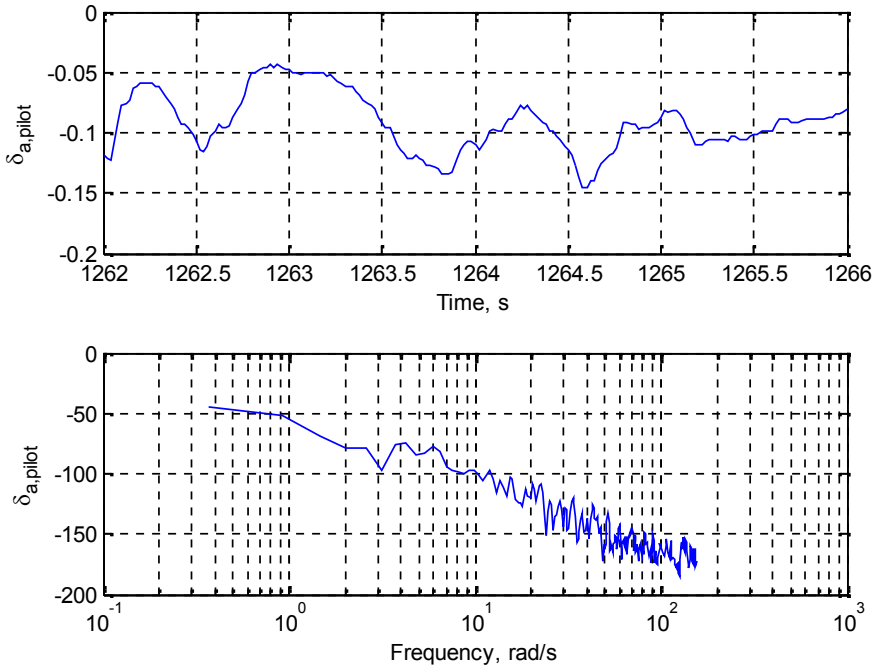

Figure 118: Input (\delta_{a,pilot}) time history and resulting PSD.

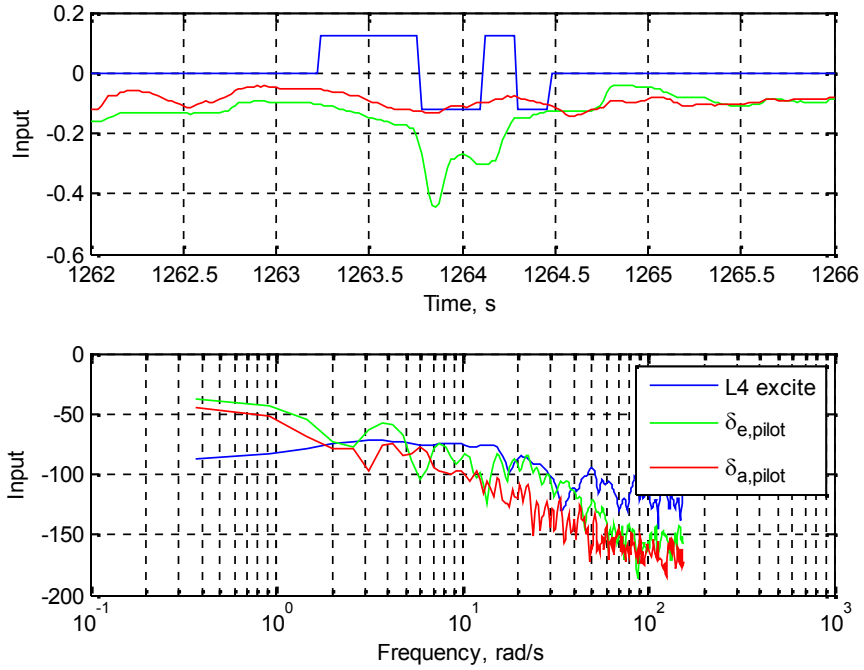

Figure 119: All inputs time histories and resulting PSDs.

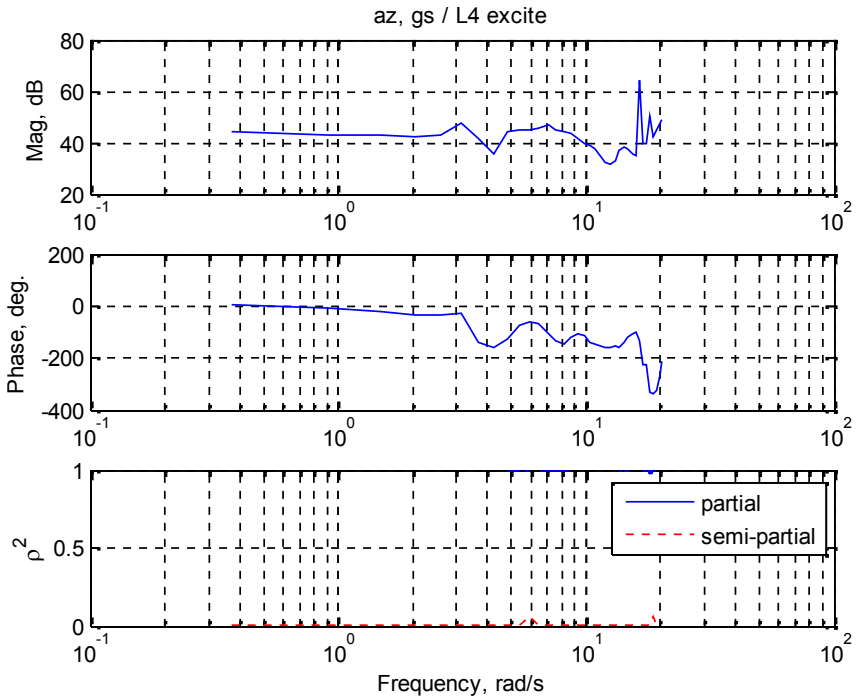

Figure 120: Identified frequency response: az, gs / L4 excite.

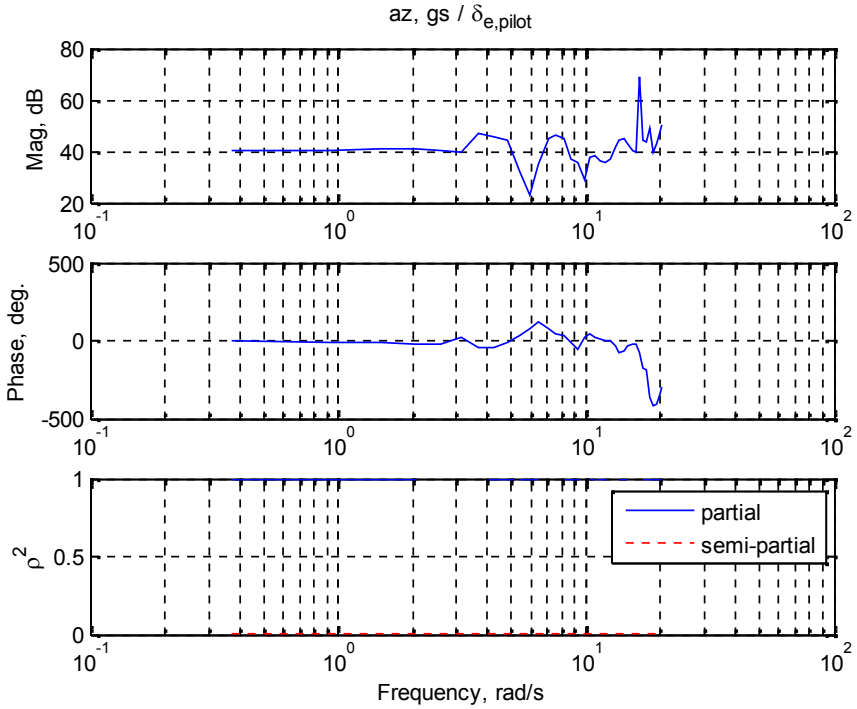

Figure 121: Identified frequency response: az, gs / \delta_{e,pilot}.

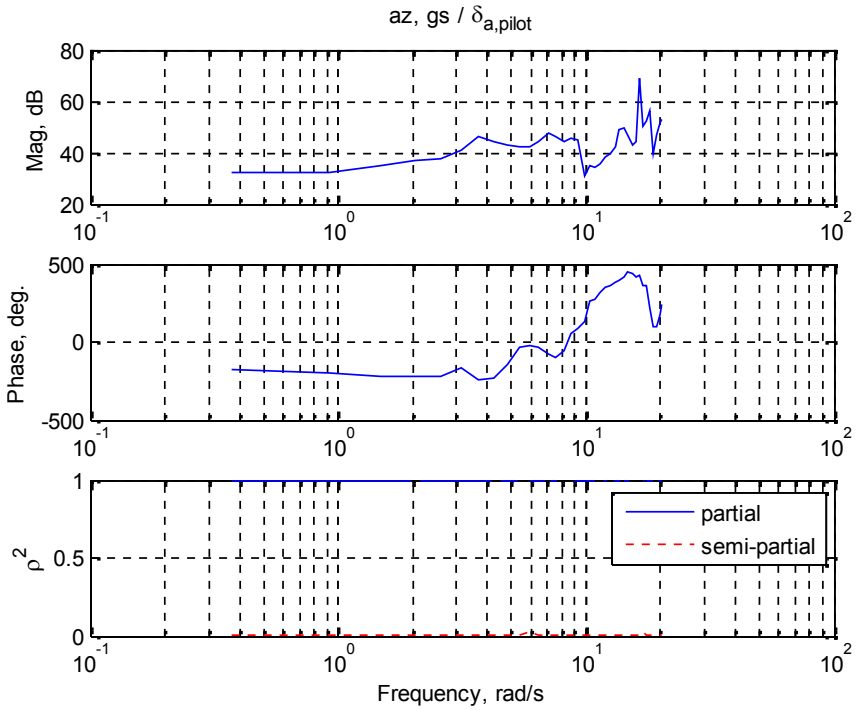

Figure 122: Identified frequency response: az, gs / \delta_{a,pilot}.

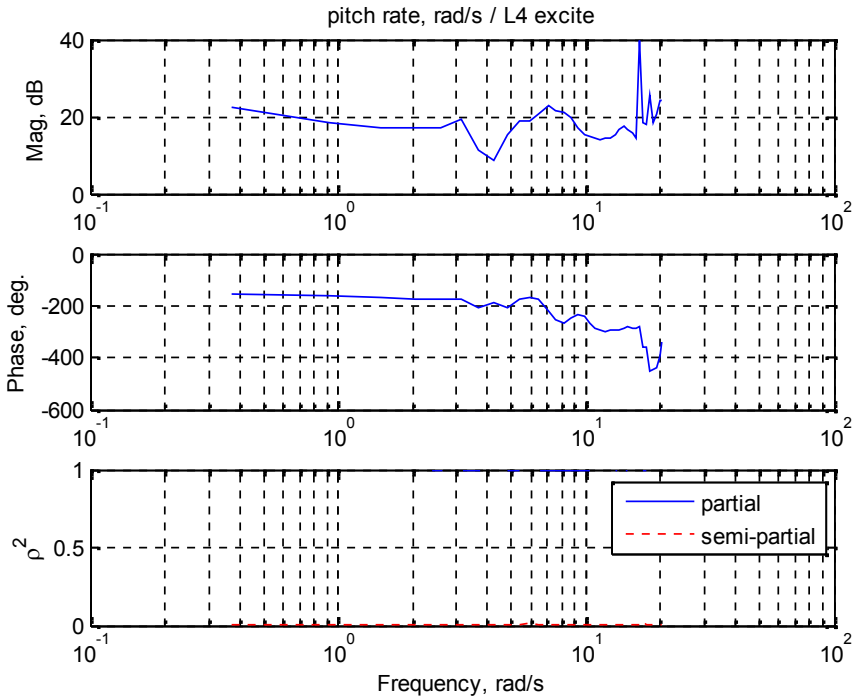

Figure 123: Identified frequency response: pitch rate, rad/s / L4 excite.

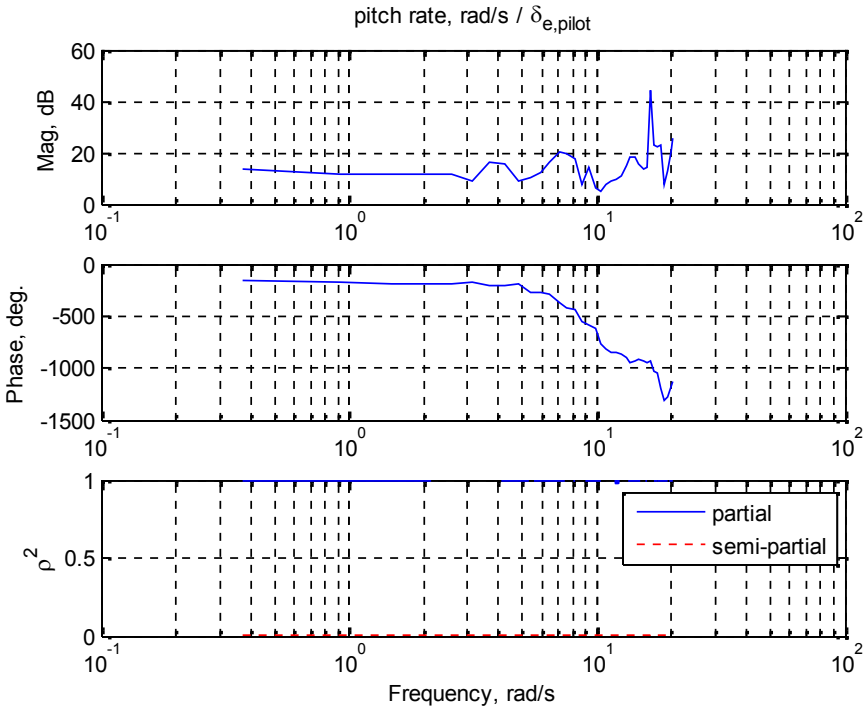

Figure 124: Identified frequency response: pitch rate, rad/s / \delta_{e,pilot}.

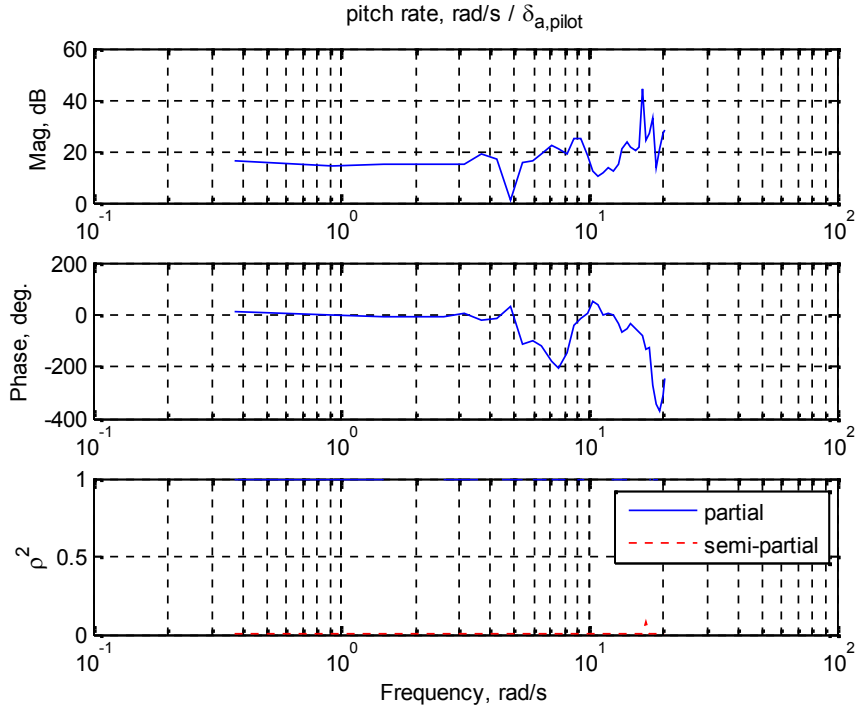

Figure 125: Identified frequency response: pitch rate, rad/s / \delta_{a,pilot}.

REFERENCES

[1] Jategaonkar, Ravindra V. "Flight vehicle system identification (a time domain methodology)." *Progress in astronautics and aeronautics* (2006).

[2] Morelli, Eugene A. "System identification Programs for aircraft (SIDPAC)," *AIAA Atmospheric Flight Mechanics Conference*, AIAA Paper 2002-4704, 2002.

[3] McRuer, Duane T., Dunstan Graham, and Irving Ashkenas. *Aircraft dynamics and automatic control*. Princeton University Press, 1973.